EFFECT OF STRUCTURAL MOTION ON THE HYDRODYNAMIC FORCING OF OFFSHORE STEEL STRUCTURES

by

ENRIQUE J. LAYA

Ingeniero Mecánico

Universidad Simón Bolívar
Caracas, Venezuela
(1977)

SUBMITTED IN PARTIAL FULFILLMENT
OF THE REQUIREMENTS OF THE
DEGREES OF

MASTER OF SCIENCE IN
MECHANICAL ENGINEERING

and

MASTER OF SCIENCE IN
CIVIL ENGINEERING

at the

MASSACHUSETTS INSTITUTE OF TECHNOLOGY

August 1980

Signature of Author_____
Departament of Mechanical Engineering
August 18, 1980

Certified by_____
Jerome J. Connor
Thesis Supervisor

Accepted by_____
Chairman, Departmental Comitee

TO MY WIFE

AND

DAUGHTER

EFFECT OF STRUCTURAL MOTION ON THE HYDRODYNAMIC FORCING OF OFFSHORE STEEL STRUCTURES

by

ENRIQUE J. LAYA

Submitted to the Departament of Mechanical Engineering and the Departament of Civil Engineering on August 18, 1980 in partial fulfillment of the requirements of the Degrees of Master of Science in Mechanical Engineering and Master of Science in Civil Engineering

ABSTRACT

The extension of Morison's equation to allow for structural motion is presently treated with two different hypotheses: (1) the relative velocity model, which replaces the fluid velocity with the relative velocity between the fluid and the structure; (2) the independent flow fields model which considers the flow to be a superposition of two unrelated flows, one due to the wave-current action on a rigid cylinder and the other due to the structural motion in still water. An iterative computational procedure that combines time domain and frequency domain analysis techniques is developed to solve the nonlinear governing equations for both models. Comparison studies are carried out for the sea states ranging from the drag dominant through the inertia dominant regimes. Results indicate that the independent flow fields model always predicts a higher displacement response, and the difference increases with wave heigth. However, the independent flow fields model is not applicable for the extreme sea states. There is negligible difference for the inertia dominant range. At intermediate sea states, which are of primary concern for fatigue analysis, the relative velocity model appears to underestimate the response, and therefore its applicability for fatigue life prediction requires further study.

Thesis Supervisor: Jerome J. Connor

Title: Professor of Civil Engineering

ACKNOWLEDGEMENTS

I will always be indebted to my advisor, Professor Jerome J. Connor, whose encouragement and thoughtful guidance have been invaluable in the accomplishment of this thesis. I cannot simply put into words my appreciation for all his attention and time spent on me.

I sincerely thank my friend Shyam Sunder S. for his suggestions and help throughout the course of this work.

The Fundación Gran Mariscal de Ayacucho funded my studies at M.I.T. The Instituto Tecnológico Venezolano del Petróleo funded this research. The financial support from these agencies is gratefully appreciated.

Also, a sincere word of thanks to Ms. Donna Masone for her excellent typing of the manuscript.

TABLE OF CONTENTS

LIST OF FIGURES

LIST OF TABLES

LIST OF SYMBOLS

Symbol	
A	Cross-sectional area
C_D	Drag coefficient, in general
C_{DS}	Drag Coefficient, based on external steady flow field
C_{DU}	Drag coefficient, based on flow field associated with structural motion
C_{DV}	Drag coefficient, based on external flow field
C_H	Hydrodynamic drag damping
$\underline{C}_H$	Hydrodynamic drag damping matrix
C_M	Inertia coefficient, in general
C_{MU}	Inertia coefficient, based on flow field associated with structural motion
C_{MV}	Inertia coefficient, based on external flow field
D	Diameter
d	Depth
D_S	Hysteretic structural damping coefficient
E	Young modulus
$\underline{F}$	Force vector, frequency domain
$\underline{f}$	Force vector, time domain
f	Force, scalar
f_D	Drag force
f_I	Inertia force
f_L	Lift force

Symbol	
f_s	Vortex shedding frequency
g	Gravity acceleration
G_η	Wave heigth spectral density function
H	Wave heigth
H_S	Significant wave heigth
I	Moment of inertia
Im[ ]	Imaginary part of a complex quantity
j	$= \sqrt{-1}$
K	Structural stiffness, scalar
$\underline{K}$	Structural stiffness matrix
k	Roughness
k	Wave number(Ch. 3)
K-C	Keulegan-Carpenter number, in general
L	Wave length
M	Mass, scalar
$\underline{M}$	Mass matrix
m	Bending moment
M_a^R	Added mass, relative velocity formulation
M_a^I	Added mass, independent flow fields formulation
N	Number of discretization points
$\underline{p}(t)$	Force vector evaluated at an iteration loop
R_E	Reynolds number, in general
S	Strouhal number

Symbol	
T	Oscillation period
T	Record legth (Ch. 4)
$T_{\dot{r}}$	Average zero crossing period of relative velocity
$T_{\dot{u}}$	Average zero crossing period of structural velocity
U	Structural displacement, defined over a continuous domain
$\underline{U}$	Structural displacement vector
u	Structural displacement, scalar
u_0	Amplitude of structural displacement
$\hat{u}$	$= \frac{u_0}{D}$, dimensionless amplitude
$\underline{V}$	Fluid velocity vector
v	Fluid velocity, scalar
v_0	Amplitude of fluid velocity
v_r	Reduced velocity
w	distributed load
X	Horizontal coordinate
Y	Vertical local coordinate
Z	Vertical coordinate
α	"proportional to" (Ch. 2)
Δ	Sampling period
δ	Dirac delta distribution
ε	Relative roughness
ε	"error" (Ch.4)
η	Instantaneous wave heigth
θ	Structural rotation

Symbol	
ℓ	Structure length
ν	Kinematic viscosity of water
ρ	Water density
σ	Root mean square (r.m.s), in general
$\sigma_{\dot{r}}$	R.M.S of relative velocity
σ_{v}	R.M.S of fluid velocity
$\sigma_{\dot{u}}$	R.M.S of structural velocity
ϕ	Random phase angle
Ω,ω	Circular frequency

CHAPTER 1

INTRODUCTION

As a result of the extensive search for oil in offshore waters during the past decade, new structural concepts such as the deep water platform have evolved. The fundamental period of these "new" structures is closer to the range of dominant periods associated with the wave loading and dynamic analysis methods are now required. They generally have low structural damping, and are susceptible to even low wave energy in the neighborhood of the fundamental period. This fact, coupled with the fatigue characteristics exhibited by the materials composing these structures, has resulted in fatigue being one of the most important design issues. A proper assessment of the dynamic behavior is now a necessity.

Dynamic response of steel offshore jacket structures is presently being evaluated by accounting for structural motion in the formulation of the force exerted by the sea through interactive terms that involve fluid and structural velocities and accelerations in a rather simple empirical expression called the Modified Morison's Formula. The modification involves replacing fluid flow measures with relative motion measures such as relative velocity, and is based on the assumption that the drag force on a flexible cylinder immersed in an oscillatory flow is equal to the force on a rigid cylinder corresponding to the actual flow conditions for the moving cylinder.

This assumption is not valid for certain flow conditions. The difficulty arises because the hypothesized drag forcing mechanism does not consider phenomenological differences resulting from extreme variations in the wake development time, which is limited by flow reversals from cycle to cycle. The use of a quasi-static flow assumption to predict the drag force on a moving cylinder, where the basic flow regime may be very different from the flow regime on a motionless cylinder, is questionable. Moe and Verley [1] have proposed a different drag force formulation based on a superposition of two "independent flow fields". They view the flow as a superposition of a far field which is unaffected by the cylinder motion and a near field resulting from the cylinder motion. Their formulation, when tested on a harmonically oscillating cylinder in line with a uniform current, indicates lower value of equivalent hydrodynamic damping compared to the relative velocity formulation. Special attention is directed here to this hypothesis because of its potential implication for a deep water platform. An overestimation of the hydrodynamic damping leads to an unconservative estimate of the fatigue life of the structure, and could result in a premature failure.

One of the objectives of this thesis is to evaluate the significance of the "independent flow fields assumption" when applied to typical flow situations for an offshore structure. The approach followed consists of:

- Use of an adequate yet computationally simple physical model for assessing the sensitivity of the dynamic response to the alternate

approaches for predicting the drag force. For this phase, a single cylindrical member representative of a typical structural element is utilized.

- Solution of the governing equations with a numerical scheme that, while capable of handling the full nonlinear equations, is reasonably inexpensive and easily implemented as an extension of the present frequency domain solution method. An interesting numerical strategy that combines the advantages of time domain and frequency domain analysis (without suffering their drawbacks) is applied to this problem.

CHAPTER 2

HYDRODYNAMIC FORCE MODELING

The prediction of hydrodynamic forces on an offshore structure is still a controversial issue in spite of the efforts of many investigators over the past 30 years. A general theoretical treatment does not exist and consequently the present approach is based on empirical formulations for special flow conditions which consider the influence of only a subset of the physical parameters involved. One has to integrate the information available for the specialized cases, assess the uncertainties, and establish a consistent mathematical formulation suitable for modeling.

This chapter starts by identifying the range of applicability of the wave force theories, and then focuses on the original Morison equation. The hydrodynamic coefficients are discussed next, starting with steady flow past a circular cylinder and then harmonic flow. An extended form of Morison's equation, which attempts to account for relative motion, is presented and the uncertainties associated with the original and relative motion formulations are examined. We then discuss the independent flow fields interactive form of Morison formula proposed by Moe and Verley. The hydrodynamic damping and added mass corresponding to the different force formulations are treated in the last section.

2.1 WAVE FORCE THEORY CLASSIFICATION

A structure in a marine environment is subjected to a time varying force resulting from the interaction of the structure and the fluid.

Two limiting cases are generally identified: i) the relative magnitude of the member diameter with respect to the incident wave length is such that the wave field is modified by the presence of the member and ii) the structure has a negligible effect on the wave field. The forcing mechanism is dictated by diffraction effects for the former case. Viscous influence is of greater influence for the later case. The key parameters which identify the relative significance of diffraction and viscous effects are the wake parameter $H/(2D)$ and the scatering parameter $2\pi D/L$. Here, H represents the wave heigth, L the wave length, and D the typical structural dimension. Fig. 2.1 summarizes the ranges of influence of both viscous and diffraction effects. The boundary lines shown are defined by $2\pi D/L = .2 \sim .1$ [2,3] and $H/(2D) \sim 2$ [5].

2.2 MORISON'S EQUATION

Most studies of in-line forces exerted by viscous oscillatory flows on circular cylinders are based on an equation proposed by Morison et al [4] in 1950. His formulation was developed for a rigid vertical cylinder inmersed in a surface wave induced flow and extending through the wave crest. Spanwise time varying flow descriptions were simulated by linear wave theory two force components were identified:

- A drag term due to the combination of pressure field effect and the viscous shear effect related to the existence of a boundary layer in the vicinity of the cylinder. The drag force acts in phase with the velocity and has the form:

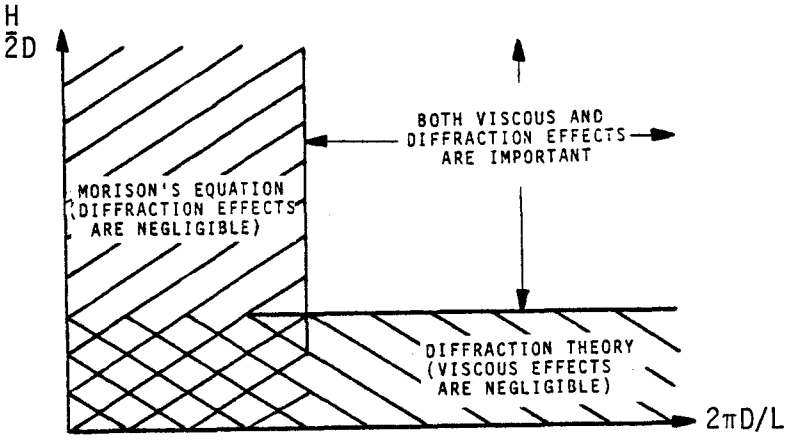

Fig. 2.1 Wave Force Theory Classification [5]

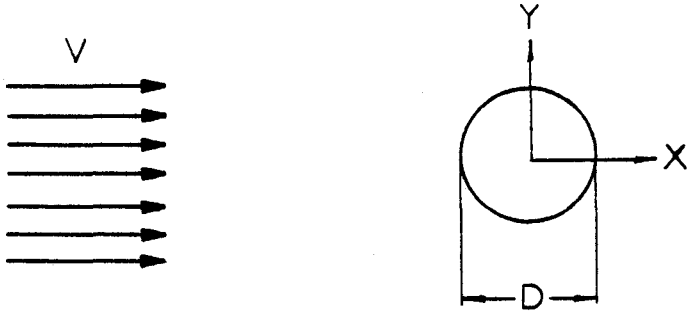

Fig. 2.2a Steady Flow Past a Rigid Circular Cylinder

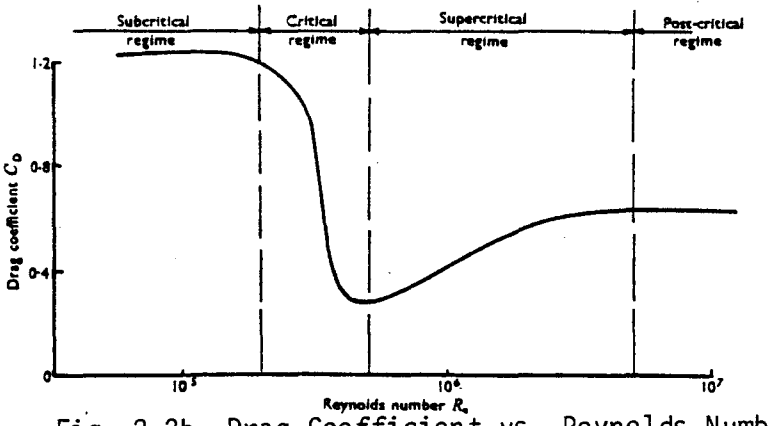

Fig. 2.2b Drag Coefficient vs. Reynolds Number for a Smooth Cylinder [3]

$$f_D = \frac{1}{2}\rho D C_D v|v| \qquad (2\text{-}1)$$

where f_D represents the drag force per unit length, ρ is the water density, D is the diameter of the cylinder, and C_D is the drag coefficient which depends on certain flow parameters to be discussed later.

- A virtual mass force (referred to here as the inertia force) which is produced by two mechanisms, the first due to the buoyancy exerted by the pressure gradient related to the acceleration field and the second due to the flow entrained by the cylinder which produces an added mass effect. The inertia force acts in phase with the acceleration and is expressed as:

$$f_I = \frac{1}{4}\rho\pi D^2\dot{v} + \frac{1}{4}\rho\pi D^2(C_M - 1)\dot{v} \qquad (2\text{-}2)$$

where f_I represents the inertia force per unit length and C_M is the inertia coefficient which also depends on certain flow properties.

The total in-line force is taken as the algebraic sum of the drag and inertia force terms:

$$f = \frac{1}{2}\rho D C_D v|v| + \frac{1}{4}\rho\pi D^2 C_M \dot{v} \qquad (2\text{-}3)$$

2.3 THE HYDRODYNAMIC COEFFICIENTS

2.3.1 INTRODUCTORY COMMENTS

When computing the hydrodynamic force on an offshore structure with Morison's equation, the question arises as to what values of C_M and C_D should be used. At present, information on the dependence of C_M and C_D with respect to all the parameters which describe the actual flow situation is unavailable. Therefore, one has to resort to data for similar simpler flows where the hydrodynamic coefficients have been evaluated. Several approximate methods for extending experimental values of these coefficients are presently in use. However, their applicability is a research issue [3]. Many experimental investigations on the behavior of the drag and/or the inertia coefficients for single cylinders at different flow conditions have been carried out following the introduction of Morison's equation. Our primary interest will be focused on the experiments for a fixed cylinder in simple harmonic flow. We first review a classical experiment that describes the features of steady flow past a fixed circular cylinder. This will provide the necessary background and perspective for the more complex case of harmonic flow.

2.3.2 STEADY FLOW PAST A FIXED CIRCULAR CYLINDER

Referring to Fig. 2.2a, we consider a stationary cylinder inmmersed in steady uniform flow perpendicular to the cylinder axis.

The properties of the flow are modeled by two parameters:

i) The Reynolds number, an indicator of the relative magnitudes of the inertia forces and viscous forces,

$$R_E = \frac{vD}{\nu}$$

where v represents the undisturbed velocity of the fluid, D the diameter and ν the kinematic viscosity.

ii) The relative roughness of the cylinder, whose effect can be viewed as increasing the apparent diameter as well as influencing the dependence of C_D on R_E (see Fig. 2.3)

$$\varepsilon = \frac{k}{D} \quad , \text{ k: surface roughness}$$

In this case, the in-line and transverse forces (also called the drag and lift forces) per unit length on the cylinder are expressed as (see Fig. 2.2a):

$$f_x = f_D = \tfrac{1}{2}\rho C_D D v^2 \tag{2-4}$$

$$f_y = f_D = \tfrac{1}{2}\rho C_L D v^2 \sin(2\pi f_s t) \tag{2-5}$$

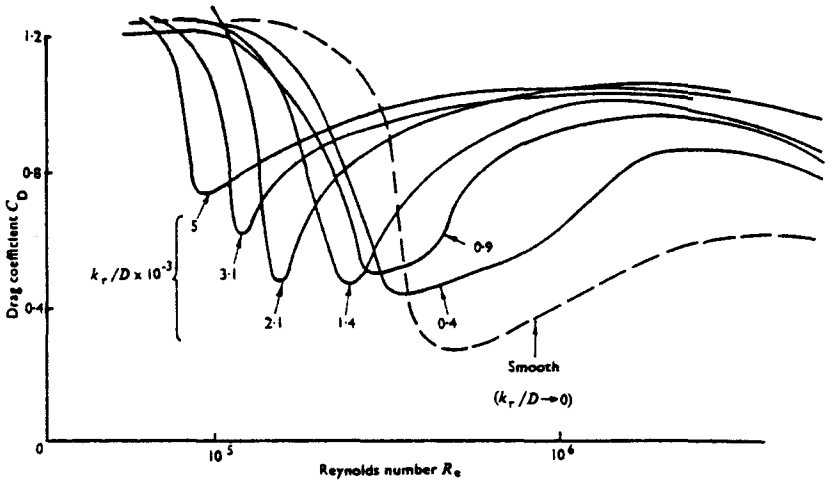

Fig. 2.3 Influence of the Relative Roughness on the Drag Coefficient [3]

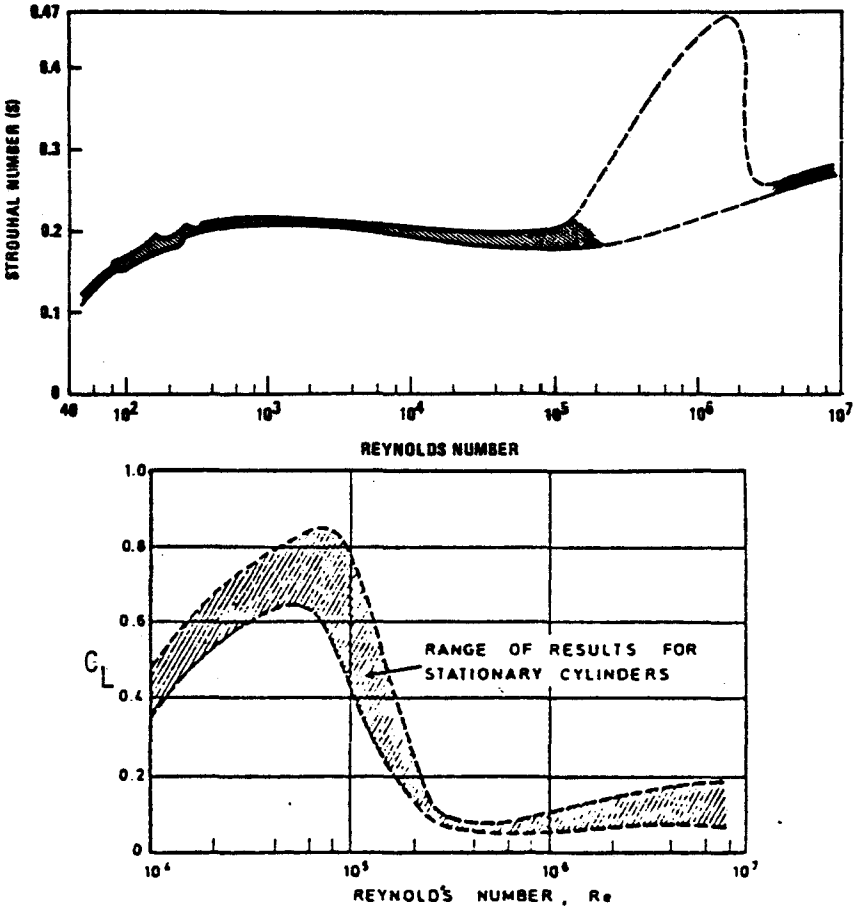

Fig. 2.4a and 2.4b Strouhal Number vs. Reynolds Number and Lift Coefficient vs. Reynolds Number [9]

where C_L is the lift coefficient and f_s is the vortex shedding frequency which depends on the dimensionless number S(S: Strouhal number),

$$f_s = S(\frac{v}{D}) \qquad (2\text{-}6)$$

The nature of the flow regime, and therefore the value of C_D, is dependent on the Reynolds number. Fig. 2.2b shows the variation of C_D with R_E and the various regimes that have been defined.

$R_E < 2\times10^5$ Subcritical range, fairly regular flow, laminar separation of boundary layer, wide wake, $C_D \simeq 1.2$.

$2\times10^5 < R_E < 5\times10^5$ Critical range, transition from laminar to turbulent regime, point of separation moves to the rear end of the cylinder, C_D diminishes considerably.

$5\times10^5 < R_E < 5\times10^6$ Supercritical range, flow is fully turbulent, C_D increases, wake widens.

$R_E > 5\times10^6$ Postcritical range, turbulent flow, C_D takes constant values within 0.6~0.7

Typical Reynolds numbers for steel jacket members near the surface are in the region $10^5 \sim 10^6$ [6] and relative roughness design values may be as high as 0.01 [7]. The influence of $\frac{k}{D}$ on C_D is shown in Fig. 2.3.

Since flow at high Reynolds number is the most common case, we will describe in detail its essential features. One of the most important features is the vorticity created at the boundaries of a rotational flow field, for example in the region near the wall of a cylindrical obstacle as shown in Fig. 2.2a. For certain flow regimes, there is an asymmetrical release of vortices from the upper and lower points of separation which generates a transverse force. This was first observed by Von-Karman in 1912. Subsequent studies have established that the frequency of vortex shedding is approximately constant, for a particular flow, and predicted by Eq. 2-6. The dependence on flow, i.e., Reynolds number, is introduced through the Strouhal number. Both the lift coefficient and the Strouhal number are functions only of Reynolds number for this experiment (see Fig. 2.4). It is interesting to note a region of drastic change in C_L and bandwidth opening for S at the critical flow regime $5\times10^5 < R_E < \sim 5\times10^6$.

2.3.2 SIMPLE HARMONIC FLOW PAST A FIXED CIRCULAR CYLINDER

A more interesting situation, which is closer to the actual problem of fluid-structure interaction in an offshore structure, is simple harmonic flow past a motionless circular cylinder. Here the additional parameter required to characterize the forcing is the Keulegan-Carpenter

number K-C=v_oT/D. It is proportional to the ratio of the distance travelled by the water particle each half cycle to the cylinder diameter. v_o represents the maximum fluid velocity over a cycle and T the period. The significance of the Keulegan-Carpenter number is that it is a gross measure of the unsteadiness of the flow. At high values of K-C (K-C>~25), the velocity of the flow varies slowly compared to the wake development time and the flow can be considered as quasi-steady. In this case, the drag component will dominate over the inertia force and the value of C_D is essentially equal to its value for steady flow. At low values of K-C (K-C<~5), the drag coefficient approaches zero and the inertia component tends to dominate. In the intermediate range, 5<K-C<25, both drag and inertia effects will be of importance. Many studies have been directed at establishing the dependence of C_D and C_M on R_E, K-C and $\frac{k}{D}$ for this type of flow although with different experimental approaches. At present, Sarpkaya's results [15] appear to be the most comprehensive. They are reproduced in Fig. 2.5.

2.4 MODIFIED MORISON'S EQUATION, A RELATIVE VELOCITY APPROACH

In section 2.2, the cylindrical element was assumed to be rigid when deriving the hydrodynamic force. Actually, there is interaction between the cylinder and the water, and the force is affected by the ensuing motion of the cylinder. This fluid-structure coupling is nonlinear and difficult to treat numerically. However, it must be considered in a dynamic response analysis since it is the source of "fluid" damping. If it is neglected, one obtains over-conservative

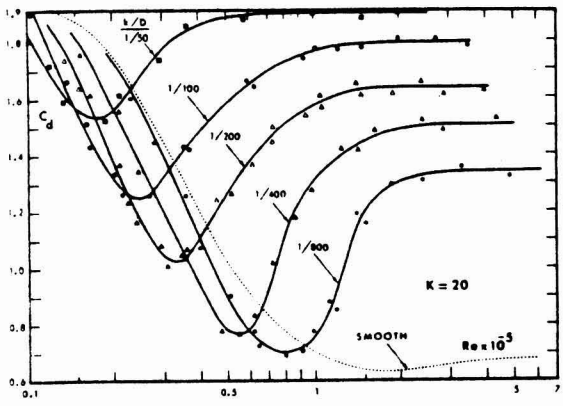

Drag coefficient versus Reynolds number for K-C=20

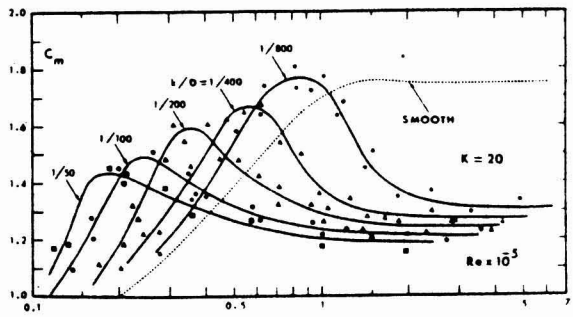

Inertia coefficient versus Reynolds number for K-C=20

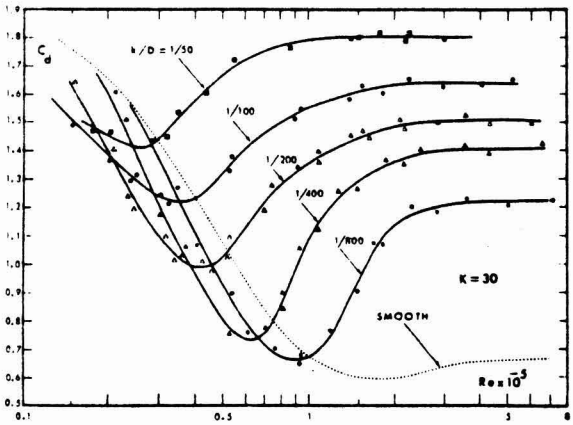

Drag coefficient versus Reynolds number for K-C=30

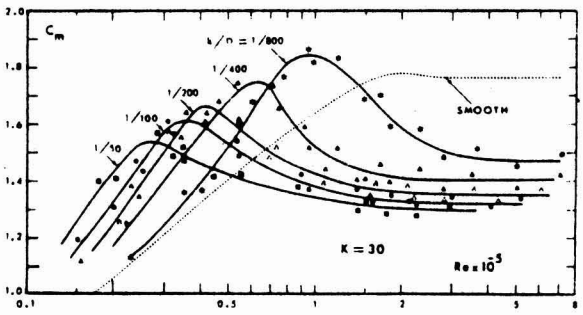

Inertia coefficient versus Reynolds number for K-C=30

Fig. 2.5 Sarpkaya's curves for C_M and C_D [15]

results.

The effect of structural motion on the drag force, which is of main concern, is accounted for by a relative velocity approach. That is, the flow pattern in the vicinity of the moving cylinder is evaluated through a coordinate transformation where a relative velocity assumption is used to determine the instantaneous flow properties. Mathematically, one replaces v in Eq. 2-1 with $v-\dot{u}$.

$$f_D = \frac{1}{2}\rho C_D D(v-\dot{u})|v-\dot{u}| \tag{2-7}$$

where $\dot{u}$ is the velocity of the cylinder and C_D is now evaluated with relative velocity "definitions" of the Reynolds number and Keulegan-Carpenter numbers:

$$R_E = \frac{(v-\dot{u})_o D}{\nu} \quad , \quad K\text{-}C = \frac{(v-\dot{u})_o T^*}{D} \tag{2-8}$$

T^* : period of the function $(v-\dot{u})$

A similar procedure is followed to account for the effect of the member acceleration, $\ddot{u}$, on the added mass term of Eq. 2-2,

$$f_I = \frac{1}{4}\rho\pi D^2\dot{v} + \frac{1}{4}\rho\pi D^2(C_M-1)(\dot{v}-\ddot{u}) \tag{2-9}$$

where C_M is also to be evaluated with R_E and K-C as defined by Eq. 2-8.

With these modifications, the total in-line force per unit length

expands to

$$f = \frac{1}{2}\rho C_D D(v-\dot{u})|v-\dot{u}| + \frac{1}{4}\rho\pi D^2 C_M(\dot{v}-\ddot{u}) + \frac{1}{4}\rho\pi D^2\ddot{u} \qquad (2\text{-}10)$$

The above expression is commonly designated as the modified form of Morison's equation. We shall refer to it here as the relative velocity interactive form of Morison's equation. This form is generally accepted as being appropriate when the cylinder diameter is a small fraction of the wave length and therefore the variation of the pressure gradient across the width of the section is insignificant. The condition, $D/L < 0.2$ [5], defines the zone of applicability. Typical offshore steel jacket members have D=O(1 m), L=O(100 m), and D/L is considerably less than 0.2.

There are a number of assumptions that are implicit in the use of Eq. 2-10. Some are related to the range of applicability of the original formulation itself (Eq. 2-3). Others are associated with the extensions introduced in 2-10. Both are important and it is worthwhile to discuss their implications.

2.5 UNCERTAINTIES ASSOCIATES WITH THE APPLICATION OF MORISON'S EQUATION

Morison's equation is based on the following assumptions:

- The in-line hydrodynamic force can be represented by the sum of the drag and inertia forces. Some investigators consider this somewhat unrealistic, partly because it expresses the drag component in terms of only the instantaneous velocity [8].

However, recognizing the ability of the hydrodynamic coefficients to account for the remaining effects, the form of the equation is adequate.

- Hydroelastic effects are not important [9]. The validity of this assumption is not questioned since Mach number ranges are within 0.3 and the flow can be regarded as truely incompressible.
- The wave field must be one-dimensional. This limitation is of importance since, in reality, no one-directional flow condition is achieved under normal sea conditions and multi-directionality effects on both C_D and C_M remain to be determined. It should also be noted that Morison's experience was with the wave propagation direction perpendicular to the cylinder axis. For non-vertical cylinders, a classical approach suggested by Borgman in 1958 [10] has been used. The wave force is evaluated with the fluid particle velocity and acceleration components perpendicular to the cylinder axis, and is assumed to act normal to the cylinder. This assumption oversimplifies the situation since the drag force is known to depend on the resultant velocity rather than on the velocity component perpendicular to the cylinder axis [11].
- The application of Eq. 2-3 assumes the effect of vortex shedding on the in-line force to be negligible. Strictly speaking, that is not true. Unsymmetrical pressure distribution patterns over the cylindrical cross section, associated with

vortex generation and oscillating transverse forces, result in fluctuation of the in-line force at a frequency equal to the shedding frequency. The additional in-line force is expressed as:

$$f_{LX} = \frac{1}{2}\rho D C_{LX} v^2 \sin(2\pi f_s + \beta)$$

C_{LX}: "in-line Lift coefficient"

β : phase angle

The intensity of this force is directly related to the vortex strength. This in turn is not only a function of instantaneous flow properties but also of its time history since vorticity progressively accumulates behind the cylinder to form large discrete vortices [13]. Studies by Sarpkaya have shown that C_L and f_s depend on R_E and $\frac{k}{D}$. At high R_E and K-C, f_s tends to its value for steady flow. Also, C_L is essentially independent of R_E for $\frac{k}{D}>0.002$ [14]. This study and a further literature review [43] suggest that the inability of

Morison's equation to model vortex shedding effects limits its applicability in the range of Keulegan-Carpenter number between ~6 and ~25, where both drag and inertia forces are of importance and vortices are generated. This range is, in fact, where Sarpkaya [15] found the highest scatter in C_D and C_M and where Keulegan and Carpenter [16] observed a region of "drastic change" in the hydrodynamic coefficients. Up to this point we have only commented on vortex shedding effects for a stationary cylinder. In reality, the cylinder will either displace normal to the flow direction or will experience externally prescribed motions which, to some degree, are independent of the flow acting on it. The analysis is more difficult since the coefficient C_L is also a non-linear function of the displacement amplitude and, at certain conditions, the shedding frequency locks into the resonant frequency of vibration. In general, transverse cylinder vibration will increase the spanwise correlation of the wake, and thus the vortex strength, which has the effect of increasing C_L [9].

In addition to these constraints, there are problems associated with the use of Eq. 2-3 in the presence of currents. Some of the uncertainties are:

- The presence of a current in the wave field can alter the direction of propagation of the waves and has the effect of concentrating or dispersing the wave energy.
- The current can substantially modify the wake and eddy formation from the members, thus

influencing the hydrodynamic coefficients. This tends to become complicated when the current runs across the axis of the wave propagation.

- A further step toward the real situation is achieved with the use of a random sea description, which considers the sea state to be comprised of a number of different regular waves propagating independently of each other. The problem here is the definition of the Keulegan-Carpenter number for a set of waves. Some authors claim it is not possible to define K-C under these circumstances [8]. Others employ a weighted average approximation for K-C [11].
- An equally uncertain situation is the determination of stripwise varying hydrodynamic coefficients on a long vertical cylinder immersed in a surface wave induced flow. As we shall see later, the fluid particles path is actually elliptical for a two-dimensional description of the flow and the velocity potential varies with depth. Thus the one-dimensional and uniform flow conditions in the experiments on which C_D and C_M are based may be quite different than the real conditions.
- Finally, the use of Eq. 2-10 implies the knowledge of the hydrodynamic coefficients. It should be recognized that this is the "penalty paid" in using a simple equation (2-10) for a highly complex problem. The oversimplifications introduced in the derivation of 2-10 have resulted in an excessive amount of "ignorance" being compensated for by the hydrodynamic coefficients.

2.6 UNCERTAINTIES ASSOCIATED WITH THE APPLICATION OF THE RELATIVE VELOCITY INTERACTIVE FORM OF MORISON'S EQUATION

An extension to Morison formula which takes into account structural motion through a relative velocity approach was introduced (Sect. 2.4). We list it again here for convenience,

$$f = \frac{1}{2}\rho C_D D(\dot{v}-\dot{u})|\dot{v}-\dot{u}| + \frac{1}{4}\rho\pi D^2 C_M \dot{v} + \frac{1}{4}\rho\pi D^2 (C_M-1)\ddot{u}$$

Malhotra and Penzien proposed this form in 1969 [12]. And it is, at present, extensively used for dynamic analysis of offshore structures. They were concerned with flexible structures, in particular the case where the magnitudes of structural and fluid velocity and acceleration are comparable. They recognized that structural motion effects are important and structural response parameters should be included in the loading function. However, no theoretical or experimental support was provided for their modification to the drag force. To date, the only work directed at confirming the validity of Eq. 2-10 is Moe and Verley's 1977 study [1]. Their experimental results for a harmonically oscillating cylinder in steady flow suggest the inapplicability of Eq. 2-7 for certain flow conditions.

At this point, it is of interest to study qualitatively the different behavioral modes generated when an external oscillatory flow is directed at an oscillating circular cylinder. This will provide some insight as to when the relative velocity interactive mechanism is likely to apply. We start by introducing an alternate interpretation

to the Keulegan-Carpenter number.

Consider a cylindrical body immersed in still water, similar to that shown in Figure 2.2a. We suddenly impose a finite velocity to the cylinder and follow it as it moves steadily upstream so as to observe the same situation as steady uniform current past a cylinder at rest (it can be shown that the two situations are entirely equivalent). Provided that $\frac{vD}{\nu}$ is sufficiently large, a wake will have started forming at time t=0 and will be tending toward its "steady" form as it appears to the observed moving with the cylinder. The term steady is intended for the statistical properties of the particle motion within the wake. The parameter of interest is the time required for the "steady" wake development. An appropriate measure is the vortex shedding period, T_s, since it defines the time needed for a vortex to form and it is thus proportional to the time taken for a wake to develop fully. The shedding period is given by:

$$T_s = \frac{1}{f_s} = \frac{1}{S}\left(\frac{D}{v}\right) \tag{2-11}$$

We consider next the case where a harmonic flow $v=v_o \sin\frac{2\pi t}{T}$ oscillates past a fixed circular cylinder. Here, we can still say that the wake development time is proportional to Ts, and for simplicity to D/v_o (R_E=constant), i.e.,

$$T_s \alpha \frac{D}{v_o} \tag{2-12}$$

However, the presence of flow reversals can inhibit the formation of the wake. A measure of the time available for a wake to develop is the period of fluid velocity oscillation T. The Keulegan-Carpenter number is defined as:

$$K\text{-}C = \frac{T}{(D/v_o)} = \frac{v_o T}{D}$$

Then, one can interpret K-C as the ratio,

$$K\text{-}C \;\alpha\; \frac{\text{Time available for a wake to form}}{\text{Time needed for a wake to form}}$$

If we now prescribe in-line oscillatory motion to the cylinder $u=u_o \sin\frac{2\pi t}{T_o}$ in addition to the external harmonic flow, there will be a total of 5 parameters describing the flow, namely $Re=\frac{v_o D}{\nu}$, $K\text{-}C=\frac{v_o T}{D}$, $\frac{k}{D}$ and,

$$v_r = \frac{v_o T_o}{D} \tag{2-13}$$

$$\hat{u} = \frac{u_o}{D} \tag{2-14}$$

where v_r is called the reduced velocity and $\hat{u}$ is a dimensionless amplitude measure. One interprets the reduced velocity in a similar way as the Keulegan-Carpenter number. Here the available time is the period of vibration for the cylinder.

All five parameters are required to describe the problem. A qualitative description of the behavior over the full range of all parameters is complicated and to some extent speculative since experimental support is available only for the case of a stationary cylinder in oscillatory flow [15] and for an oscillating cylinder in steady current [1]. In terms of the non-dimensional parameters, the former case is equivalent to $v_r = \hat{u} = 0$ whereas the later deals with K-C $\to \infty$ and $\frac{k}{D} \to 0$. Although the two experiments were aimed at different problems and are totally different with respect to objectives, conditions, and experimental arrangement, they are useful for establishing an understanding of the behavior at these limiting conditions.

Pursuing this behavioral assessment further, we consider the case where K-C, v_r and $\hat{u}$ are varied, assuming some typical orders of magnitude, say $R_E \sim 10^5 - 10^6$ (turbulent) and $\frac{k}{D} \sim .01$ (rough cylinders) for the other parameters. We start with the situation where K-C and v_r are both very high, and $\hat{u}$ has an extremely high value. This may occur for a compliant tower or a tension leg platform. Here two characteristic time points can be identified. The first point is when the outer oscillatory flow is about to reverse. All the surrounding water is essentially still except in the vicinity of the cylinder where a wake may be starting to form or has already formed earlier, depending on the direction of the cylinder motion prior to reversal of the flow. In either case a wake is expected to develop eventually, and it will experience a slow change in form due the small acceleration achieved by the cylinder. The second point is when the external flow is at its

peak. A fully formed turbulent wake has already reached an essentially steady configuration. The effect of the cylinder's motion is to supply or remove kinetic energy from the wake, depending again on the sense of the relative motion between the water particles and the cylinder. Based on the quasi-steadiness of the flow, one can argue that the drag force will result from the superposition of two dependent flow fields: one due to a "steady" flow past the cylinder at rest and the other due to the motion of the cylinder through otherwise still water. If this were the true situation, the in-line force per unit length would be given by $f=\frac{1}{2}\rho DC_D(v-\dot{u})^2$. However, since both the cylinder and the external flow oscillate, the sense has to be accounted for. One replaces $(v-\dot{u})^2$ with $(v-\dot{u})|v-\dot{u}|$ and introduces an inertia term to represent the acceleration effect. It is important to recognize that the relative velocity form of the drag term is based on the existence of a well defined wake and a quasi-steady flow.

We consider next the effect of $\hat{u}$. Suppose $\hat{u}$ is very small and K-C and v_r are very high. At time instants where the external flow reverses, the cylinder is capable of initiating a vortex as it moves if its amplitude of vibration is large enough. However, $\frac{u_o}{D}$ is very small and separation will hardly occur (backflow is unlikely to occur on an oscillating circular cylinder which reverses its motion after reaching a distance smaller than about D/6 irrespectively of the accelerations achieved [17]). In this situation Eq. 2-7 predicts a drag coefficient based essentially on the maximum external flow velocity which is only appropriate for the external velocities associated with peaking con-

ditions. Hence for small $\hat{u}$ and high K-C and v_r, the use of a constant average value of C_D seems somewhat unrealistic.

Finally, we consider the case where either K-C or v_r is very small and $\hat{u}$ has a moderate value, say of about .4~.7. The case of high K-C and small v_r corresponds to a rapidly vibrating cylinder with a significant amplitude in a slowly oscillating external flow. When the external flow is about to reverse, the cylinder is oscillating in essentially calm water, and the vibrations are so rapid that any vortex initiation is virtually eliminated by the cylinder. In this case, the drag force is roughly zero and the forcing mechanism is inertia. A high speed stream acts on the cylinder at peak external flow but, due to the high rate of vibration, the water particles cannot follow either motion and a wildly disorganized and unsteady flow pattern exists near the cylinder. Here, a relative velocity hypothesis is highly suspect. To assume that a cylinder vibrating at such high frequencies will directly exchange energy with the external flow is equally questionable. The same level of uncertainty exists for the case of low K-C and high v_r, i.e., when the external flow oscillates at high frequency and the cylinder vibrates at low frequency. Figure 2.6 summarizes the qualitative discussion of the range of applicability of the relative velocity expression, 2-7. In the next section, we present the equation proposed by Moe and Verley [1] as more appropriate for the zone where the relative velocity model is not valid. Their study was restricted to steady external flow, which corresponds to K-C $\to\infty$ in Figure 2.6.

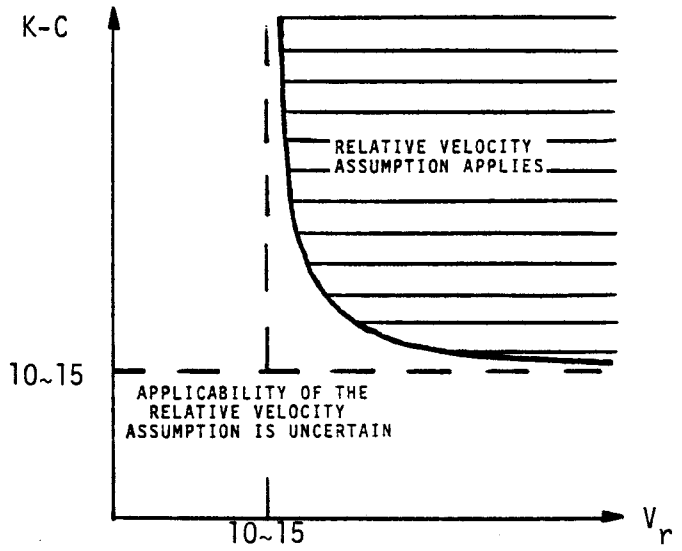

Fig. 2.6 Range of Uncertainty for the Applicability of the Relative Velocity Assumption

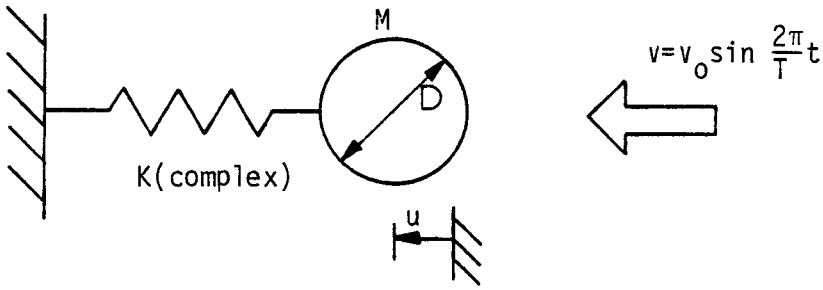

Fig. 2.7 Hypothetical Single Degree of Freedom Structure

2.7 INDEPENDENT FLOW FIELDS INTERACTIVE FORM OF MORISON'S EQUATION

In view of the uncertainties associated with the application of the relative velocity interactive form of Morison formula, a different form of the drag forcing term was proposed for the case of an oscillating cylinder in steady current at low v_r by Moe and Verley in 1978 [1]. Their formulation is based on the superposition of two independent flow fields, a far field unaffected by the cylinder motion and a near field due to the cylinder motion. No theoretical support is provided, only some qualitative indications deduced from an experimental study conducted by Pedley [18] on oscillating boundary layers in a free stream without flow reversal. However, they do present experimental results which show that the relative velocity approach is not appropriate for small values of v_r in a steady current. As a replacement they suggest:

$$f_D = \frac{1}{2}\rho C_{DS} D v^2 - \frac{1}{2}\rho C_{DU} \dot{u}|\dot{u}| \quad . \tag{2-15}$$

where v is the steady velocity; and C_{DS} is the steady drag coefficient for a smooth cylinder, and C_{DU} is the oscillatory drag coefficient for a smooth cylinder vibrating in still water. The range of applicability of Eq. 2-15, indicated by their experimental results, is v_r<10~15.

Their formulation, intended originally for external steady currents, is extended in this study to oscillatory external flow $v=v_o \sin\frac{2\pi t}{T}$. Eq. 2-15 is transformed to

$$f_D = \frac{1}{2}\rho D C_{DV} v|v| - \frac{1}{2}\rho C_{DU} \dot{u}|\dot{u}| \tag{2-16}$$

where C_{DV} is the oscillatory drag coefficient on a stationary cylinder. The total force per unit length consists of the drag term, 2-16, and an inertia term which is derived below.

When the cylinder is fixed with respect to the fluid, the inertia component is determined with Morison's original formula (Eq. 2-2)

$$f_{IV} = \frac{1}{4}\rho\pi D^2 C_{MV} \dot{v} \tag{2-17}$$

f_{IV} accounts for both the in-line buoyancy and the added mass effect. Cmv depends on $R_E = v_o D/\nu$ and $K\text{-}C = v_o T/D$. If the fluid is at rest, the force due to the cylinder's acceleration, $\ddot{u}$, is

$$f_{IU} = -\frac{1}{4}\rho\pi D^2 (C_{MU}-1)\ddot{u} \tag{2-18}$$

f_{IU} contains the added mass effect of the displaced fluid; C_{MU} is evaluated for the same conditions as C_{DU}. Superposing the two flow fields yields:

$$f_I = \frac{1}{4}\rho\pi D^2 C_{MV} \dot{v} - \frac{1}{4}\rho\pi D^2 (C_{MU}-1)\ddot{u} \tag{2-19}$$

Finally, the total force has the form:

$$f = \frac{1}{2}\rho D[C_{DV} v|v| - C_{DU} \dot{u}|\dot{u}|] + \frac{1}{4}\rho\pi D^2[C_{MV}\dot{v} - (C_{MU}-1)\ddot{u}] \qquad (2\text{-}20)$$

where the hydrodynamic coefficients are proposed as:

$$(C_{DV}, C_{MV}) \text{ functions of } \left(\frac{v_o D}{\nu}, \frac{v_o T}{D}, \frac{k}{D}\right)$$

$$(C_{DU}, C_{MU}) \text{ functions of } \left(\frac{\dot{u}_o D}{\nu}, \frac{\dot{u}_o T_o}{D}, \frac{k}{D}\right) \qquad (2\text{-}21)$$

2.8 HYDRODYNAMIC DAMPING AND ADDED MASS IMPLIED BY THE ALTERNATE APPROACHES

In the different cases considered so far, we have prescribed two sets of input, namely the descriptors for the external flow and the parameters characterizing the cylinder motion. The real case is that where an external flow acts on a given structure which then reacts in accordance with a dynamic equation of motion. Consider, for example, the hypothetical structure shown in Figure 2.7. The governing equation of motion is the familiar relationship:

$$M\ddot{u} + Ku = f(t)\ell \qquad (2\text{-}22)$$

where M and K are the structural mass and complex stiffness, ℓ is the cylinder length and f(t) is a forcing function such as Eq. 2-10 or 2-20. If a relative velocity formulation is used for f(t) in 2-22, the resulting form is:

$$M\ddot{u} + Ku = \frac{1}{2}\rho DC_D(v-\dot{u})|v-\dot{u}|\ell + \frac{1}{4}\rho\pi D^2 C_M\dot{v}\,\ell - \frac{1}{4}\rho\pi D^2(C_M-1)\ddot{u}\,\ell \qquad (2\text{-}23)$$

For the sake of illustration, let us assume $|\dot{u}| << |v|$ as an average condition. Actually, this assumption is valid for most fixed offshore structures. Then the drag term can be expressed as [9]:

$$(v-\dot{u})|v-\dot{u}| \simeq v|v| - \dot{u}|v| \qquad (2\text{-}24)$$

Substituting 2-24 into 2-23 and rearranging we obtain:

$$[M + M_a^R]\ddot{u} + C_H^R\dot{u} + KU = \frac{1}{2}\rho DC_D v|v|\ell + \frac{1}{4}\rho\pi D^2 C_M\dot{v}\,\ell \qquad (2\text{-}25)$$

where M_a^R is called the added mass and C_H^R represents the hydrodynamic drag damping,

$$M_a^R = \frac{1}{4}\rho\pi D^2(C_M-1)\ell \qquad (2\text{-}26)$$

$$C_H^R = \frac{1}{2}\rho DC_D|v|\ell \qquad (2\text{-}27)$$

The superscript R is included to indicate their connection with the relative velocity assumption.

If Eq. 2-20 is used for f(t), we obtain a different set of expressions for the hydrodynamic damping, C_M^I, and the added mass, M_a^I,

$$M_a^I = \frac{1}{4}\rho\pi D^2(C_{MU}-1)\ell \qquad (2\text{-}28)$$

$$C_H^I = \frac{1}{2}\rho D C_{DU} |\dot{u}| \ell \qquad (2\text{-}29)$$

Even if there is a significant difference in the added mass terms, its effect is unlikely to be important for large values of M, a typical condition of submerged members of offshore jackets, and relatively close ranges of C_M and C_{MU}. However, a comparison of the damping components shows that 2-27 generates higher hydrodynamic damping for typical values of $|\dot{u}| << |v|$ and comparable magnitudes of C_D and C_{DU}. Hence the use of Eq. 2-10 will result in a lower response than predicted by 2-20. This difference becomes more critical near resonance if the internal structural damping is very small.

CHAPTER 3

SYSTEM MODELING

3.1 STRUCTURAL MODEL

In order to predict the motion, one needs to define a physical model for the structural system. In this section, we discuss the basic structural system and the essential features of wave-structure interaction. A simplified model representing the structure is developed in 3.1.1. Sections 3.1.2 and 3.1.3 treat the mathematical aspects of the structural response model.

3.1.1 SELECTION OF STRUCTURE

A fixed steel offshore structure is a space frame comprised of tubular steel members which are welded together at the nodes. A common characteristic of these structures is that they are supported on piles driven through either the main legs or sleeves surrounding the legs. The deck rests on the top of the tower and houses the production hardware and other facilities. Deck weight varies widely depending on the particular case. For example, the Hondo platform (Gulf of Mexico) has a deck of about 1600 tons weight [19] while the Ninian (North Sea) platform's deck weight is approximately 26,000 tons [20]. At this time, the tallest offshore structure is the Cognac Platform, installed in the Gulf of Mexico in 1025 feet of water and having a total height of 1265 feet [21].

A deep water platform is designed to resist a broad range of loads acting from the construction stage throughout the life of the

structure. Only the hydrodynamic load acting on the submerged portion of the structure is considered in this study as this usually provides the main source of dynamic excitation. Its dominant period ranges from about 17 seconds in severe storm conditions to about 7.4 seconds at very low wave heights. The natural periods of vibration of a deep water platform may be as high as 4.5 seconds(Cognac Platform). Two limiting behavioral modes can be identified. For a high sea state, the energy is concentrated in the high wave period zone and drag forces tend to dominate for the members in the upper submerged zone of the structure. The structural response is quasi-static since the fundamental structural period is significantly lower than the dominant wave period. At the other extreme, i.e., when the wave height is relatively low, the energy distribution is more uniform, the dominant period shifts to the shorter range and approaches the natural period of the structure. Inertia loads are dominant for most structural members and the system oscillates essentially at its natural frequency. For moderate sea states, both quasi-static and resonant response are expected [22]. Although these basic structural response features have been observed and simulated [23,24],the sensitivity of the structural response over the full range of sea state to the two different forcing functions described in the previous chapter has not been investigated. Our objective is to carry out a detailed comparison of the two hypotheses. We could consider a complete structure but interpreting the results, particularly the role of the alternate forcing formulations, would be very difficult. Therefore we restrict our attention to a single vertical element having a diameter comparable to a typical component of the structure. This allows us to

simulate the local element-fluid interaction and at the same time adjust the natural frequency so that it is representative of deep water structures.

3.1.2 PRELIMINARY ASSUMPTIONS

Before initiating the mathematical formulation of the structural response model, we introduce some assumptions which provide the simplifications needed for a formulation that is directed to the non-linear fluid-structure interaction rather than to the general structural behavior problem. They are as follows:

- The slenderness ratio L/D of the cylindrical element is sufficiently large so that it can be analyzed as a beam rather than as a shell structure. Also the shear deformation can be neglected since it is small compared with the bending deformation at the frequencies of interest.
- The cylinder material behavior is linear elastic.
- Geometric non-linearities are negligible. This uncouples axial and transverse behavioral modes, i.e., the transverse force equilibrium equation does not involve the axial force.
- Rotatory inertia is neglected. This is consistent with neglecting transverse shear deformation.

3.1.3 EQUATIONS OF MOTION

Referring to Fig. 3.1 we establish the governing equations for the planar cylindrical element under the action of the distributed load w(y,t). The deformed configuration of the member is described by the coordinate U(y,t). With this notation, the equilibrium and geometrical compatibility equations take the following form,

$$\frac{\partial^2 U}{\partial y^2} = \frac{m}{EI} \tag{3-1}$$

$$w = \rho A \frac{\partial^2 U}{\partial t^2} + \frac{\partial^2 m}{\partial y^2} \tag{3-2}$$

where ρ is the material density, A is the cross-sectional area, and I is the moment of inertia. We consider the cross section and material parameters to be constant. Combining these expressions results in,

$$\rho A \frac{\partial^2 U}{\partial t^2} + EI \frac{\partial^4 U}{\partial y^4} = w \tag{3-3}$$

In addition to assuming small rotation and negligible transverse shear deformation, the material damping has been ignored.

The complete formulation consists of eq. 3-3 and six additional conditions, namely:

- Two essential boundary conditions
- Two natural boundary conditions
- Two initial conditions

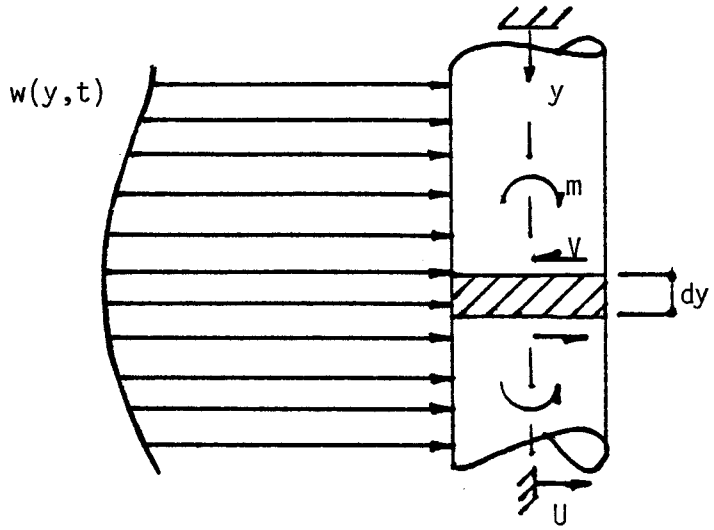

Fig. 3.1 Cylindrical Element Subjected to Hydrodynamic Load

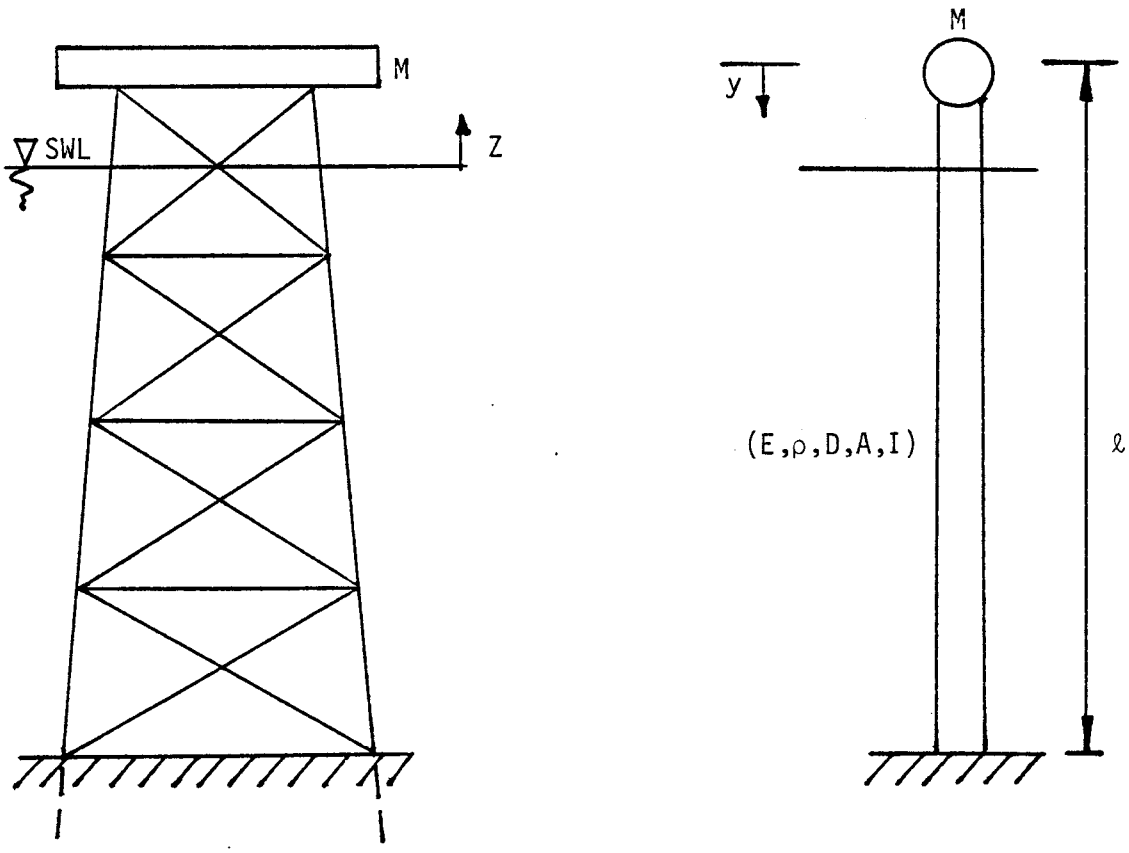

Fig. 3.2 Physical Model of the Structure

We are interested in the clamped-free case shown in Fig. 3.2 . The appropriate boundary conditions are:

$$U(L,t) = \frac{\partial U}{\partial y}(y,t)\Big|_{y=\ell} = 0 \qquad \frac{\partial^2 U}{\partial y^2}(y,t)\Big|_{y=0} = 0$$

$$\frac{\partial^3 U}{\partial y^3}(y,t)\Big|_{y=0} = -\frac{M}{EI}\frac{\partial^2 U}{\partial y^2}(y,t)\Big|_{y=0} \tag{3-4}$$

We could also consider the system to be initially at rest.

$$U(y,0) = \frac{\partial U}{\partial t}(y,t)\Big|_{t=0} = 0$$

This structure is used for response simulation studies. The parameters ℓ, A, I, and M have been chosen so as to approximate the natural frequency of vibration of a deep water structure whereas the member diameter D has been kept comparable with a typical local member diameter.

The solution of eq. 3-3 is our immediate objective. However, procedures for generating analytical solutions of partial differential equations of this type are practical only for relatively simple forcing functions w(y,t). Unfortunately, that is not the case here. Some effort was devoted to solving eq. 3-3 directly, but it was terminated for the following reasons:

- The forcing function w(y,t) cannot be expressed as a product of independent time and space functions when both drag and inertia terms are considered.

- The application of a modal superposition approach to eq. 3-3 leads to an integral term for the modal load participation factor which involves response-dependent terms and the use of an iterative scheme to calculate and update the dynamic response by integrating at each iteration loop is numerically inefficient.
- It is rather difficult to handle general boundary conditions.
- A considerable amount of effort must be invested in solving for U(y,t) in order to obtain other quantities of interest, say for example u(0,t).

In view of these difficulties an alternate solution strategy was adopted. Instead of evaluating the resulting form of the continuous variable U(y,t), a set of points are identified on the axis of the member and the state variable U(y,t) is calculated at each of these so-called nodal points. Interpolation is used to define the variation between nodal points. This procedure is commonly refered to as a finite element discretization. The reader is refered to [25] for a detailed treatment of the subject. We will only point out here the key issues considered in the generation of the system matrices. Fig. 3.3 shows an equivalent discrete beam consisting of a number of segments with lumped masses at the nodal points levels. The concentrated loads associated with each degree of freedom represent resultants of the stepwise distributions. The mass matrix is assumed to be a diagonal

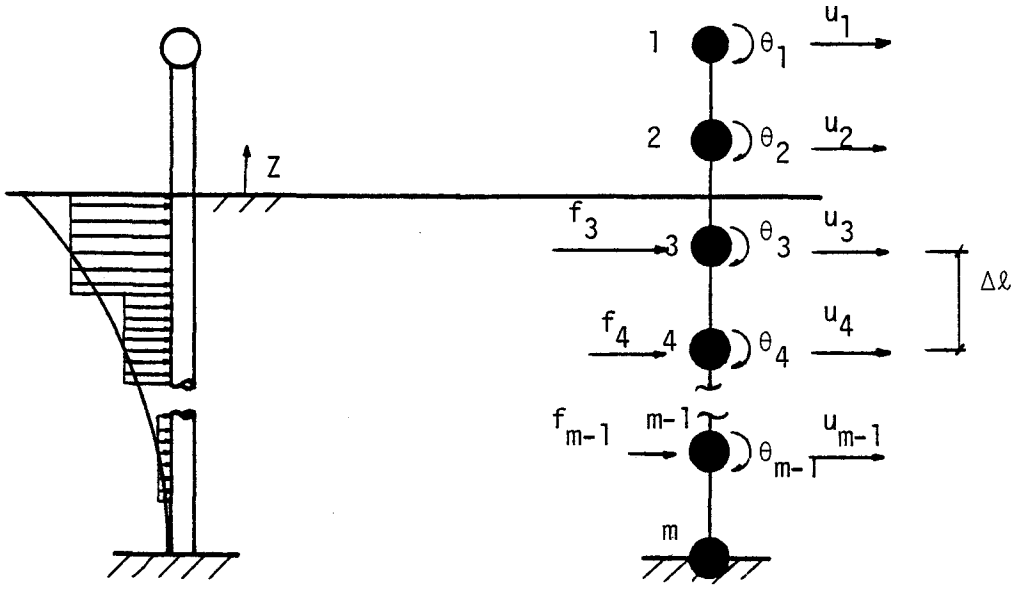

Fig. 3.3 Structural Response Model

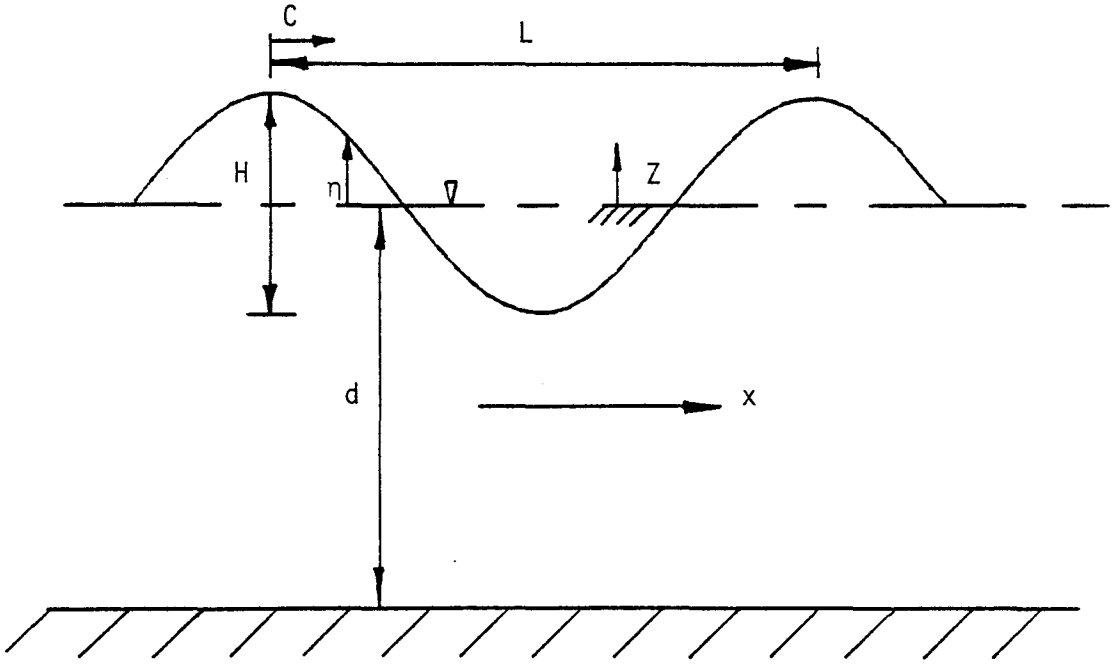

Fig. 3.4 Single Harmonic Wave

matrix with zeroes at the corresponding locations of the rotational degrees of freedom, and nonzero elements consisting of the contribution of the tributary translational masses associated with the node.

The equations of motion for the assembled system are expressed as:

$$\underline{M}\ddot{\underline{U}} + \underline{K}\underline{U} = \underline{f} \tag{3-5}$$

where

$$\underline{U} = \{u_1, \theta_1, u_2, \theta_2 \ldots\ldots u_m, \theta_m\}^T$$

$$\underline{f} = \{f_1, 0, f_2, 0 \ldots\ldots f_m, 0\}^T \tag{3-6}$$

The system stiffness matrix $\underline{K}$ is complex. Its real part is generated by assembling the m-1 beam element stiffness matrices, each of which comprises four degrees of freedom and is a square symmetric matrix of size 2*n. The imaginary part Im[$\underline{K}$] introduces a structural hysteretic damping term which is proportional to the displacement and acts in phase with the velocity. We express Im[$\underline{K}$] in terms of a hysteretic structural damping coefficient, D_s

$$\text{Im}[\underline{K}] = 2D_s\underline{K} \tag{3-7}$$

3.2 EVALUATION OF FORCE VECTOR

To completely define the problem, we need to relate the fluid flow properties with the wave surface height which is specified as input. In what follows, we first discuss briefly linear wave theory. Simulation of fluid kinematics for a random sea state is based on linear wave theory, and is described in section 3.2.2.

3.2.1 SINGLE HARMONIC WAVE AND LINEAR WAVE THEORY

Fig. 3.4 shows a single oscillatory wave characterized by its height H, length L, and period T propagating with a celerity C over a two-dimensional fluid domain of still water depth d. The fluid flow measures of interest are the velocity and acceleration. Linear wave theory is based on the following assumptions:

- Two dimensional, inviscid flow
- Small wave steepness, H/L
- Convective acceleration terms are negligible
- Boundary terms dependent on η are negligible.

We omit the solution details and just list the resulting expression for the velocity potential [6]

$$\phi = \frac{Hg}{2\omega} \frac{\cosh[k(1+z/d)]}{\cosh kd} \sin(kx-\omega t) \qquad (3\text{-}8)$$

where k is the wave number and ω is the circular frequency. They are related by the dispersion equation:

$$\omega^2 = kg \tanh kd \tag{3-9}$$

The horizontal fluid particle velocity and acceleration are given by [6]:

$$V_x = \frac{\partial \phi}{\partial x} = \frac{H}{2}\left(\frac{gT}{\ell}\right) \frac{\cosh[kd(1+z/d)]}{\cosh kd} \cos(kx-\omega t) \tag{3-10}$$

$$\dot{V}_x = \frac{\partial V_x}{\partial t} = \frac{H}{2}\left(\frac{2\pi g}{\ell}\right) \frac{\cosh[kd(1+z/d)]}{\cosh kd} \sin(kx-\omega t) \tag{3-11}$$

3.2.2 RANDOM SEA STATE REPRESENTATION AND KINEMATICS

The linearity assumption allows one to represent the flow beneath a randomly varying sea surface as the superposition of flows corresponding to a finite set of wave components assumed to comprise the irregular wave. This leads to a rather simple representation of a random sea state characterized by a wave amplitude spectral density function $G(\omega)$, which can be interpreted as a measure of the amplitude of the linear wave component having frequency ω. Randomness is incorporated in the description by allowing for random phase angles ϕ_n, uniformly distributed between 0 and 2π. The sea state descriptor used in this analysis is the two parameter one-sided Pierson-Moskowitz spectrum, (see Fig. 3.5):

$$G_\eta(\omega) = \frac{A}{\omega^5} \exp[-B/\omega^4]$$
$$A = 4\pi^3 H_s^2/T_z^4 \tag{3-12}$$
$$B = 16\pi^3/T_z^4$$

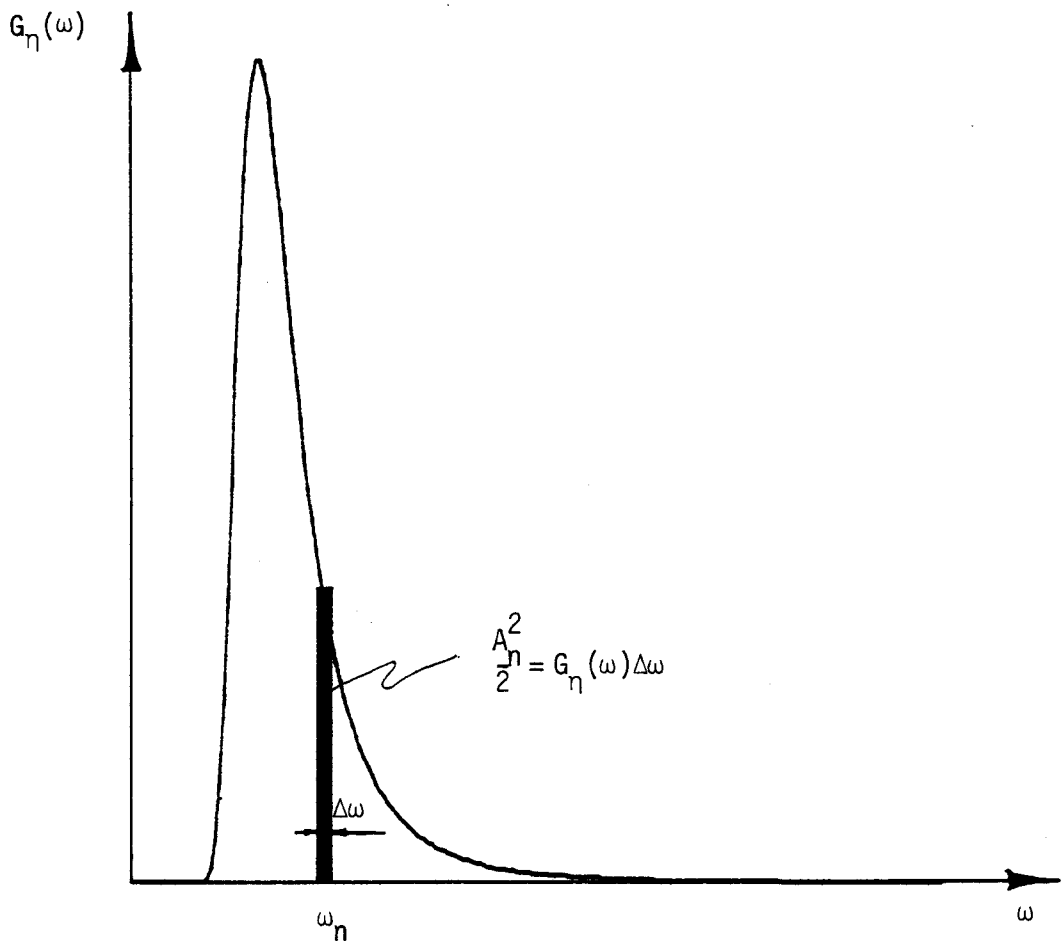

Fig. 3.5 Modified Pierson-Moskowitz Wave Height Spectrum

where H_s is the significant wave height and T_z is the average zero crossing period. Given the spectral density function for the wave surface elevation, one discretizes the frequency axis into M segments $\Delta\omega$ and represents the variation as a superposition of linear waves [38,39] as follows:

$$\eta(t) = \sum_{n=1}^{M} A_n \cos(k_n x - \omega_n t + \phi_n) \tag{3-13}$$

The parameter A_n defines the amplitude for the n'th wave component,

$$A_n = \sqrt{2G_n(\omega_n)\Delta\omega} \tag{3-14}$$

Applying linear wave theory, horizontal fluid particle velocity and acceleration are determined with,

$$V = \sum_{n=1}^{M} \omega_n A_n G_n \cos(-\omega_n t + k_n x + \phi_n) \tag{3-15}$$

$$\dot{V} = \sum_{n=1}^{M} \omega_n^2 A_n G_n \sin(-\omega_n t + k_n x + \phi_n) \tag{3-16}$$

where G_n defines the vertical distribution of fluid velocity and acceleration,

$$G_n = \frac{\cosh[k_n(z+d)]}{\sinh k_n d} \tag{3-17}$$

and k_n and ω_n are related through the dispersion relation, Eq. 3-9.

The expression for the force vector simplifies when matrix notation is introduced. We define

$$\underset{\sim}{(V-\dot{U})|V-\dot{U}|} = \{(V_1-\dot{U}_1)|V_1-\dot{U}_1|, 0, \ldots\ldots, (V_n-\dot{U}_n)|V_n-\dot{U}_n|, 0\}^T \qquad (3\text{-}18)$$

$$\underset{\sim}{V|V|} = \{V_1|V_1|, 0, \ldots\ldots\ldots\ldots, V_n|V_n|, 0\}^T \qquad (3\text{-}19)$$

$$\underset{\sim}{\dot{U}|\dot{U}|} = \{\dot{U}_1|\dot{U}_1|, 0, \ldots\ldots\ldots\ldots, \dot{U}_n|\dot{U}_n|, 0\}^T \qquad (3\text{-}20)$$

Then, the vector forms of the relative and independent flow fields formulations are:

$$\underline{f}^R = \tfrac{1}{2}\rho D\Delta\ell\ \underline{C}_D\ \underset{\sim}{(V-\dot{U})|V-\dot{U}|} - \tfrac{1}{4}\rho\pi D^2\Delta\ell[\underline{C}_M-\hat{\underline{I}}]\ \ddot{\underline{U}} + \tfrac{1}{4}\rho\pi D^2\Delta\ell\ \underline{C}_M\ \dot{\underline{V}} \qquad (3\text{-}21)$$

$$\underline{f}^I = \tfrac{1}{2}\rho D\Delta\ell[\underline{C}_{DV}\ \underset{\sim}{V|V|} - \underline{C}_{DU}\ \underset{\sim}{\dot{U}|\dot{U}|}] - \tfrac{1}{4}\rho\pi D^2\Delta\ell[\underline{C}_{MU}-\hat{\underline{I}}]\ddot{\underline{U}} + \tfrac{1}{4}\rho\pi D^2\Delta\ell\ \underline{C}_{M_V}\ \dot{\underline{V}} \qquad (3\text{-}22)$$

where the hydrodynamic coefficient matrices are diagonal, and have the form:

$$\underline{C}_M = \begin{bmatrix} C_{M1} & & & & & \\ & 0 & & & & \\ & & C_{M2} & & & \\ & & & 0 & & \\ & & & & \ddots & \\ & & & & & C_{Mm} \\ & & & & & & \underline{0} \end{bmatrix} \tag{3-23}$$

Also, we have introduced the matrix $\hat{\underline{I}}$

$$\hat{\underline{I}} = \begin{bmatrix} 1 & & & & & \\ & 0 & & & & \\ & & 1 & & & \\ & & & 0 & & \\ & & & & \ddots & \\ & & & & & 1 \\ & & & & & & \underline{0} \end{bmatrix} \tag{3-24}$$

to simplify the notation for the added mass matrices,

$$\underline{M}_a^R = \tfrac{1}{4}\rho\pi D^2 \Delta\ell [\underline{C}_M - \hat{\underline{I}}] \tag{3-25}$$

$$\underline{M}_a^I = \tfrac{1}{4}\rho\pi D^2 \Delta\ell [\underline{C}_{MU} - \hat{\underline{I}}] \tag{3-26}$$

Incorporating the real and added mass terms leads to the "final" form of the system of equations,

$$[\underline{M} + \underline{M}_a]\underline{\ddot{U}} + \underline{KU} = \underline{\overset{*}{f}} \tag{3-27}$$

where $\underline{\overset{*}{f}}$ denotes either 3-22 or 3-23 with the added mass terms deleted.

CHAPTER 4

SOLUTION OF EQUATIONS OF MOTION

The last two chapters have discussed the development of the mathematical model that is employed to predict the response of a simplified offshore jacket. Since the model is non-linear, its solution is not straightforward. This chapter addresses the solution phase. Sections 4.1 and 4.2 provide some background on the numerical procedures which are applicable to this general problem, and section 4.3 presents a detailed description of the solution strategy followed here.

4.1 INTRODUCTORY COMMENTS

The nature of forcing processes associated with natural phenomena such as waves is random and thus a specific determination of the resulting spatial and temporal load distribution is not possible. One has to specify the loading in terms of the statistical properties of the process. Loadings defined this way are called stochastic or non-deterministic. Similarly, solution methods that operate on stochastic input are refered to as non-deterministic methods.

Solution methods are grouped in two basic categories: time domain and frequency domain. Time domain techniques are deterministic by nature. Frequency domain methods are often viewed as non-deterministic since they are usually associated with spectral techniques which relate the response spectra to the forcing spectra via a transfer function. However, with a frequency domain method, one can also transform a deterministically generated loading to the frequency domain and solve the equations expressed

in terms of Fourier frequency components. This procedure is refered to here as the "deterministic frequency domain" method.

An additional classification according to the treatment of the non-linear drag term is also introduced. As we shall see in the following sections, they fall into three categories: linear, higher order and non-linear. The first two solution techniques approximate the drag force with equivalent polynomial expansions, and the other method works with the full non-linear form.

4.2 NON-DETERMINISTIC FREQUENCY DOMAIN METHODS

4.2.1 LINEAR ITERATIVE METHODS

The solution strategy is based on linearizing the drag term in either forcing function 3.22 or 3.23. A linearization technique was first applied to Eq. 3.22 (relative velocity drag force) by Malhotra and Penzien [12] and Foster [27], and is outlined below:

One expresses $(v-\dot{u})|v-\dot{u}|$ as:

$$(v-\dot{u})|v-\dot{u}| = \alpha(v-\dot{u}) \tag{4-1}$$

and obtains the value of α by minimizing the error,

$$\varepsilon = (v-\dot{u})|v-\dot{u}| - \alpha(v-\dot{u}) \tag{4-2}$$

in a mean square sense. Setting $E\left[\frac{\partial(\varepsilon)^2}{\partial\alpha}\right] = 0$ results in the following expression,

$$\alpha = \frac{E[(v-\dot{u})^2|v-\dot{u}|]}{E[(v-\dot{u})^2]} \tag{4-3}$$

The sea surface fluctuation over a short period of time, in the order of one hour, can be considered to be as a zero mean stationary Gaussian process. When linear wave theory is applicable, the water particles velocity and acceleration will also be zero mean Gaussian processes. Further, if the response is assumed zero mean, normally distributed, it can be shown that,

$$\alpha = \sqrt{\frac{8}{\pi}}\ \sigma_{\dot{r}} \tag{4-4}$$

where $\sigma^2_{\dot{r}}$ is the mean square value of $\dot{r} = v - \dot{u}$. Substituting for 4-1 and 4-4 results in:

$$[M + M_a]\ \underline{\ddot{U}}_G + \tfrac{1}{2}\rho D\Delta\ell\ \underline{C_D}\sigma_{\dot{r}}\ \underline{\dot{U}}_G + \underline{K}\ \underline{U}_G = \tfrac{1}{2}\rho D\ \underline{C_D}\sigma_{\dot{r}}\ \underline{V}\Delta\ell + \tfrac{1}{4}\rho\pi D^2\ \underline{C_M}\ \underline{\dot{V}}\Delta\ell \tag{4-5}$$

where the subscript G indicates the connection with the Gaussian approximation. The solution, $\underline{U}_G$, is the best Gaussian approximation to the response $\underline{U}$ in the minimum mean square error sense, based on a first order approximation for the relative velocity drag term (Eq. 4-1).

We express $\underline{V}$ and $\underline{\dot{V}}$ in terms of the discretized wave spectral density function $G(\omega)$ using 3-15 and 3-16. After some algebra, the force expression reduces to:

$$f_j = \mathrm{Im}\left[\sum_{n=1}^{M} A_n\ F_{jn}\ \exp(j(-\omega_n t + \phi_n))\right] \tag{4-6}$$

where A_n and F_{jn} are known coefficients. Since the response model is linear, the solution can be expressed as a superposition corresponding to the $\underline{M}$ discrete frequencies.

$$\underline{U_{G_n}} = \text{Im}\left[\sum_{n=1}^{M} A_n \underline{U_{G_n}} \exp(j(-\omega_n t + \phi_n))\right] \tag{4-7}$$

Substituting in 4-5 leads to the set of equations for $\underline{U_{G_n}}$.

$$[\underline{K} - i\omega_n \underline{C_H} - \omega_n^2 (\underline{M} + \underline{M_a})]\underline{U_{G_n}} = \underline{F_n} \tag{4-8}$$

where $\underline{C_H}$ represents the equivalent hydrodynamic damping matrix. Iteration is required. Equation 4-8 has to be solved for the M discrete frequencies within an iteration loop. Also, the added mass and the hydrodynamic coefficients have to be updated after each iteration since they depend on the r.m.s value and average zero crossing period of the relative velocity.

4.2.2 HIGHER ORDER ITERATIVE METHODS

The linearization procedure outlined in the preceeding section can be extended to allow for higher order expansions. Various polynomial expansions for $v|v|$ were obtained by Borgman [28]. For example, the cubic approximation has the form:

$$v|v| \simeq \sqrt{\frac{2}{\pi}}\left[\sigma_v v + \frac{v^3}{3\sigma_v}\right] \tag{4-9}$$

When v is a zero mean Gaussian process. Comparison studies [29] have shown that 4-9 is a very good approximation.

Expansions of this type are handled by iterative non-deterministic methods. Dunwoody [30] considers the cubic expansion for the relative velocity term $(v-\dot{u})|v-\dot{u}|$ and applies the Gaussian closure technique [31] to evaluate higher statistical moments in terms of second moments. The key assumption which makes the approach feasible is the the excitation and response joint processes are Gaussian, zero mean. For example, the fourth moment involving the random variables a, b, c, and d, can be expressed as:

$$E[abcd] = E[ab]\,E[cd] + E[ac]\,E[bd] + E[ad]\,E[bc] \qquad (4\text{-}10)$$

With relations of this type, all fourth and sixth moments are decomposed and the resulting second moments are expressed as auto-and cross-correlation functions which are then Fourier transformed to auto- and cross-spectra. Combining appropriate terms and solving results in the least mean square error, cubic expansion based, Gaussian approximation to the response $\underline{U}$. Numerical implementation requires iteration on the response spectra.

Gudmestad and Connor [29] consider the case where there is a current superimposed on the wave field, and propose a method for calculating the response which does not require an evaluation of the force spectral density function. They employ a cubic polynomial expansion for $|v|v$. The presence of current introduces constant and second degree terms.

Their approach is based on employing the recurrence formula

$$\left[\sum_{n=n_o}^{M} v_n \cos(n\Delta\omega t+\alpha_n)\right]^k \simeq \sum_{n=n'_o} [v'_n \cos(n\Delta\omega t) + v''_n \sin(n\Delta\omega t)], \quad k=2,3 \tag{4-11}$$

to transfer the non-linear forcing term to a form similar to the linear relation, 4-6. They assume $v >> \dot{u}$ and approximate $|v-\dot{u}|(v-\dot{u})$ with $v|v| - |v|\dot{u}$ as suggested by Blevins [9]. This method does not assume the response to be Gaussian and therefore is a more "exact" procedure. Smith has shown that the probability density function for the drag force deviates considerably from the Gaussian form in the high force region [32]. Additional numerical studies are needed in order to evaluate the practicality of Gudmestad and Connor's method.

4.3 SOLUTION STRATEGY

4.3.1 A DETERMINISTIC NONLINEAR ITERATIVE FREQUENCY DOMAIN METHOD

A different approach based on a coupling of deterministic and non-linear, iterative, frequency domain methods is investigated in this study. The rational for this choice is as follows:

- Hydrodynamic damping is dependent on the sea state. A simple and inexpensive evaluation is difficult to obtain by directly integrating the equations in the time domain. Time domain methods, although capable of handling non-linearities, are not suitable for a practical assessment of the hydrodynamic damping. Also, an inherent problem with time domain schemes is the

isolation of starting transients.

- A simpler and cheaper answer to the hydrodynamic damping question could be obtained with a non-deterministic frequency domain method. Unfortunately, they cannot deal with the drag term in its full non-linear form, and work with modified forms which partially account for the non-linearities, but require certain approximations related to the response statistics. The response is generally assumed to be normally distributed. This only seems appropriate when the drag force is small compared to the inertia force. For the case of drag dominant load, Appendix A discusses the errors introduced in the force spectrum by the modifications in the drag term.

In summary, the objectives of this study cannot be achieved with either of these methods. It is necessary to work with the full non-linear forcing term and, at the same time, obtain a "simple" assessment of the hydrodynamic damping implied by the different forcing assumptions. A deterministic, iterative, frequency domain method described by Fish and Rainey [33] appears to be a likely candidate. In what follows we discuss in detail the application of this method to our problem.

Our starting point is Eq. 3-2 (the * on $\underline{f}$ has been dropped).

$$[\underline{M} + \underline{M}_a]\, \ddot{\underline{U}}(t) + \underline{K}\, \underline{U}(t) = \underline{f}(\dot{\underline{U}},t) \qquad (4\text{-}12)$$

Rather than operate on the present form of $\underline{f}(\dot{\underline{U}},t)$, we expand it in a second order Taylor series about an assumed function $\dot{\underline{U}}_o(t)$,

$$[\underline{M} + \underline{M}_a]\,\ddot{\underline{U}}(t) + \underline{K}\,\underline{U}(t) = \underline{f}(\dot{\underline{U}}_o,t) + \left.\frac{d\underline{f}}{d\dot{\underline{U}}}\right|_{(\dot{\underline{U}}_o,t)} (\dot{\underline{U}} - \dot{\underline{U}}_o) + \frac{1}{2}\left.\frac{d^2\underline{f}}{d\dot{\underline{U}}}\right|_{(\dot{\underline{U}}_o,t)} (\dot{\underline{U}} - \dot{\underline{U}}_o)^2 \qquad (4\text{-}13)$$

The solution of 4-13 is obtained by iterating on the right hand side. We determine the first estimate for $\underline{U}$ using only $\underline{f}(\dot{\underline{U}}_o,t)$, update the r.h.s., and solve again for $\underline{U}$. This generates a sequence $\underline{U}_1(t)$, $\underline{U}_2(t)$, $\underline{U}_3(t)$... which converges to the solution $\underline{U}(t)$.

In 4-13, the second order expansion for $\underline{f}(\dot{\underline{U}},t)$ differs from the scheme proposed in [33], where only a first order truncation is used. The presence of higher order derivatives is desirable since they accelerate convergence. However, as we shall see in section 4.3.2.4, it is not possible to incorporate third and higher order derivatives because of numerical difficulties. As a point of interest, the added mass term in (4-12) corresponds to the particular case where the dependence of $\underline{f}$ on $\ddot{\underline{U}}$ is linear (except for the inertia coefficient) and since it is constant, we include it in the l.h.s. of the equation. However, in a more accurate model both the inertia and drag loads for the members located in the splash zone depend on the instantaneous surface elevation. This effect can be treated with this solution scheme, but is not considered here. Extended formulations which also include slamming forces are presented in [34] and [35].

Returning to(4-13),the derivatives of r.h.s. corresponding to the relative velocity form of $\underline{f}(\dot{\underline{U}}_o,t)$ (Eq. 3-21 without the added mass) are:

$$\underline{f}_R(\dot{\underline{U}}_o,t) = \tfrac{1}{2}\rho D\ \underline{C}_D\Delta\ell(\underline{V}-\dot{\underline{U}})\,|\underline{V}-\dot{\underline{U}}| + \tfrac{1}{4}\rho\pi D^2\ \underline{C}_M\Delta\ell\dot{\underline{V}} \tag{4-14}$$

$$\frac{d\underline{f}_R}{d\dot{\underline{U}}}(\dot{\underline{U}}_o,t) = -\rho D\ \underline{C}_D\Delta\ell\,|\underline{V}-\dot{\underline{U}}_o|$$

$$\tfrac{1}{2}\frac{d^2\underline{f}_R}{d\dot{\underline{U}}^2}(\dot{\underline{U}}_o,t) = -\tfrac{1}{2}\rho D\ \underline{C}_D\Delta\ell\ \mathrm{sign}(\underline{V}-\dot{\underline{U}}_o) \tag{4-15}$$

Equation (4-13) expands to

$$\begin{aligned}[\underline{M} + \underline{M}_a^R]\ \ddot{\underline{U}}(t) + \underline{K}\ \underline{U}(t) &= \tfrac{1}{2}\rho D\ \underline{C}_D\Delta\ell(\underline{V}-\dot{\underline{U}}_o)\,|\underline{V}-\dot{\underline{U}}_o| \\ &+ \tfrac{1}{4}\rho\pi D^2\ \underline{C}_M\ \dot{\underline{V}}\Delta\ell - \rho D\ \underline{C}_D\Delta\ell|\underline{V}-\dot{\underline{U}}_o|(\dot{\underline{U}}-\dot{\underline{U}}_o) \\ &- \tfrac{1}{2}\rho D\ C_D\Delta\ell\ \mathrm{sign}(\underline{V}-\dot{\underline{U}}_o)(\dot{\underline{U}}-\dot{\underline{U}}_o)^2\end{aligned} \tag{4-16}$$

The form corresponding to the independent flow fields formulation of $\underline{f}(\dot{\underline{U}},t)$ is:

$$\begin{aligned}[\underline{M} + \underline{M}_a^I]\ \ddot{\underline{U}}(t) + \underline{K}\ \underline{U}(t) &= \tfrac{1}{2}\rho D\Delta\ell[C_{\underline{D}V}\ \underline{V}|\underline{V}| - C_{\underline{D}U}\ \dot{\underline{U}}_o|\dot{\underline{U}}_o|] \\ &+ \tfrac{1}{4}\rho\pi D^2\ C_{\underline{M}V}\ \dot{\underline{V}}\Delta\ell - \rho D\ C_{\underline{D}U}\Delta\ell|\dot{\underline{U}}_o|(\dot{\underline{U}}-\dot{\underline{U}}_o) \\ &- \tfrac{1}{2}\rho D\ C_{\underline{D}U}\Delta\ell\ \mathrm{sign}(\dot{\underline{U}}_o)(\dot{\underline{U}}-\dot{\underline{U}}_o)^2\end{aligned} \tag{4-17}$$

The solution strategy can be viewed as a variant of a Newton-Raphson iteration. When applying the standard Newton-Raphson method to a non-

linear equation, the solution is approached by iterating from point to point in time. For example, the solution sought here is the displacement time function. The modified version generates a sequence of frequency domain solutions $\underline{U}_1(\Omega)$, $\underline{U}_2(\Omega)$, etc. corresponding to iterated linearized forms of the equations.

The first "linear" form assumes $\dot{\underline{U}}(t)=\underline{0}$ in the r.h.s. of either Eq. 4-16 or 4-17 (depending on which formulation is being considered) and selects values for the hydrodynamic coefficients, these are fitted to Sarpkaya's data [15] through r.m.s. values of certain combinations of the assumed function $\dot{\underline{U}}_0(t)$ and the prescribed velocity function $\underline{V}(t)$. The hydrodynamic coefficients are updated within the iteration process, these are proposed as:

$$
\begin{aligned}
&(C_D, C_M)_i \quad \text{functions of } \left(\frac{\sigma_{\dot{r}} D}{\nu}, \frac{\sigma_{\dot{r}} T_{\dot{r}}}{D}, \frac{k}{D}\right)_i \\
&(C_{DV}, C_{MV})_i \quad \text{functions of } \left(\frac{\sigma_v D}{\nu}, \frac{\sigma_v T_z}{D}, \frac{k}{D}\right)_i \\
&(C_{DU}, C_{MU})_i \quad \text{functions of } \left(\frac{\sigma_{\dot{u}} D}{\nu}, \frac{\sigma_{\dot{u}} T_u}{D}, \frac{k}{D}\right)_i
\end{aligned}
\tag{4-18}
$$

where $T_{\dot{r}}$: Average zero crossing period of $(V-\dot{U})_i$

T_u : Average zero crossing period of $(\dot{U})_i$

"i": Refers to the node i

Successive equations are obtained by modifying the right hand side, and updating the added mass. An equation generated within the iterative procedure has the form:

$$\underline{M}\,\ddot{\underline{u}} + \underline{K}\,\underline{u} = \underline{p}(t) \tag{4-19}$$

Note that the hydrodynamic damping is included in $\underline{p}(t)$.

We can express the solution of 4-19 as a convolution of the impulse response matrix (complex) and the loading vector in the time domain,

$$\underline{u}(t) = \int_{-\infty}^{\infty} \underline{h}(t-\tau)\, p(\tau)\, d\tau \tag{4-20}$$

However, we prefer to work in the frequency domain. Introducing Fourier transforms for $\underline{h}$ and $\underline{p}$,

$$\underline{H}(\Omega) = \int_{-\infty}^{\infty} \underline{h}(t)\, \exp(-j\Omega t)\, dt \tag{4-21}$$

$$\underline{F}(\Omega) = \int_{-\infty}^{\infty} \underline{p}(t)\, \exp(-j\Omega t)\, dt \tag{4-22}$$

allows us to write the solution as

$$\underline{U}(\Omega) = \underline{H}(\Omega)\, \underline{F}(\Omega) \tag{4-23}$$

where

$$\underline{H}(\Omega) = [\underline{K} - \Omega^2\, \underline{M}]^{-1} \tag{4-24}$$

Since the loading is independent of the structural displacement, we need to evaluate only the velocity, which is obtained directly from the inverse transform,

$$\dot{\underline{u}}(t) = \frac{1}{2\pi} \int_{-\infty}^{\infty} j\Omega \underline{U}(\Omega) \exp(j\Omega t)\, d\Omega = \frac{j}{2\pi} \int_{-\infty}^{\infty} \underline{H}(\Omega)\, \underline{F}(\Omega) \exp(j\Omega t)\, d\Omega \qquad (4\text{-}25)$$

Starting with $\dot{\underline{U}}_0(t)$, we compute the first estimate of $\dot{\underline{U}}(t)$. The derivative terms are then updated, and a second estimate is evaluated. In subsequent iterations $\dot{\underline{U}}_0$ is also updated to accelerate convergence. For example, we replace $\dot{\underline{U}}_0$ with the first estimate when computing the third estimate. The basic features of the method are summarized below:

- Deterministic specifications of $\underline{V}(t)$ and $\dot{\underline{V}}(t)$ are generated with the wave surface height spectral density function as described in section 3.2.2.
- The full non-linear form of the drag term is used and no assumptions concerning the response statistics are introduced.
- The equations are solved in the frequency domain. An efficient Fast Fourier Transform algorithm is employed for the discrete spectral analysis of the force time history.
- The solution scheme differs somewhat from Fish and Rainey's approach. As previously mentioned, second derivatives are included to accelerate convergence. Also, the iteration algorithms are different. In the original method, $\underline{f}(\dot{\underline{U}}_0, t)$ is considered to be constant and only the terms associated with $\dot{\underline{U}}$ are corrected at each iteration. Here, all variables are continuously updated. This involves more work per iteration but the overall effort is reduced. Section 4.3.2.4 discusses these points in more detail.

4.3.2 NUMERICAL IMPLEMENTATION

This section is concerned with the numerical implementation aspects. We start by briefly reviewing some issues related to the application of the Discrete Fourier Transform algorithm (DFT). The accuracy that one obtains is dependent on how the DFT is applied, and an understanding of its limitations is essential.

4.3.2.1 APPLICATION OF THE DISCRETE FOURIER TRANSFORM

The numerical solution requires firstly, operating in discrete frequency and discrete time domains, and secondly, use of finite duration time histories for both load and response.

The discrete, finite version of equations 4-22, 4-24 and 4-25 are respectively [36]:

$$\underline{F}(k) = \sum_{r=0}^{N-1} \underline{p}(r) \exp(-j(2\pi k\, r/N)) \tag{4-26}$$

$$\underline{H}(k) = [\underline{K} - j(\frac{2\pi k}{T})^2 \underline{M}]^{-1} \tag{4-27}$$

$$\dot{\underline{u}}(r) = \frac{1}{N} \sum_{k=0}^{N-1} \underline{H}(k)\, \underline{F}(k)\, j(\frac{2\pi k}{T}) \exp(j(2\pi k\, r/N)) \tag{4-28}$$

where N represents the number of equally spaced time points; T is the signal length; $\underline{p}(r)$ is the value of $\underline{p}$ at $t=r\frac{T}{N}=r\Delta$. The discrete series $\underline{F}(k)$ is periodic, of period N. Also, the real part is symmetric, and the imaginary part is anti-symmetric about $k=\frac{N}{2}$, which corresponds to the Nyquist frequency $\Omega_0=\frac{\pi}{\Delta}$. Therefore, only the first half of the complex

series $\underline{F}(k)$ is required, since the rest of the information is redundant. The importance of the Nyquist frequency follows from the time domain sampling theorem, which states: if the Fourier transform $Q(\Omega)$ of a function $q(t)$ is zero for $\Omega_0 < |\Omega|$, the continuous function $q(t)$ is uniquely determined from a set of discrete values sampled at equal time intervals not exceeding $\frac{\pi}{\Omega_0}$. When the transform is not band-limited, as is the case of $\underline{F}(\Omega)$, the consequence of not sampling at an infinitely small rate produces overlapping extraneous wave forms centered at the Nyquist frequency. This distortion is known as aliasing.

In our problem, the frequency content of $\underline{p}(t)$ is related to the wave surface height spectral density function and thus aliasing can be minimized by a judicious choice of Δ. The peaks present in $(F(\Omega))$ at multiple odd frequencies of $\omega_p k$ (ω_p=peak frequency of the wave surface height spectrum) $3\omega_p$, $5\omega_p$, etc., are due to the non-linear, zero mean drag term and can be resolved up to, for example $9\omega_p$, where the energy content is negligible. This becomes obvious upon inspection of the high frequency tail of a Fourier spectrum of the load (see Fig. A.3). It should also be noted that when the structure is stiff, the sampling rate has to be sufficiently small so that the behavior in the neighborhood of the fundamental frequency can be resolved.

4.3.2.2 SAMPLING OF THE RESPONSE VELOCITY

We comment here on the problem encountered in sampling the response velocity signals. As an illustration, we consider the case of a single harmonic wave, and drag dominant hydrodynamic force. The drag

force $f(t)=f_o \sin \omega_o t|\sin \omega_o t|$, is plotted in Fig. 4.1a. Figure 4.1b shows the displacement response for a stiff single degree of freedom system. The response is essentially quasi-static since the system's natural frequency is significantly higher than the loading frequency. The problem arises when the structural velocity is derived from the displacement response. At the transition points (point A in Fig. 4.1b), the velocity decreases rapidly to zero and then increases again. The behavior is characterized by sharp peaks, i.e., cusps. Figure 4.1c illustrates the response velocity corresponding to a sampling period of T/160, where T is the wave period. When the wave is irregular, some of the cusps may be last if the sampling period is too large. This problem is encountered with response velocity records associated with high sea state cases, where the load is drag dominant (for certain diameters and depths) and the dominant loading frequencies are small in comparison to the structural natural frequency. The effect of the inertia load in the single harmonic wave case is to displace these peaks horizontally, as indicated in Fig. 4.2b.

4.3.2.3 THE CONVOLUTION INTEGRAL

The solution of the sequential differential equation 4-19 can be represented as the linear convolution of $\underline{h}(t)$ and $\underline{p}(t)$,

$$\underline{u}(t) = \underline{h}(t) * \underline{p}(t) = \int_{-\infty}^{\infty} \underline{h}(t-\tau)\, \underline{p}(\tau)\, d\tau \qquad (4\text{-}29)$$

When $\underline{p}(t)$ is time limited, the output $\underline{U}(t)$ has a duration equal

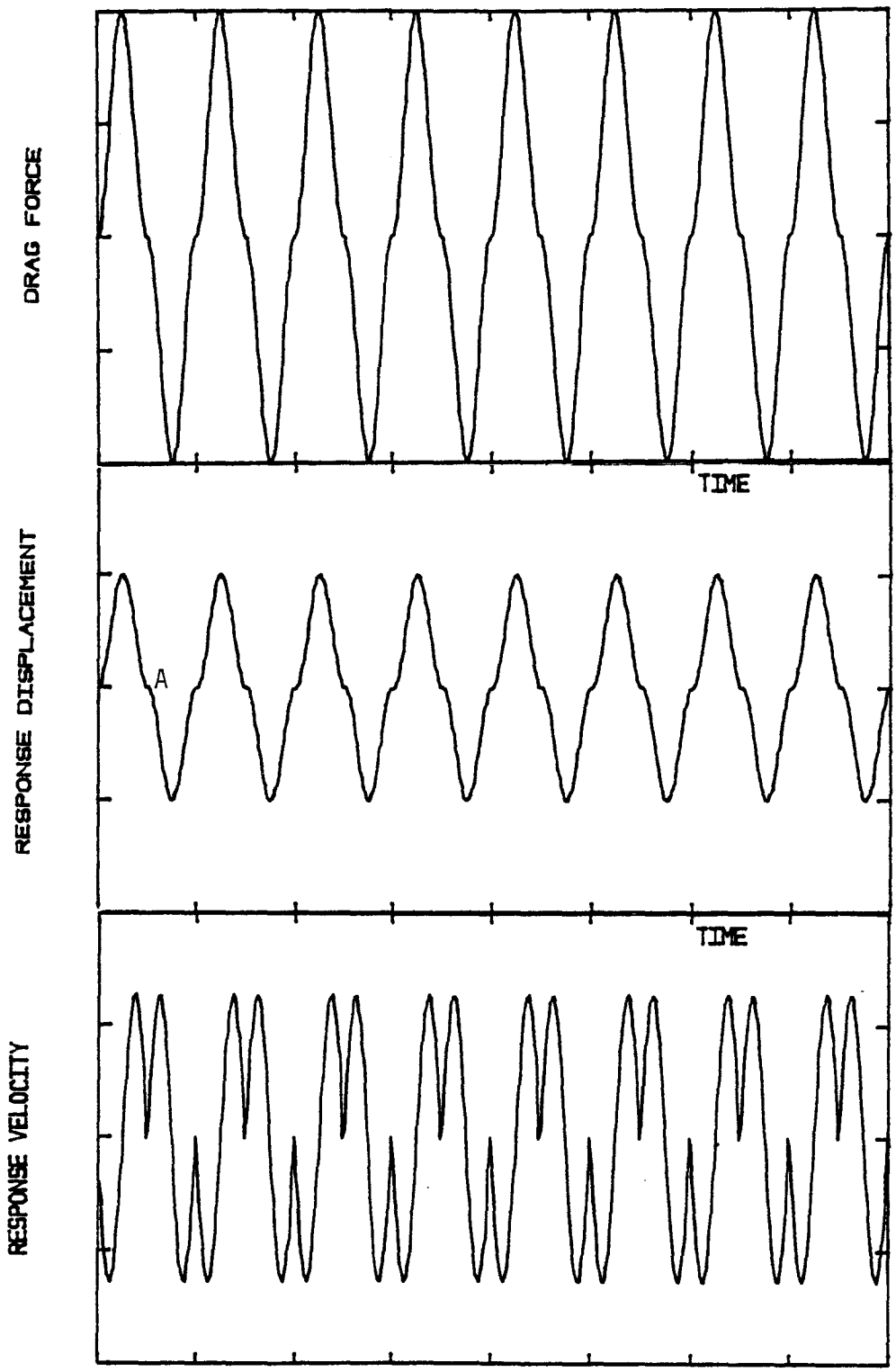

Figs. 4.1a, 4.1b and 4.1c Drag Load Associated with a Single Harmonic Wave, and Single d.o.f. Response

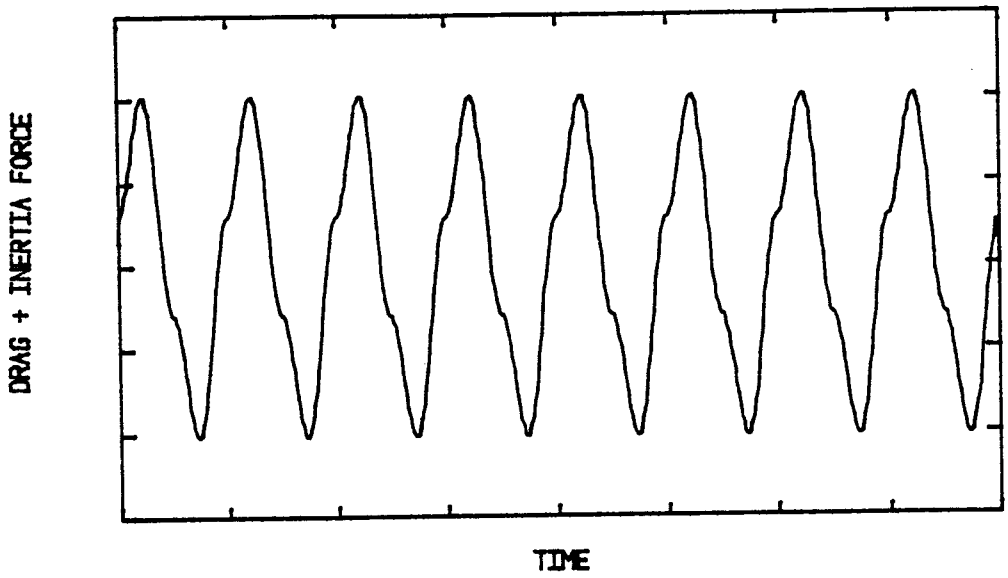

Fig. 4.2a Superposition of Drag and Inertia Forces

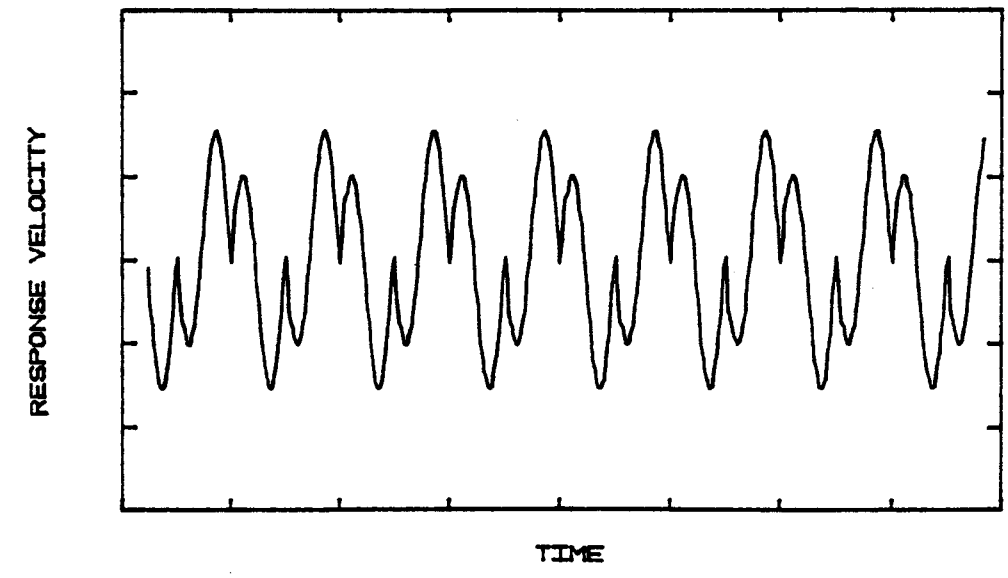

Fig. 4.2b Single d.o.f. System Velocity Response to Drag and Inertia Forces Associated with a Single Harmonic Wave

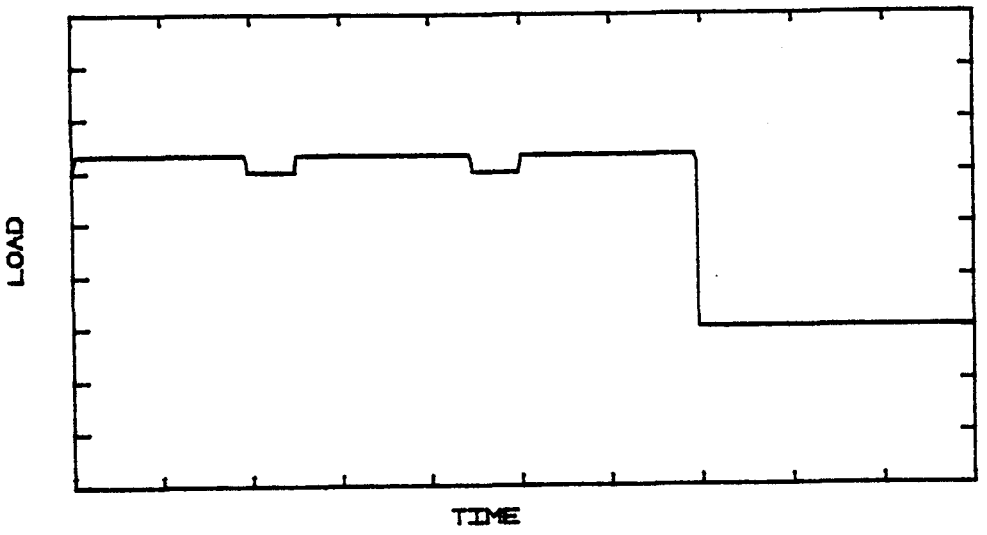

Fig. 4.3a Load Function

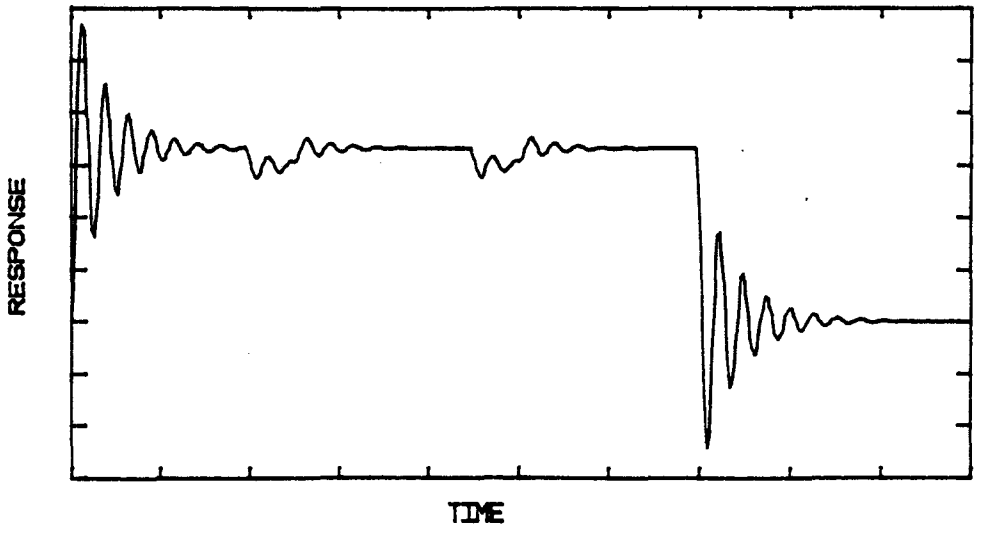

Fig. 4.3b Response Function Resulting From the Application of Linear Convolution

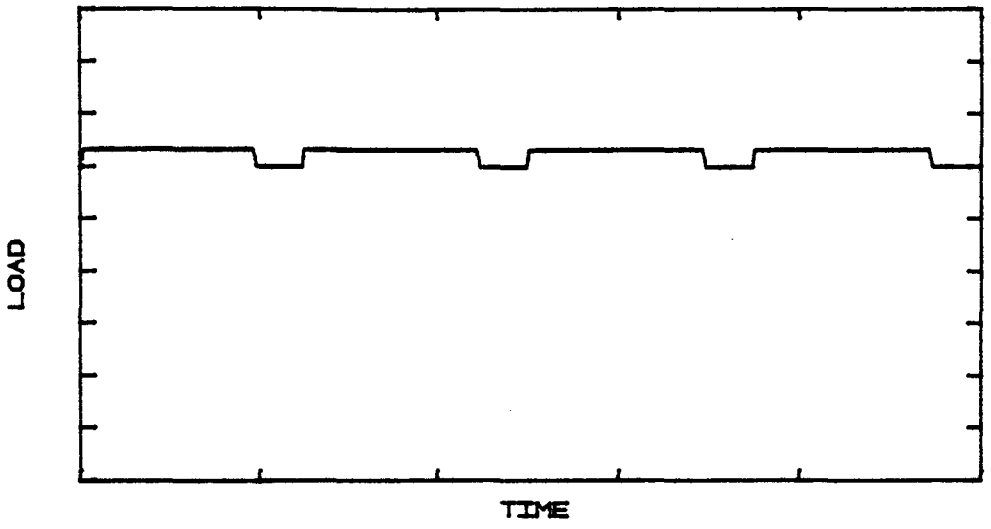

Fig. 4.4a Load Function

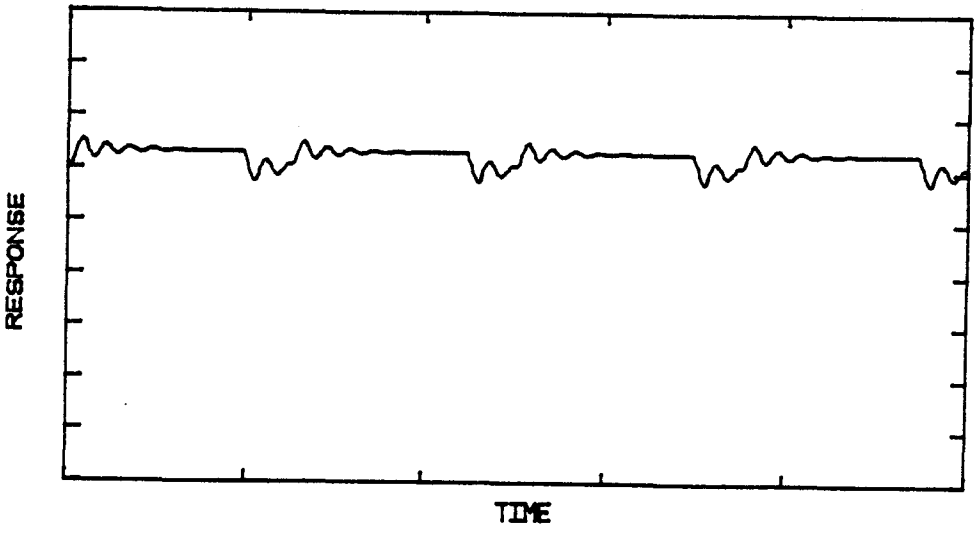

Fig. 4.4b Response Function Resulting from the Application of Circular Convolution

to the sum of the duration of $\underline{p}$ and the length of the system impulse function, $\underline{h}(t)$, which depends on the system damping. In addition, transients are present in the initial and end regions of the response.

Fig. 4.3 illustrates the convolution ofna set of pulses with a typical time-impulse response of an elastic, damped single degree of freedom system. Both the starting and ending transients are clearly identified. When the system is very ligthtly damped, starting transients may extend through a significant portion of the response signal. For a stationary periodic load, one can work with the actual load period. By using a frequency domain approach it is possible to derive the steady state solution without the presence of transients by applying circular rather than linear convolution [36]. Fig. 4.4 illustrates this procedure.

4.3.2.4 CONVERGENCE

In order to asses convergence, one needs to select a measure of the solution. Both discrete and integrated measures are used here. We compare the peak difference in two consecutive velocity time histories, and also the r.m.s values. The r.m.s measure is usually of interest in nondeterministic methods where the output information refers to spectral quantities. The peak difference in consecutive time histories is a "sharper" criteria and is useful for evaluating convergence of stress quantities. We use an r.m.s measure for the initial iterations since it is easy to evaluate and is also needed to update the hydrodynamic coefficients. When the solution is approaching convergence,we check on both r.m.s and peak differences. The two

criteria are:

$$\left| \frac{(\sigma_{\dot{U}_i})^2_{n+1} - (\sigma_{\dot{U}_i})^2_{n}}{(\sigma_{\dot{U}_i})^2_{n+1}} \right| < \varepsilon_{\sigma}, \quad i=1,2,3,\ldots N_o \tag{4-30}$$

$$\left| \frac{(\dot{U}_i(r))_{n+1} - (\dot{U}_i(r))_{n}}{(\dot{U}_i(r))_{n+1}} \right| < \varepsilon_{\dot{u}}, \quad i=1,2,3,\ldots N_o \tag{4-31}$$

where n+1 refers to the current iteration and N_o is the number of interactive degrees of freedom (translation of submerged nodes).

Convergence can be improved by including artificial damping in the dynamic response model. One has to add the same term on the right hand side so that the load is correct. For example, the equations for the relative velocity hypothesis are modified by adding $\underline{C}\,\dot{\underline{U}}$,

$$\begin{aligned}[\underline{M} + \underline{M}_a^R]\,\ddot{\underline{U}}(t) + \underline{C}\,\dot{\underline{U}}(t) + \underline{K}\,\underline{U}(t) = {} & \tfrac{1}{2}\rho D\,\underline{C}_D\Delta\ell(\underline{V}-\dot{\underline{U}}_o)|\underline{V}-\dot{\underline{U}}_o| \\ & + \tfrac{1}{4}\rho\pi D^2\,\underline{C}_M\Delta\ell\,\dot{\underline{V}}_o \\ & + \rho D\,\underline{C}_D\Delta\ell\,|\underline{V}-\dot{\underline{U}}_o|(\underline{U}(t) - \underline{\dot{U}}_o(t)) \\ & + \tfrac{1}{2}\rho D\Delta\ell\,\mathrm{sign}(\dot{\underline{V}}-\dot{\underline{U}}_o)(\dot{\underline{U}}-\dot{\underline{U}}_o)^2 + \underline{C}\,\dot{\underline{U}}\end{aligned} \tag{4-30}$$

The advantage of this modification is that it provides, in the first iteration an approximation for a hydrodynamic damping which would

otherwise be ignored. With an appropriate choice of $\underline{C}$, the first function $\underline{U}(t)$ is not excessively over or under-estimated. The selection of $\underline{C}$ may be the hydrodynamic damping resulting from a linear, Gaussian expansion of the drag force (section 4.2.1).

Convergence is also dependent on the form of the iteration algorithm. Our method considered only the first two derivatives of the drag force,

$$\frac{d\underline{f}_R}{d\dot{\underline{U}}} = -\rho D \, \underline{C}_D \Delta\ell \, |\underline{V}-\dot{\underline{U}}| \tag{4-31}$$

$$\frac{d^2\underline{f}_R}{d\dot{\underline{U}}^2} = -\rho D \, \underline{C}_D \Delta\ell \, \text{sign}(\underline{V}-\dot{\underline{U}}) \tag{4-32}$$

the third derivative is

$$\frac{d^3\underline{f}_R}{d\dot{\underline{U}}^3} = -\rho D \, \underline{C}_D \Delta\ell \, \delta(\underline{V}-\dot{\underline{U}}) \tag{4-33}$$

Numerical evaluation of the first two terms is straightforward. However, the third derivative is difficult to evaluate, and therefore has not been included in the expansion.

CHAPTER 5

PRESENTATION AND DISCUSSION OF RESULTS

The numerical simulations carried out in this investigation are directed at assessing the sensitivity of an offshore jacket structural response model to the alternate formulations for the hydrodynamic loading. We discuss first the effect of using a limited selection of random phase angles in the generation of time histories for fluid particle velocity and acceleration and then examine convergence of the iteration solution procedure and the hydrodynamic drag damping corresponding to the two force hypotheses.

5.1 SENSITIVITY OF THE FORCE FOURIER TRANSFORM TO DIFFERENT SPECIFICATIONS OF RANDOM PHASE ANGLES

The solution procedure requires time histories of the fluid particle velocity and acceleration. In order to evaluate these variables, a random number generator is used to generate phase angles, and the question arises as to how sensitive is the response to this "random" choice. Comparison studies were carried out for the rigid cylinder and sea state defined in table A-1. Two series of phase angle generations were investigated: 10 simulations (case A) and 20 simulations (Case B). The mean of the Force Fourier magnitude for the 20 different phase angle selections is plotted in Fig. 5.1. Cases A and B are indistinguishable.

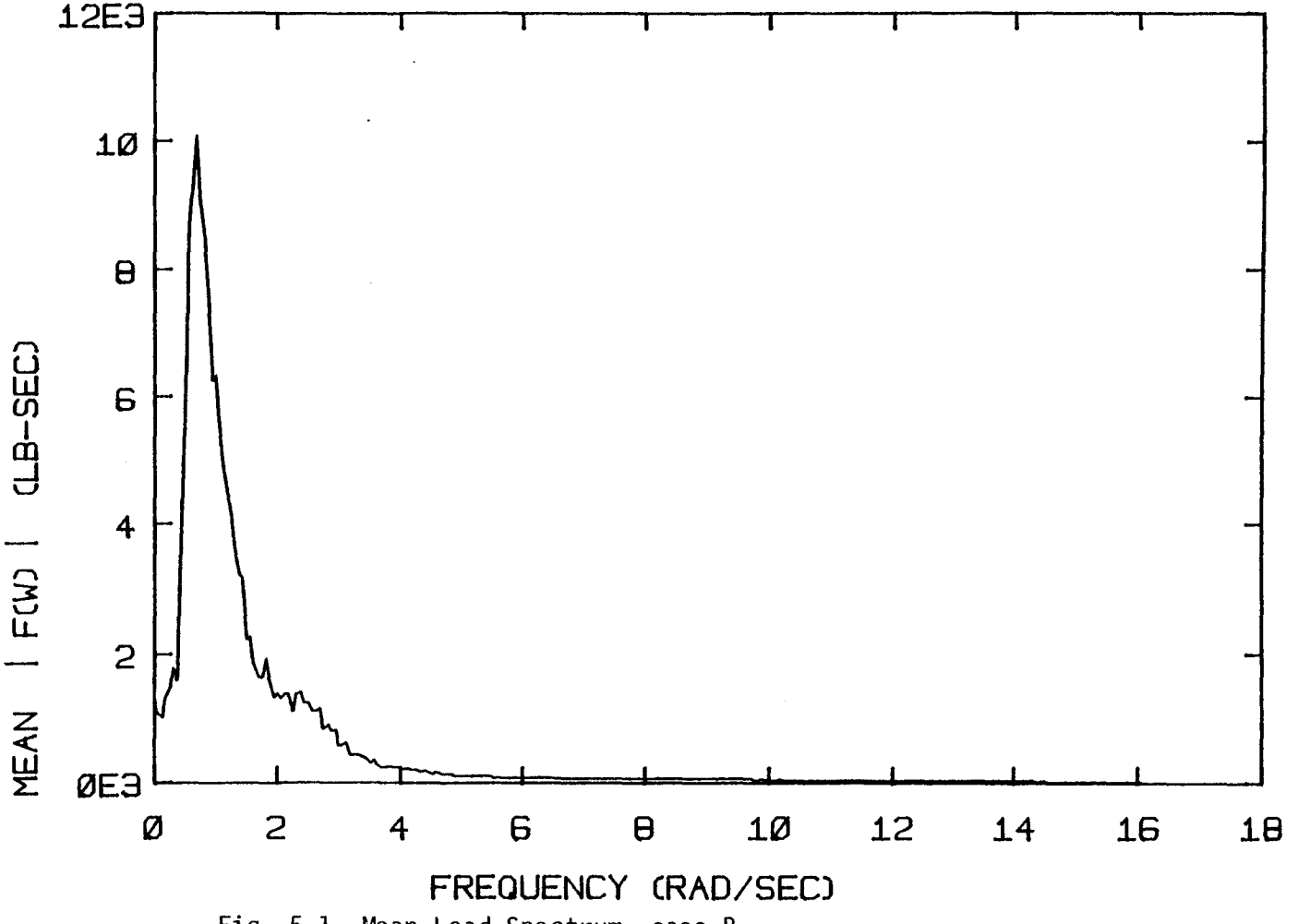

Fig. 5.1 Mean Load Spectrum, case B

for the scale employed in Fig. 5.1. The standard deviation of the Force Fourier magnitude for the various discrete frequencies is shown in Fig. 5.2. Peak values are about 17 % of the mean and they tend to be lower for case B, i.e., as the number of simulations is increased, the statistical variability decreases. The first and second moment statistics for both cases are summarized in table 5-1. The standard deviation of the phase angles across the ensemble provides a measure of their randomness. Results are plotted in Fig. 5.3; all random phase angles have been divided by 2π. The theoretical value of the standard deviation for the distributions is $\frac{1}{\sqrt{12}} \simeq 0.29$, and we observe that case B tends towards this value.

5.2 SENSITIVITY OF THE RESPONSE TO THE ALTERNATE HYDRODYNAMIC FORCE HYPOTHESES

The offshore jacket structure employed for the sensitivity study consists of a single cylinder clamped at the base. Fig. 5.4 defines the structural geometry and also shows the discrete structural model. The essential structural model parameters are listed in table 5-2. Five different sea state cases, which cover the spectrum from drag dominant through inertia dominant loading, are plotted in Fig. 5.5.

Time histories of fluid particle velocity and acceleration at the submerged nodes are generated for a duration of 100 s., with an interval of $\Delta = 0.390625$ s. There are 256 time points ($N=2^8$) and the corresponding Nyquist frequency is $\Omega_0 = \frac{\pi}{\Delta} = 8.04$ rad/sec. Since this is an upper bound on the frequency, the upper wave cut-off frequency has to be sufficiently below this value so that the higher harmonics resulting from the nonlinea-

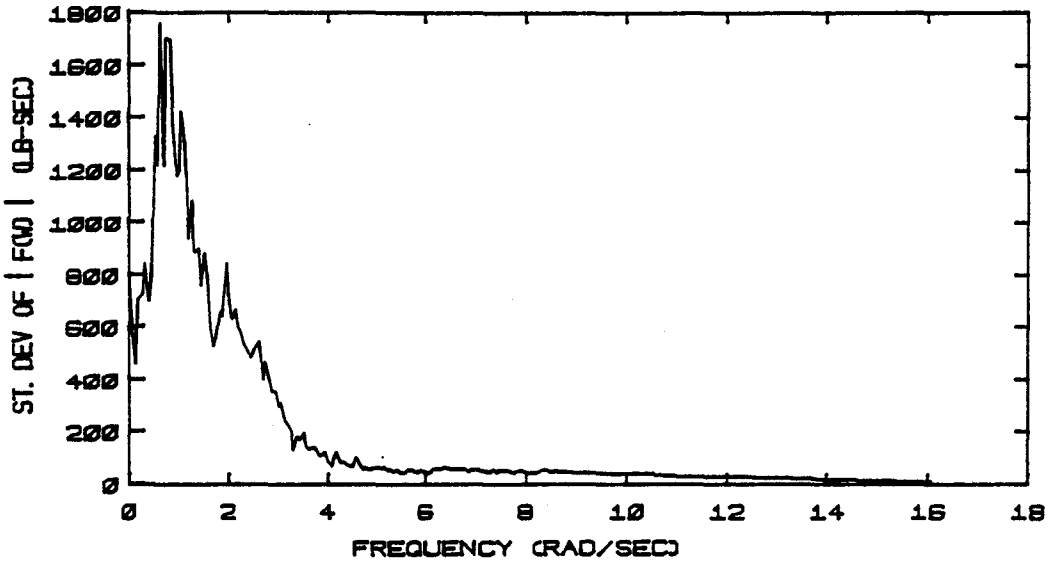

Fig. 5.2a Standard Deviation Spectrum, case A

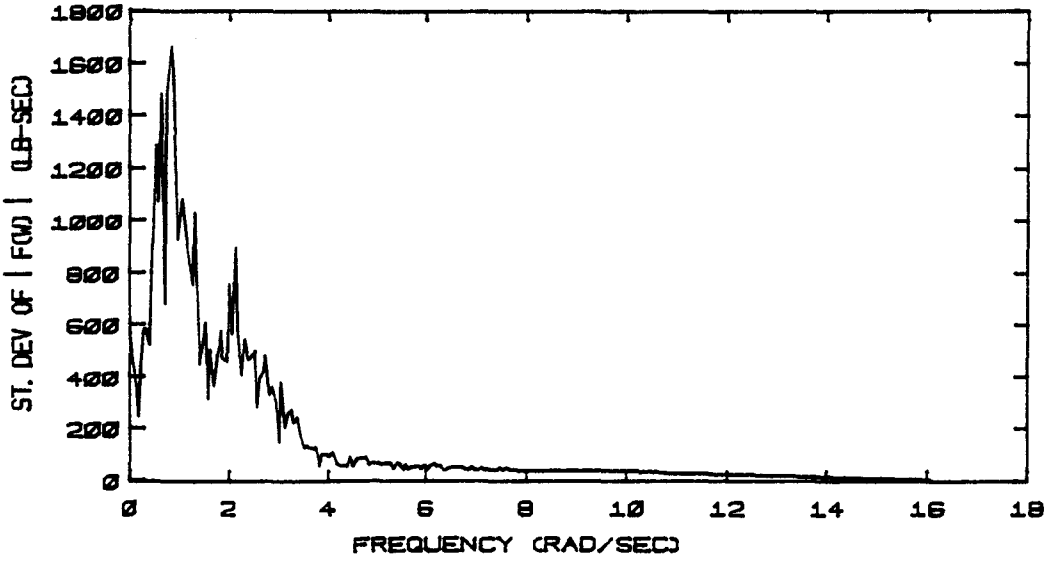

Fig. 5.2b Standard Deviation Spectrum, case B

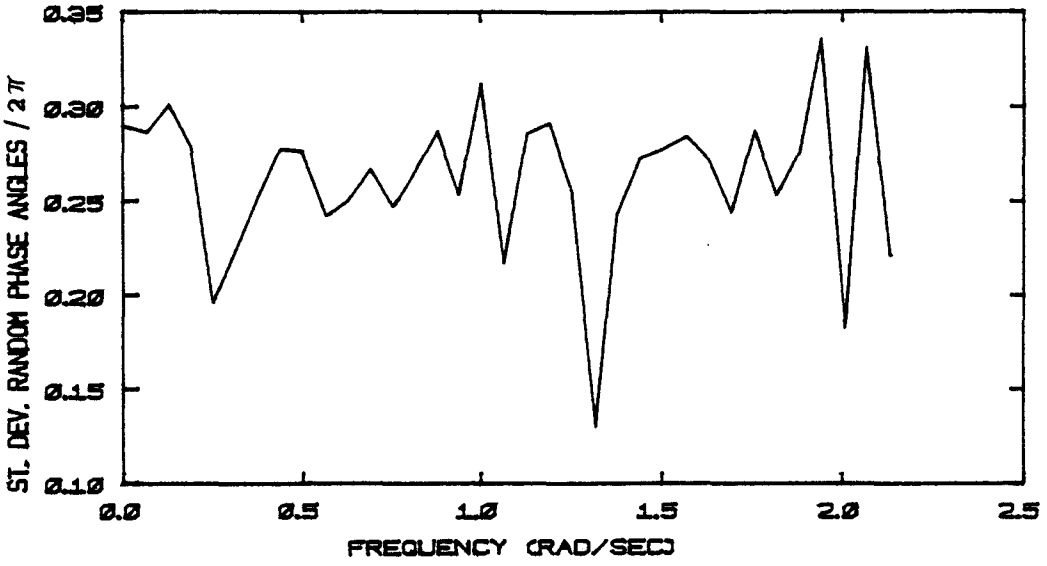

Fig. 5.3a Standard Deviation of Random Phase Angles, case A

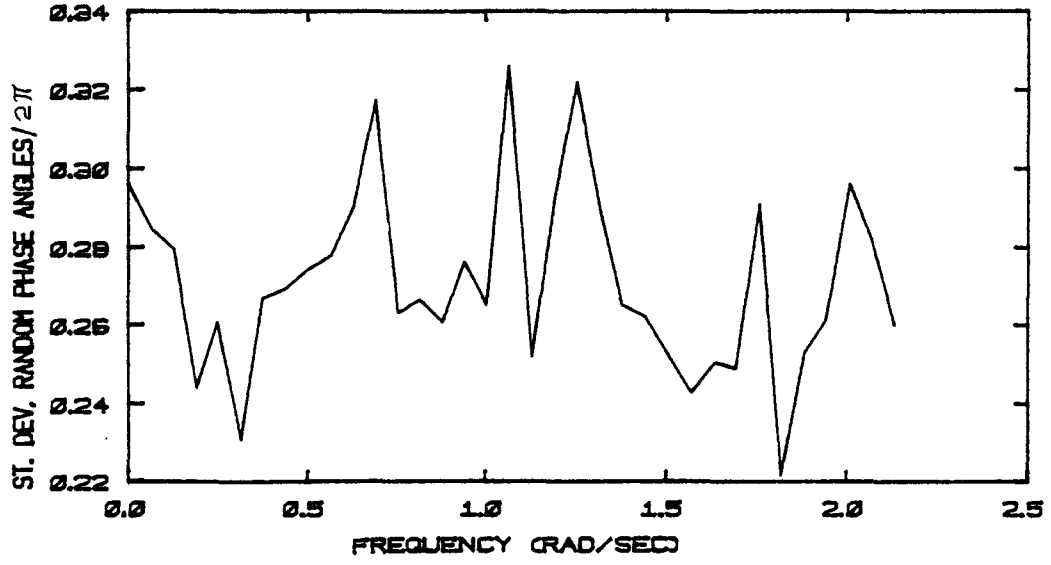

Fig. 5.3b Standard Deviation of Random Phase Angles, case B

TABLE 5-1

FIRST AND SECOND MOMENT STATISTICS

	CASE A		CASE B	
	Mean	St. Dev.	Mean	St. Dev.
First Spectral Moment (lb/sec)	5914.8	1130.6	5805.5	928.2
Second Spectral Moment (lb/sec^2)	6285.6	1201.5	6105.4	903.6

TABLE 5-2

STRUCTURAL MODEL PARAMETERS

Heigth:	70 feet
Diameter:	15 in.
Thickness:	0.5 in.
Number of Free Degrees of Freedom:	6(3 transl., 3 rot.)
Top Mass:	7000 lbs
Lower nodes Translational Masses:	1817 lbs
Foundation Condition:	Clamped
Natural Frequency:	~2.1 rad/sec
Hysteretical Damping Coeff.:	0.02

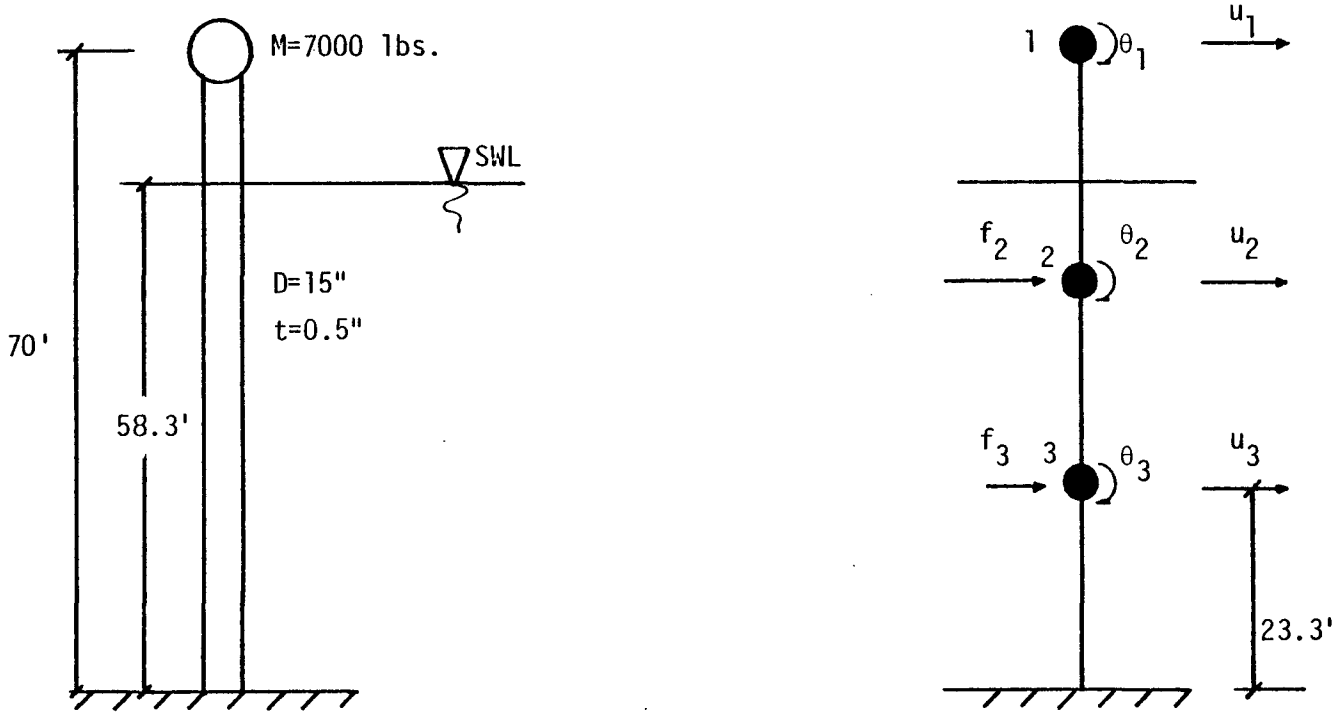

Fig. 5.4 Structural and Dynamic Response Model

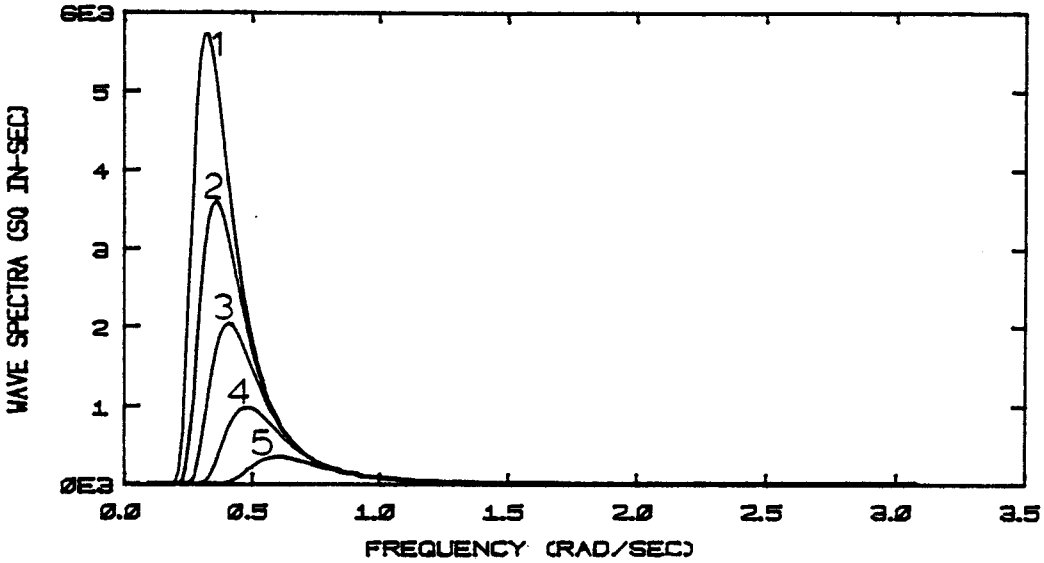

Fig. 5.5 Wave heigth Spectral Density Functions

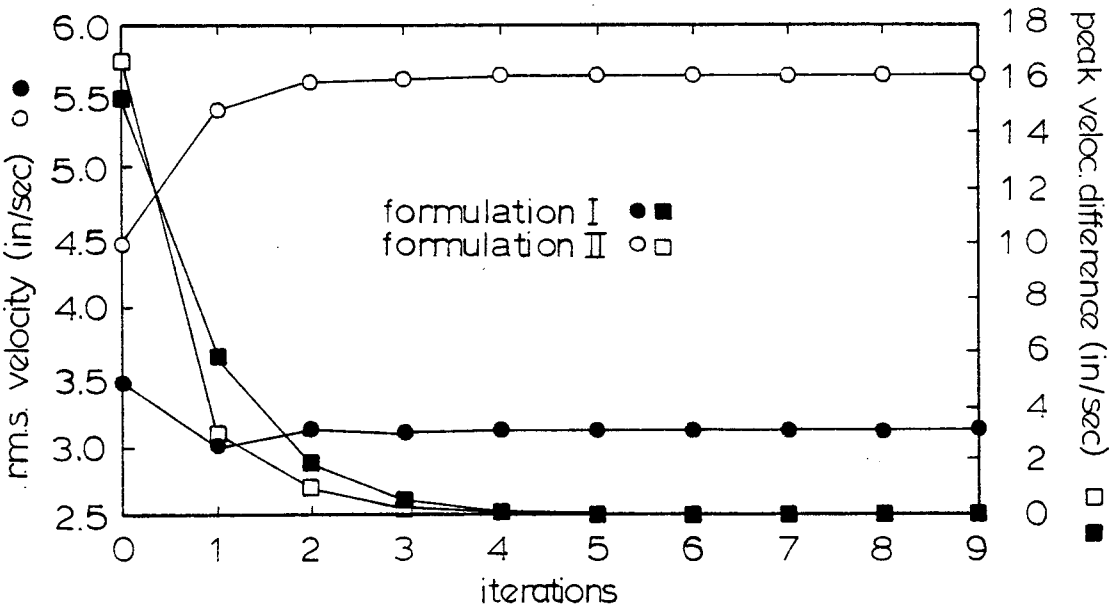

Fig. 5.6 Convergence History of Case 1

rity will fall within this limit. The time histories are treated as periodic functions, of period 100 s., and circular convolution is applied to generate the response. Circular convolution avoids the problem of transients which is encountered with linear convolution.

Artificial damping as a fraction of the linear hydrodynamic damping, $\underline{C} = \alpha[\frac{1}{2}\rho D \underline{C}_{DV} \frac{8}{\pi}\underline{\sigma}_V \Delta\ell]$, is included in the equations for all the cases studied. We assume $\alpha = 1$ for the relative velocity formulation (FORMULATION I). Since the hydrodynamic damping is less for the independent flow fields hypothesis (FORMULATION II), we use $\alpha = 0.3$ for this case. As discussed in Chapter 4, the hydrodynamic coefficients are based on Sarpkaya's data. Subroutine COEFF of POSEIDON, developed by S. Shyam Sunder, selects values for C_D and C_M corresponding to the values of Reynolds number, Keulegan-Carpenter number, and relative roughness. Iteration is required, but the process converges rapidly.

The first case ($H_S = 12'$, $T_Z = 6.912$ s.), a typical drag dominant situation, is described in detail to illustrate the procedure. Table 5-3 summarizes the results. Convergence of the structural r.m.s and peak velocity difference between succesive iterations for the upper submerged node (node 2) is shown in Fig. 5.6. From an engineering point of view, convergence of the relative velocity formulation is obtained after 3 cycles. This includes one cycle for the first estimate, one cycle for defining the first Taylor series expansion about $\dot{\underline{U}}_0$, and one cycle with the Taylor series forcing function. Fig. 5.6 shows that two iterations provided the response within a ~1 % r.m.s error from the converged response. Slightly faster convergence was obtained with formulation II

TABLE 5-3

SUMMARY OF RESULTS FOR CASE 1

SEA STATE PARAMETERS

Significant Wave Heigth	(H_S)	12	feet
Av. Zero Crossing Period	(T_Z)	6.91	sec
Lower Cut-off Frequency	(ω_1)	0.376991	rad/sec
Higher Cut-off Frequency	(ω_M)	2.513279	rad/sec
Frequency increment	$(\Delta\omega)$	0.062832	rad/sec

		node 2	node 3
R.M.S Fluid Velocity	(σ_v)(in/s.)	26.17	18.76
FORMULATION I RESULTS			
Number of Iterations	4		
Converged Struct. R.M.S Vel.	$(\sigma_{\dot{u}})$(in/s.)	3.10	0.92
Reynolds Number	$(\frac{\sigma_{\dot{r}}D}{\nu})x10^{-5}$	2.78	1.97
Keulegan-Carpenter Number	$(\frac{\sigma_{\dot{r}}T_{\dot{r}}}{D})$	13.68	11.44
Hydrodynamic Coefficients	C_M	1.22	1.34
	C_D	1.70	1.42
Reduced Velocity	$(\frac{\sigma_v T_{\dot{u}}}{D})$	6.7	4.8
FORMULATION II RESULTS			
Number of iterations	4		
Converged Struct. R.M.S Vel.	$(\sigma_{\dot{u}})$(in/s.)	5.62	1.6
Far Field Reynolds Number	$(\frac{\sigma_v D}{\nu})x10^{-5}$	2.73	1.95
Near Field Reynolds Number	$(\frac{\sigma_{\dot{u}}D}{\nu})x10^{-5}$	0.58	0.17
Far Field Keulegan-Carpenter No.	$(\frac{\sigma_v T_Z}{D})$	12.07	8.65
Near Field Keulegan-Carpenter No.	$(\frac{\sigma_{\dot{u}}T_u}{D})$	1.07	0.31
Hydrodynamic Coefficients	C_{MV}	1.31	1.5
	C_{MU}	1.94	1.98
	C_{DV}	1.5	1.07
	C_{DU}	0.12	0.03

since the rate of change of the load with respect to the structural velocity is lower. This is due to the lower values of C_{DU} compared to C_D, and lower r.m.s. structural velocity in comparison to r.m.s. relative velocities. Consequently, lower hydrodynamic damping and therefore higher response amplitudes are predicted with formulation II.

The top node displacement time histories and Fourier magnitudes for I and II are plotted in Figs. 5.7 and 5.8.

Fig. 5.9 compares the "converged" Force Fourier magnitude for node 2. The initial estimate, shown in Fig. 5.10a, is based on assuming a rigid structure, and therefore is the same for both formulations (the same set of random phase angles has been used). Fig. 5.10b displays the time history. The difference between the "starting" and "converged" force is due to the structural velocity term and its effect on the hydrodynamic damping. One possible approach for deriving an equivalent linear viscous damping measure would be to average in a r.m.s. sense the frequency dependent, complex, translation damping diagonal terms,

$$C_i = \frac{[F_0(\Omega) - F_N(\Omega)]}{j\Omega U_i(\Omega)} \qquad (5\text{-}1)$$

where i refers to the translational node number, $F_0(\Omega)$ and $F_N(\Omega)$ are the starting and converged force transforms and $U_i(\Omega)$ is the displacement transform. This procedure has not been carried out here. It represents a natural extension of this work.

Since structural damping is relatively low ($D_S = 0.02$), the

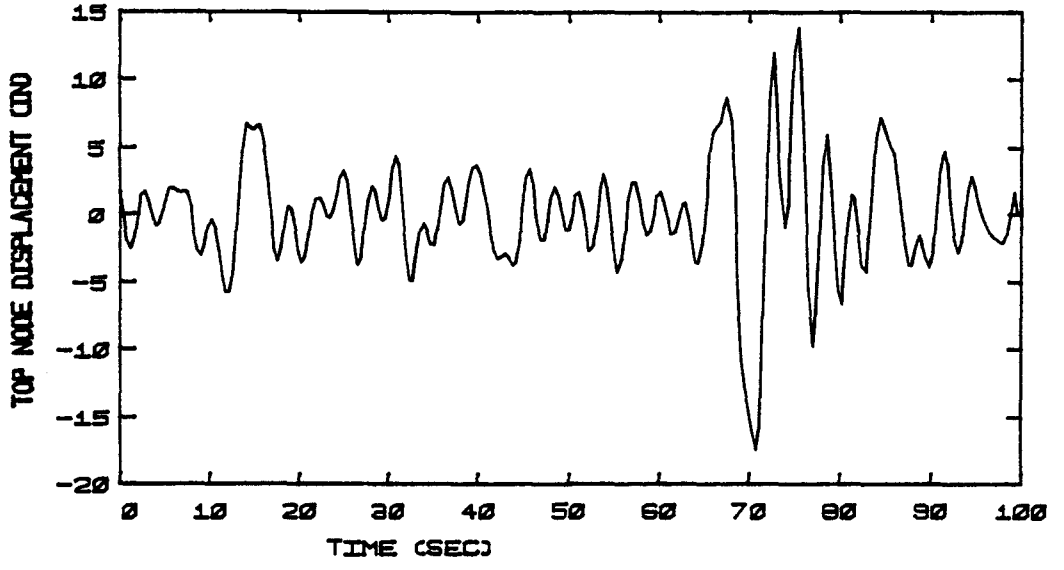

Fig. 5.7a Time History of Top Node Displacement, Case 1, Formulation I

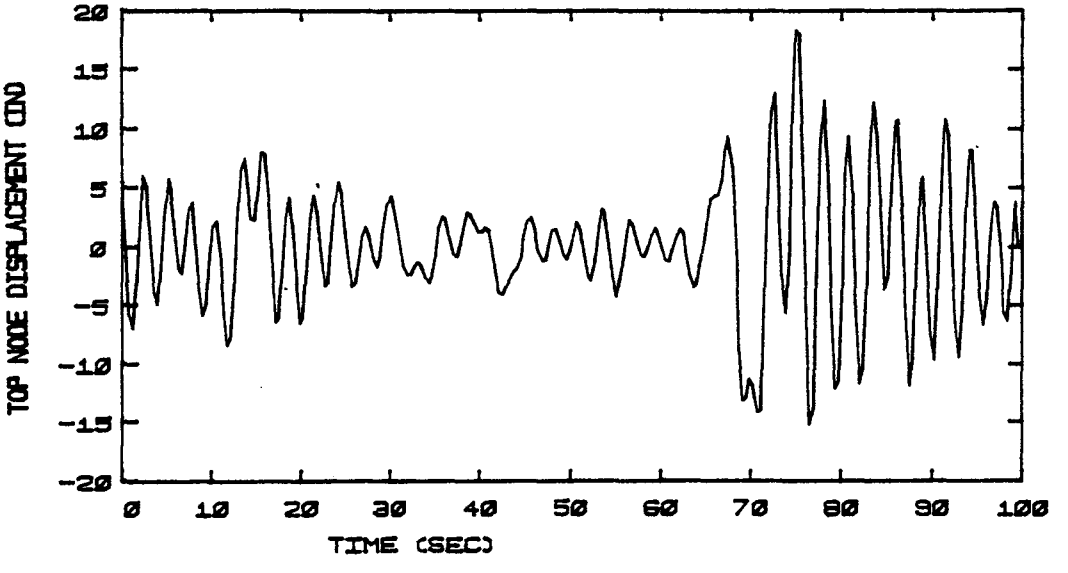

Fig. 5.7b Time History of Top Node Displacement, Case 1, Formulation II

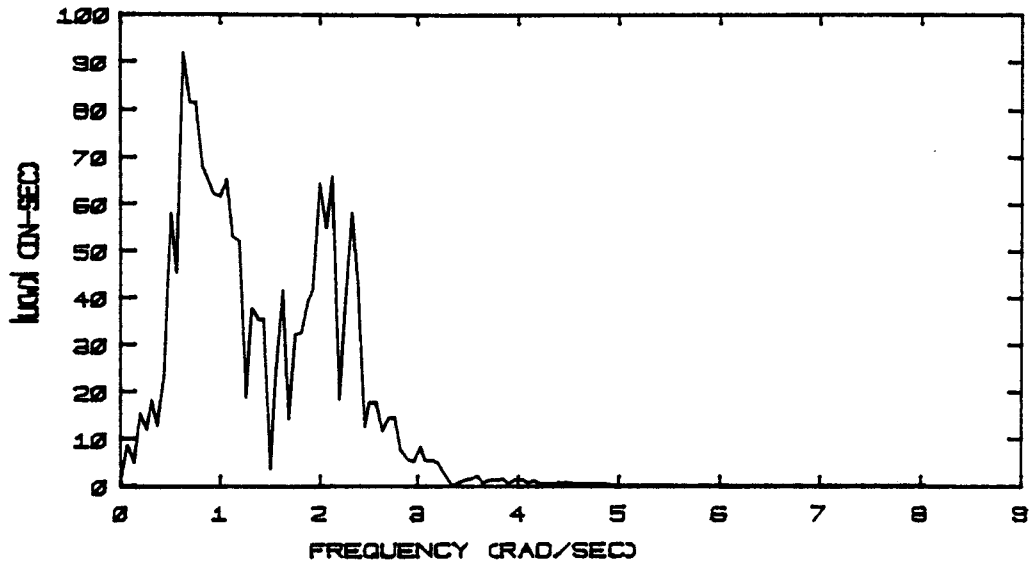

Fig. 5.8a Top Node Displacement Spectrum, Case 1, Formulation I

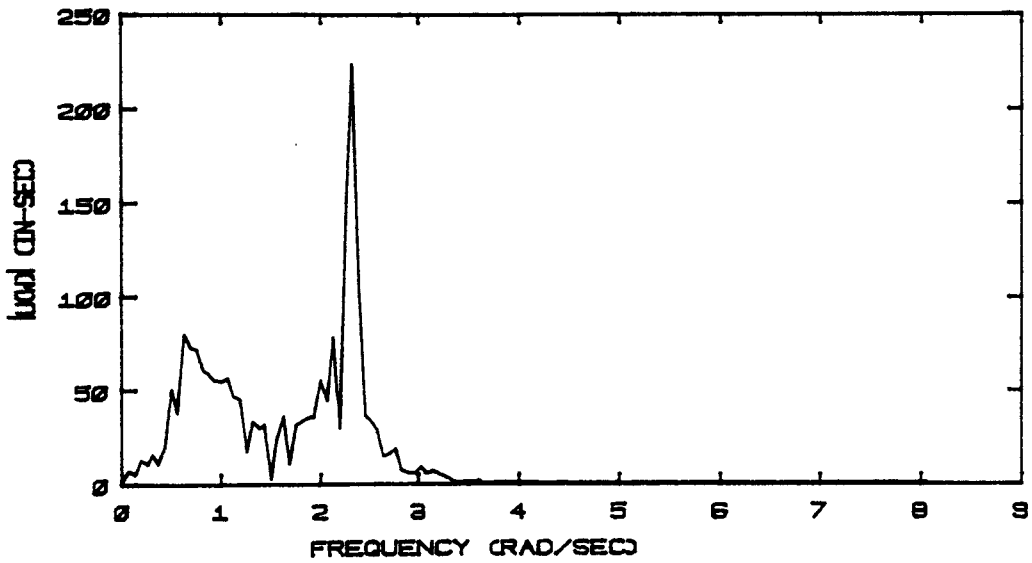

Fig. 5.8b Top Node Displacement Spectrum, Case 1, Formulation II

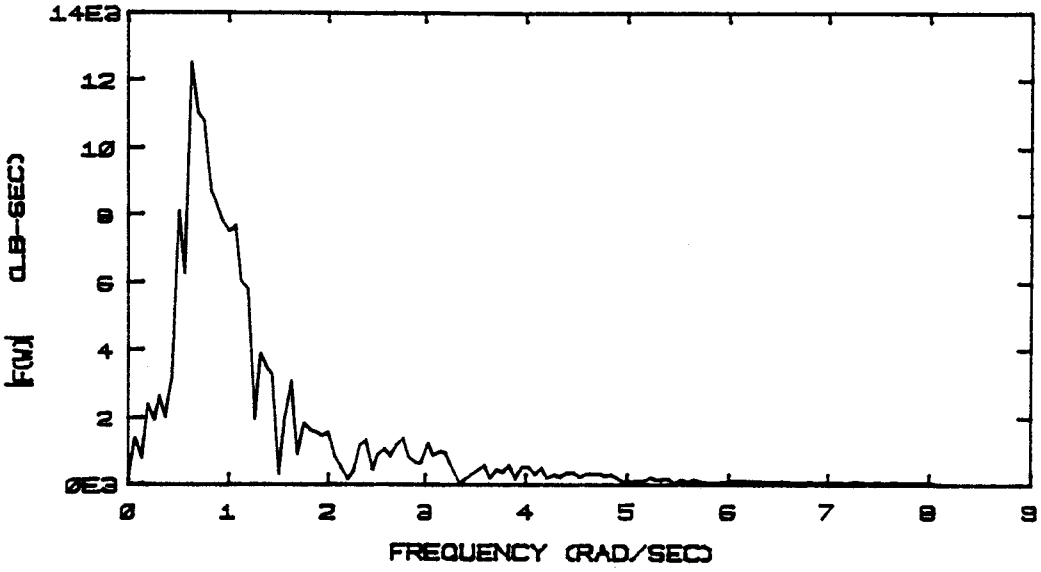

Fig. 5.9a Converged Force Spectrum, Case 1, Formulation I

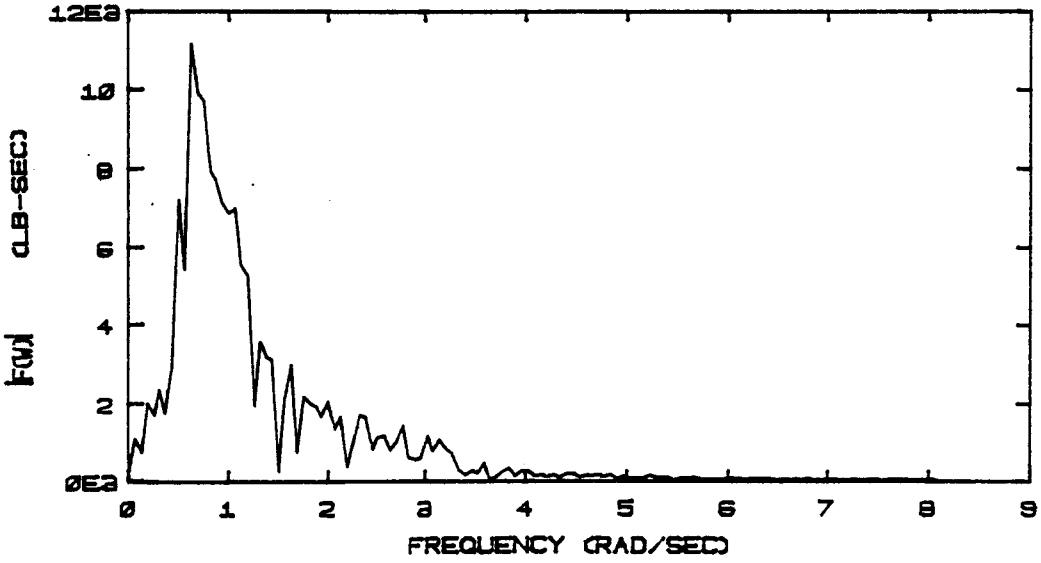

Fig. 5.9b Converged Force Spectrum, Case 1, Formulation II

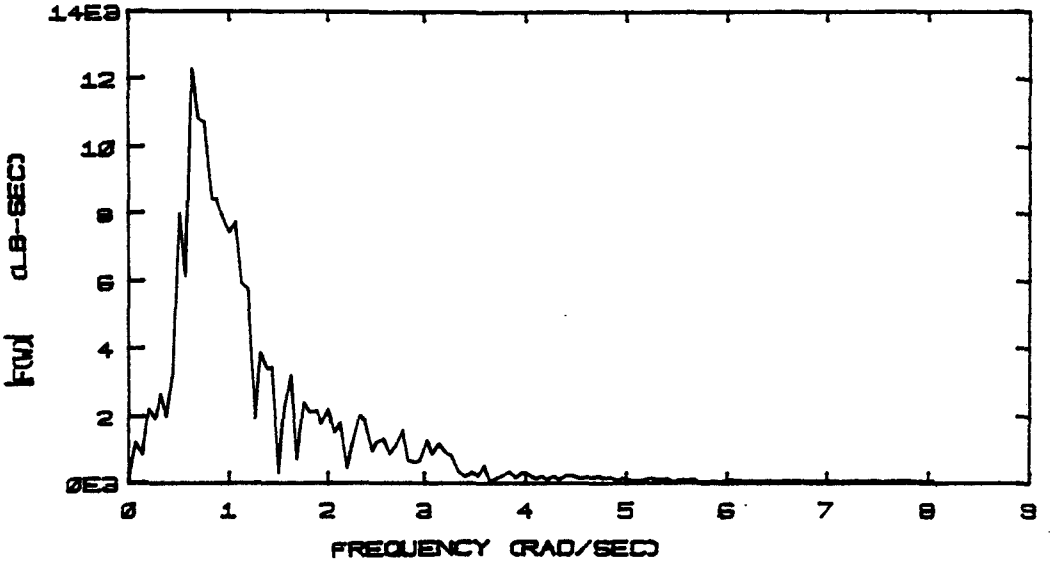

Fig. 5.10a Starting Force Spectrum, Case 1

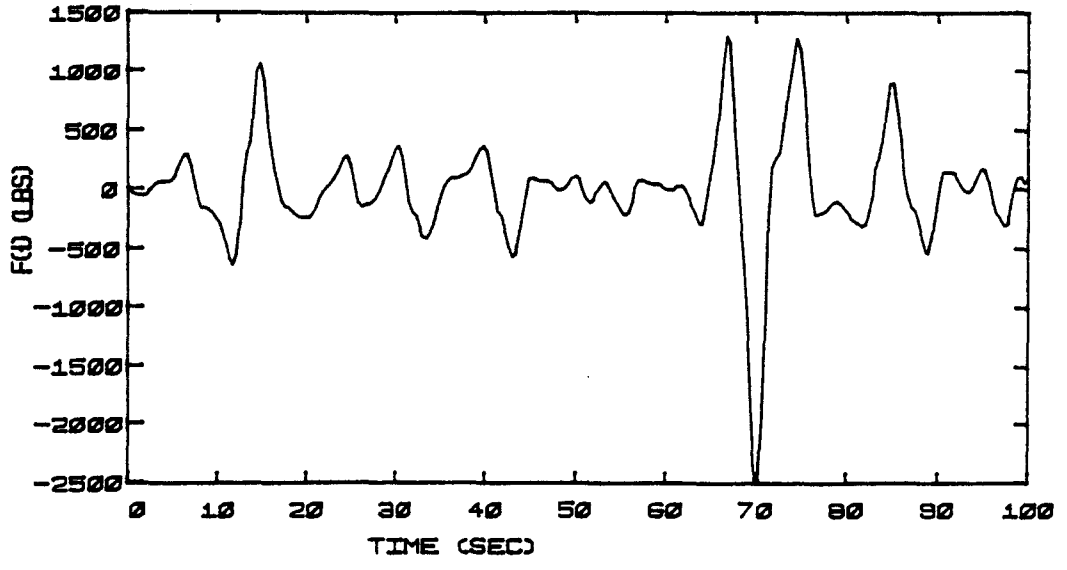

Fig. 5.10b Starting Force Time History, Case 1

difference in hydrodynamic damping between the two formulations can lead to significantly different behavior near resonance.

Fig. 5.11 shows the top node response to a quasi-white noise applied at nodes 2 and 3. Hydrodynamic damping is not considered. However, the added mass was included in the computational model, and this required iteration on the inertia coefficient, leading to a variation of the natural frequency from cycle to cycle. The effect is most significant in the initial cycles since the added masses are of the same order as the nodal masses, and the ratio of top node mass to submerged nodal masses is quite low ($\frac{m_1}{m_2} = \frac{m_1}{m_3} \simeq 3.85$).

Convergence can also be assessed by comparing the velocity correction at each iteration. Focussing on node 2, we show first the time history of the fluid velocity in Fig. 5.12. The solution for the structural velocity after the first cycle is plotted in Fig. 5.13. It is equal to the first correction since the structural velocity is assumed initially to be zero. It also depends on the artificial damping assumed in the solution. Subsequent corrections are plotted in Figs. 5.14 through 5.16. The distribution of convergence throughout the signal is uneven due to a "beat" present in the force signal towards the end of the record.

The effect of the corrective terms is to zero out the smoother part of the record and to lower the overshooting waves at the end. There is a slight phase shift from cycle to cycle due to the sequential action of the hydrodynamic damping in the iterative process, i.e., the time domain difference in consecutive response velocities is due to both magnitude and phase differences.

Experience gained with similar records suggests that the time region

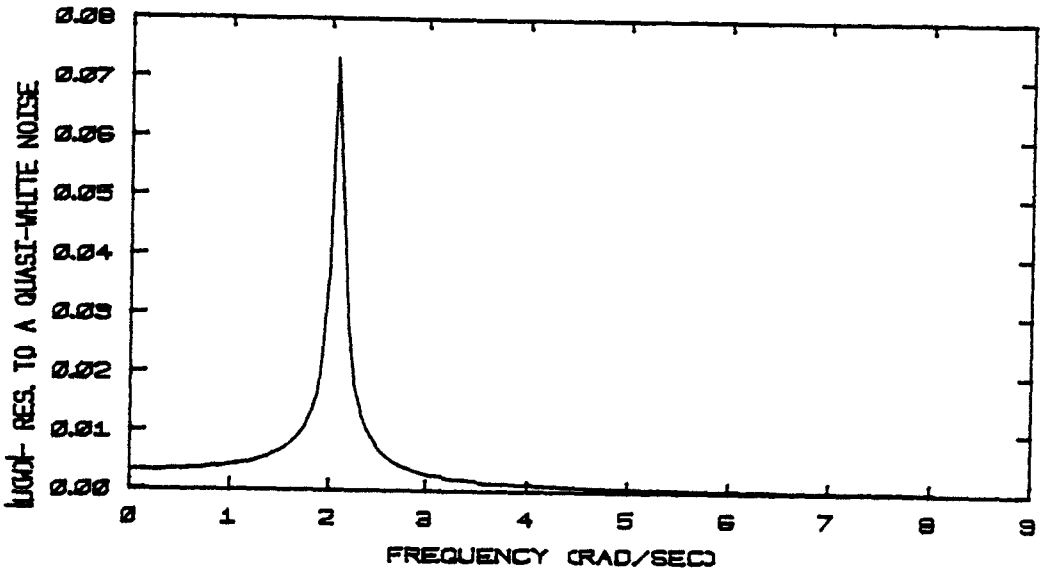

Fig. 5.11 Top Node Response to a Quasi-White Noise, Case 1

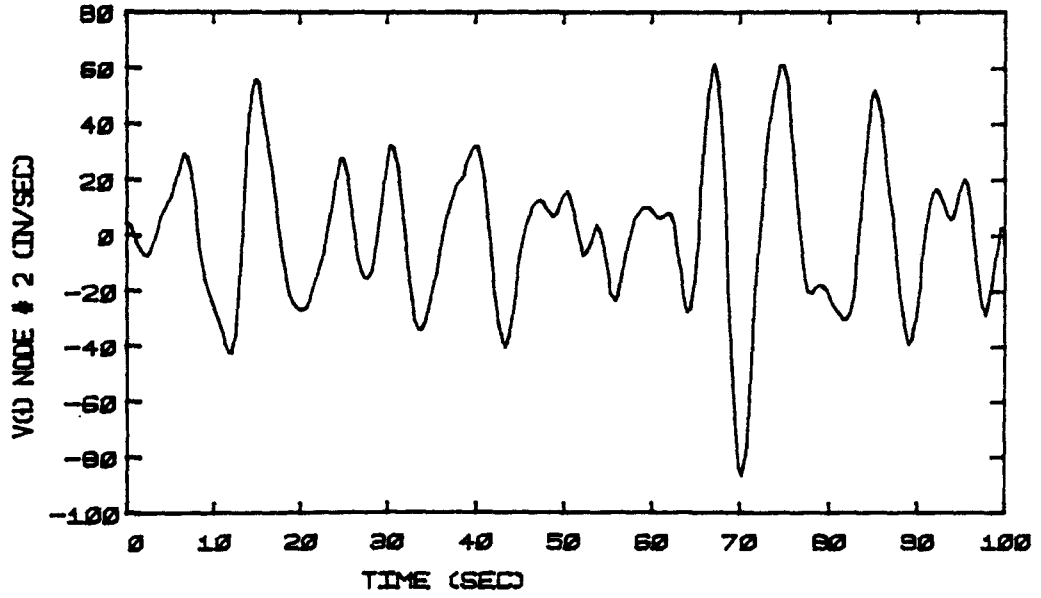

Fig. 5.12 Time History of Fluid Velocity, Case 1

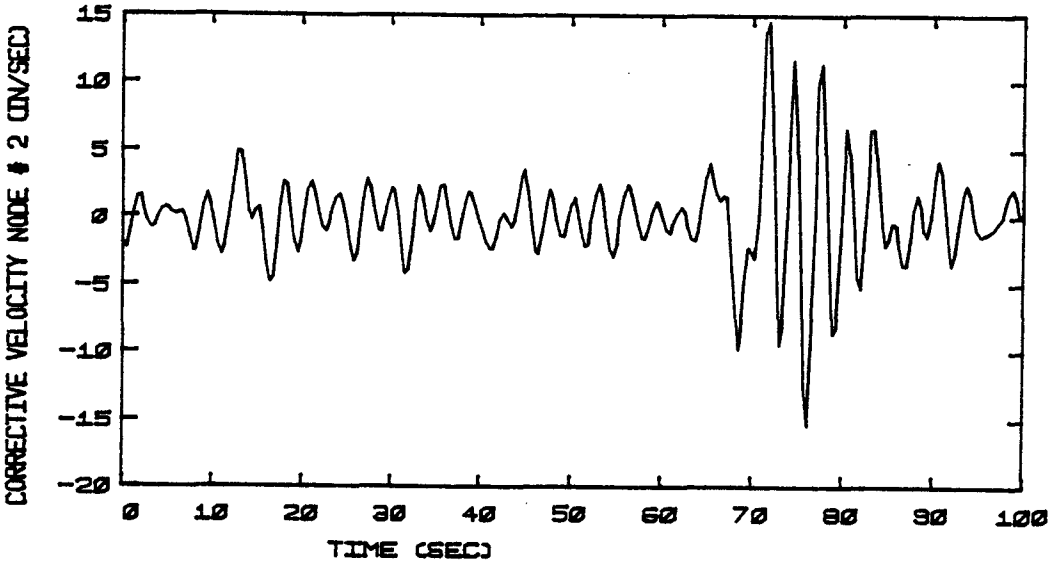

Fig. 5.13 Time History of First Estimate of Response Velocity, Case 1, Formulation I

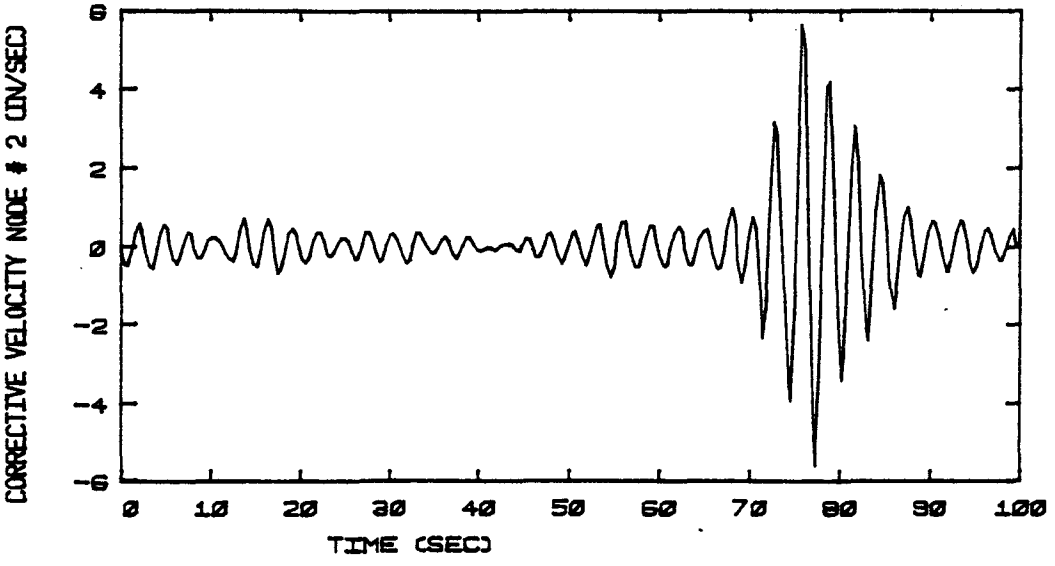

Fig. 5.14 Corrective Velocity, Iteration 1, Case 1, Formulation I

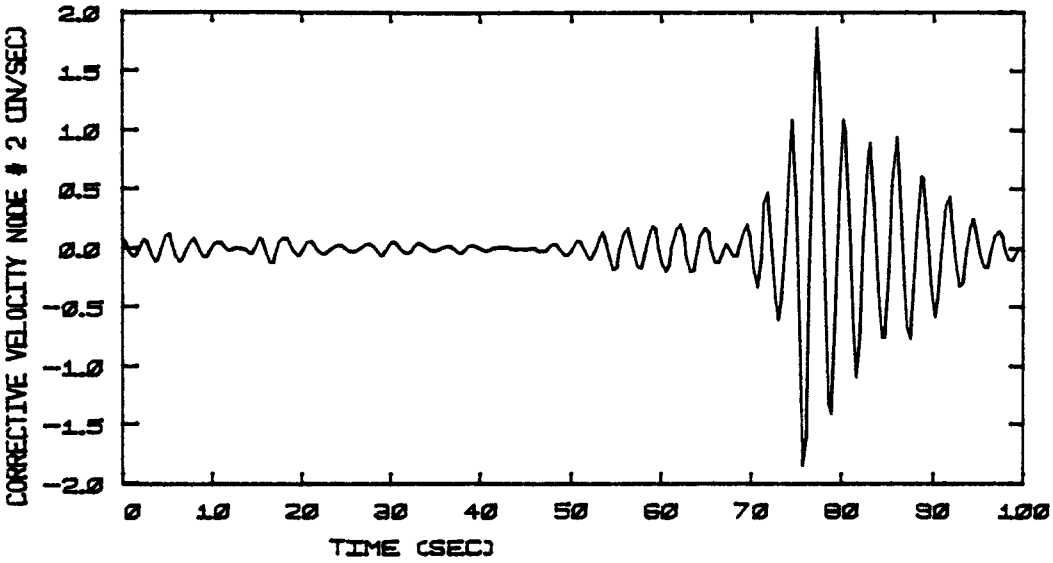

Fig. 5.15 Corrective Velocity, Iteration 2, Case 1, Formulation I

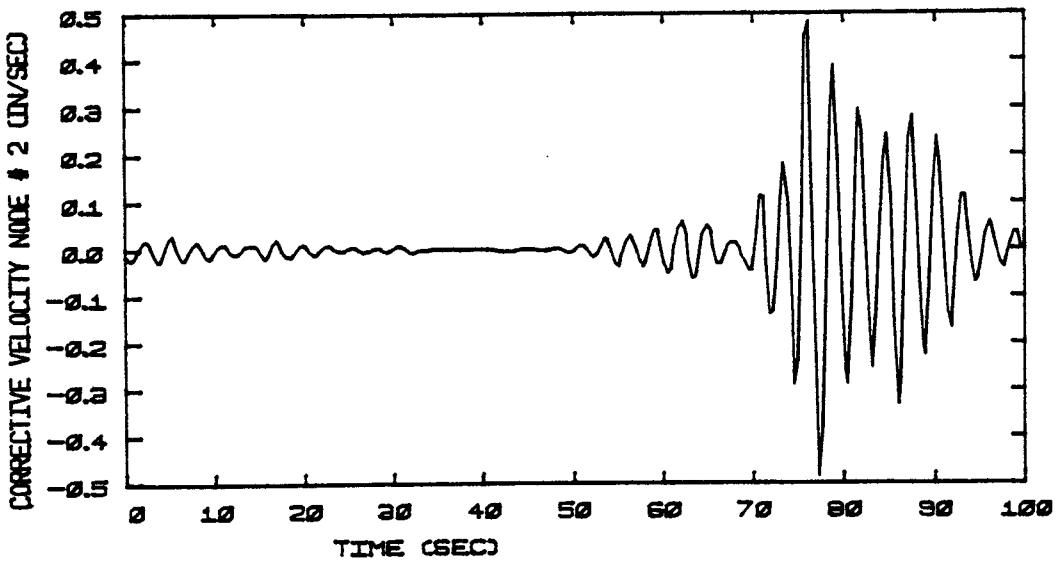

Fig. 5.16 Corrective Velocity, Iteration 3, Case 1, Formulation I

affected by a beat is equal to the duration of the impulse-response function of the system. This is partially seen in Figs. 5.14 to 5.16. As a point of interest, note that the perturbation extends only to the rigth of the signal and does not shift to the left in subsequent iterations. This behavior is related to the causal property of the system; it responds only to past loads.

We next illustrate the "starting effect" of the artificial damping. Case 1 was rerun using two widely different values of α. Table 5-4 lists percentage of r.m.s converged top node response obtained at subsequent cycles for both formulations I and II using α = 0.4, 1.6 and α = 0.05, 1.0 respectively. These results show that convergence can be improved with an appropiate choice of α. In this case, the better estimates are α= 1.6 in I and 0.05 in II.

Results for the remaining cases are summarized in tables 5-5 through 5-8. The starting force at node 2 and converged top node displacement Fourier magnitudes are plotted in Figs. 5.17 to 5.28. Case 2 results indicate drag dominance; there is a gradual progression towards inertia dominance for cases 3 through 5. Also, dynamic amplification becomes more pronounced as the region of highest energy content in the Force Fourier magnitude spectrum approaches the natural frequency of the structure. The Keulegan-Carpenter number and the reduced velocity measure indicate the applicability of the independent flow fields assumption for all cases. This formulation always predicts a higher dynamic response, and the difference in r.m.s response tends to be insignificant as the inertia load becomes more dominant. Case 5 represents this extreme case.

TABLE 5-4

HISTORY OF PERCENTAGE OF CONVERGED RESPONSE

FOR DIFFERENT FRACTIONS OF ARTIFICIAL DAMPING

	Formulation I		Formulation II	
Cycle	$\alpha = 0.4$	$\alpha = 1.6$	$\alpha = 0.05$	$\alpha = 1.0$
1	136.97	96.99	95.83	57.1
2	108.4	99.29	100.6	77.34
3	104.13	99.45	99.97	88.30
4	102.00	99.80	99.99	94.80

TABLE 5-5

SUMMARY OF RESULTS FOR CASE 2

SEA STATE PARAMETERS

Significant Wave Heigth	(H_S)	10	feet
Av. Zero Crossing Period	(T_Z)	6.25	sec
Lower Cut-off Frequency	(ω_1)	0.376991	rad/sec
Higher Cut-off Frequency	(ω_M)	2.513279	rad/sec
Frequency increment	$(\Delta\omega)$	0.062832	rad/sec

		node 2	node 3
R.M.S Fluid Velocity	(σ_v) (in/s.)	21.65	14.46

FORMULATION I RESULTS

Number of Iterations	4		
Converged Struct. R.M.S Vel.	$(\sigma_{\dot{u}})$(in/s.)	2.29	0.67
Reynolds Number	$(\frac{\sigma_{\dot{r}} D}{\nu})\times 10^{-5}$	2.32	1.52
Keulegan-Carpenter Number	$(\frac{\sigma_{\dot{r}} T_{\dot{r}}}{D})$	11.41	8.85
Hydrodynamic Coefficients	C_M	1.35	1.49
	C_D	1.42	1.10
Reduced Velocity	$(\frac{\sigma_v T_{\dot{u}}}{D})$	5.34	3.56

FORMULATION II RESULTS

Number of iterations	4		
Converged Struct. R.M.S Vel.	$(\sigma_{\dot{u}})$(in/s.)	2.61	0.75
Far Field Reynolds Number	$(\frac{\sigma_v D}{\nu})\times 10^{-5}$	2.26	1.51
Near Field Reynolds Number	$(\frac{\sigma_{\dot{u}} D}{\nu})\times 10^{-5}$	0.27	0.08
Far Field Keulegan-Carpenter No.	$(\frac{\sigma_v T_Z}{D})$	9.02	6.03
Near Field Keulegan-Carpenter No.	$(\frac{\sigma_{\dot{u}} T_u}{D})$	0.51	0.15
Hydrodynamic Coefficients	C_{MV}	1.48	1.65
	C_{MU}	1.97	1.99
	C_{DV}	1.12	0.75
	C_{DU}	0.05	0.01

TABLE 5-6

SUMMARY OF RESULTS FOR CASE 3

SEA STATE PARAMETERS

Significant Wave Heigth	(H_S)	8	feet
Av. Zero Crossing Period	(T_Z)	5.51	sec
Lower Cut-off Frequency	(ω_1)	0.502655	rad/sec
Higher Cut-off Frequency	(ω_M)	2.6389	rad/sec
Frequency increment	$(\Delta\omega)$	0.062832	rad/sec

		node 2	node 3
R.M.S Fluid Velocity	(σ_v)(in/s.)	17.09	10.29

FORMULATION I RESULTS

Number of Iterations	4		
Converged Struct. R.M.S Vel.	$(\sigma_{\dot{u}})$(in/s.)	1.91	0.56
Reynolds Number	$(\frac{\sigma_{\dot{r}} D}{\nu})\times 10^{-5}$	1.86	1.08
Keulegan-Carpenter Number	$(\frac{\sigma_{\dot{r}} T_{\dot{r}}}{D})$	7.44	5.36
Hydrodynamic Coefficients	C_M	1.57	1.7
	C_D	0.93	0.66
Reduced Velocity	$(\frac{\sigma_v T_{\dot{u}}}{D})$	4.22	2.54

FORMULATION II RESULTS

Number of iterations	4		
Converged Struct. R.M.S Vel.	$(\sigma_{\dot{u}})$(in/s.)	2.05	0.59
Far Field Reynolds Number	$(\frac{\sigma_v D}{\nu})\times 10^{-5}$	1.78	1.07
Near Field Reynolds Number	$(\frac{\sigma_{\dot{u}} D}{\nu})\times 10^{-5}$	0.21	0.06
Far Field Keulegan-Carpenter No.	$(\frac{\sigma_v T_Z}{D})$	6.28	3.78
Near Field Keulegan-Carpenter No.	$(\frac{\sigma_{\dot{u}} T_u}{D})$	0.40	0.12
Hydrodynamic Coefficients	C_{MV}	1.64	1.79
	C_{MU}	1.98	1.99
	C_{DV}	0.78	0.47
	C_{DU}	0.04	0.01

TABLE 5-7

SUMMARY OF RESULTS FOR CASE 4

SEA STATE PARAMETERS

Significant Wave Heigth	(H_S)	6	feet
Av. Zero Crossing Period	(T_Z)	4.69	sec
Lower Cut-off Frequency	(ω_1)	0.628319	rad/sec
Higher Cut-off Frequency	(ω_M)	2.7646	rad/sec
Frequency increment	$(\Delta\omega)$	0.0628318	rad/sec

		node 2	node 3
R.M.S Fluid Velocity	(σ_v) (in/s.)	12.46	6.33
FORMULATION I RESULTS			
Number of Iterations	4		
Converged Struct. R.M.S Vel.	$(\sigma_{\dot{u}})$(in/s.)	1.99	0.57
Reynolds Number	$(\frac{\sigma_{\dot{r}} D}{\nu}) \times 10^{-5}$	1.39	0.67
Keulegan-Carpenter Number	$(\frac{\sigma_{\dot{r}} T_{\dot{r}}}{D})$	4.69	2.41
Hydrodynamic Coefficients	C_M	1.73	1.87
	C_D	0.58	0.3
Reduced Velocity	$(\frac{\sigma_v T_{\dot{u}}}{D})$	2.7	1.37
FORMULATION II RESULTS			
Number of iterations	4		
Converged Struct. R.M.S Vel.	$(\sigma_{\dot{u}})$(in/s.)	2.1	0.62
Far Field Reynolds Number	$(\frac{\sigma_v D}{\nu}) \times 10^{-5}$	1.3	0.66
Near Field Reynolds Number	$(\frac{\sigma_{\dot{u}} D}{\nu}) \times 10^{-5}$	0.2	0.05
Far Field Keulegan-Carpenter No.	$(\frac{\sigma_v T_Z}{D})$	3.9	1.93
Near Field Keulegan-Carpenter No.	$(\frac{\sigma_{\dot{u}} T_u}{D})$	0.43	0.12
Hydrodynamic Coefficients	C_{MV}	1.77	1.89
	C_{MU}	1.98	1.99
	C_{DV}	0.48	0.24
	C_{DU}	0.04	0.01

TABLE 5-8

SUMMARY OF RESULTS FOR CASE 5

SEA STATE PARAMETERS

Significant Wave Heigth	(H_S)	4	feet
Av. Zero Crossing Period	(T_Z)	3.74	sec
Lower Cut-off Frequency	(ω_1)	0.753982	rad/sec
Higher Cut-off Frequency	(ω_M)	2.89	rad/sec
Frequency increment	$(\Delta\omega)$	0.0628318	rad/sec

		node 2	node 3
R.M.S Fluid Velocity	(σ_v) (in/s.)	7.69	2.83

FORMULATION I RESULTS

Number of Iterations	4		
Converged Struct. R.M.S Vel.	$(\sigma_{\dot{u}})$(in/s.)	2.20	0.62
Reynolds Number	$(\frac{\sigma_{\dot{r}} D}{\nu}) \times 10^{-5}$	0.91	0.32
Keulegan-Carpenter Number	$(\frac{\sigma_{\dot{r}} T_{\dot{r}}}{D})$	2.65	1.13
Hydrodynamic Coefficients	C_M	1.85	1.95
	C_D	0.32	0.1
Reduced Velocity	$(\frac{\sigma_v T_{\dot{u}}}{D})$	1.55	0.57

FORMULATION II RESULTS

Number of iterations	4		
Converged Struct. R.M.S Vel.	$(\sigma_{\dot{u}})$(in/s.)	2.27	0.66
Far Field Reynolds Number	$(\frac{\sigma_v D}{\nu}) \times 10^{-5}$	0.8	0.29
Near Field Reynolds Number	$(\frac{\sigma_{\dot{u}} D}{\nu}) \times 10^{-5}$	0.23	0.07
Far Field Keulegan-Carpenter No.	$(\frac{\sigma_v T_Z}{D})$	1.92	0.71
Near Field Keulegan-Carpenter No.	$(\frac{\sigma_{\dot{u}} T_u}{D})$	0.43	0.12
Hydrodynamic Coefficients	C_{MV}	1.89	1.96
	C_{MU}	1.98	1.99
	C_{DV}	0.23	0.06
	C_{DU}	0.03	0.01

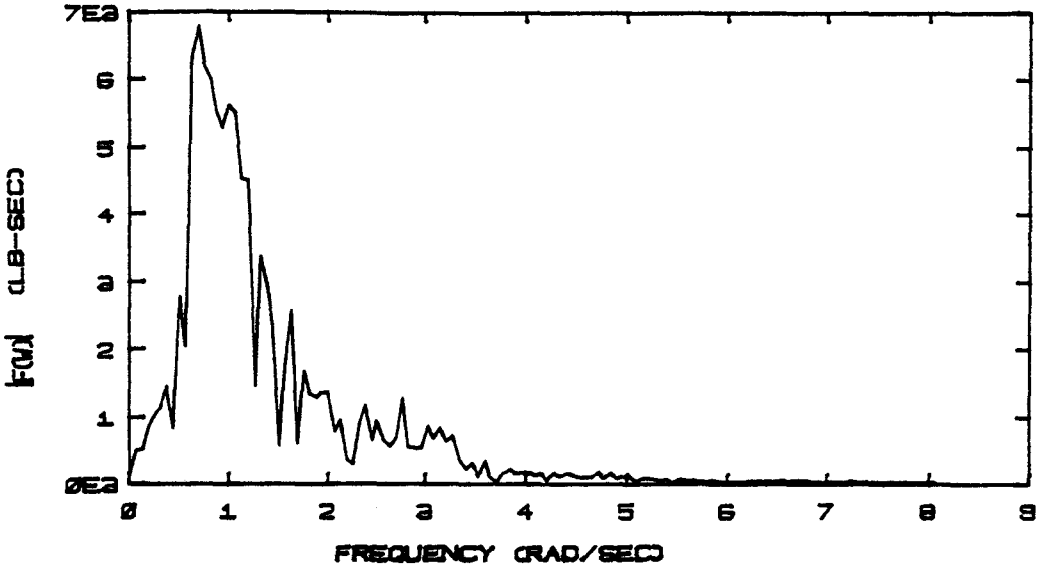

Fig. 5.17 Starting Force Spectrum, Case 2

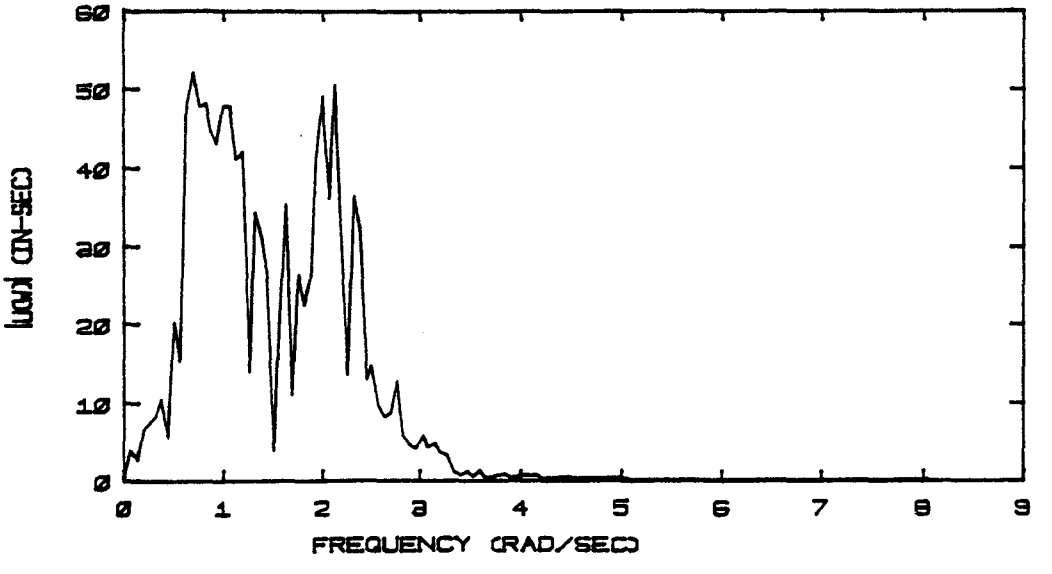

Fig. 5.18 Top Node Displacement Spectrum, Case 2, Formulation I

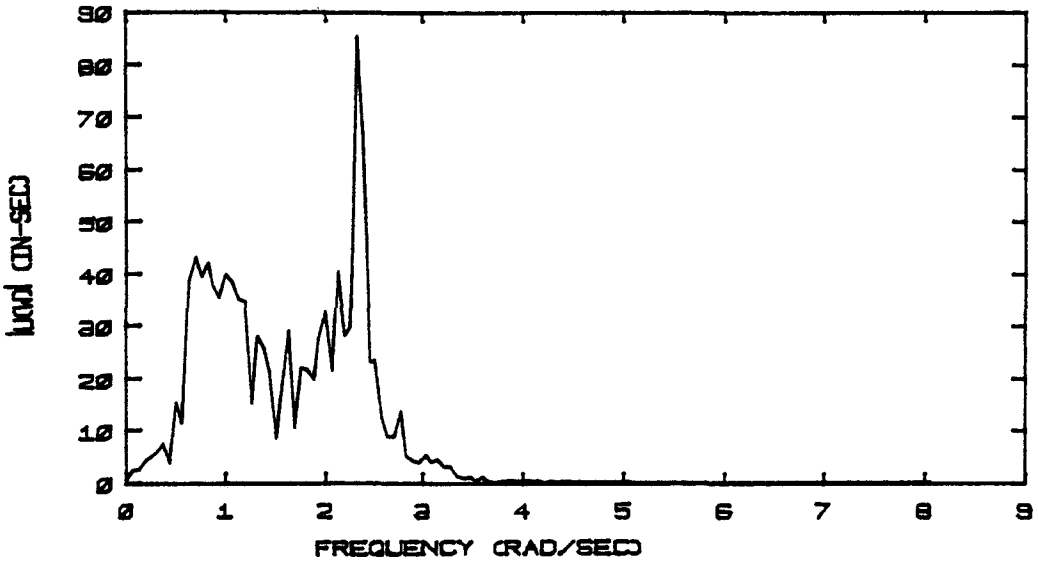

Fig. 5.19 Top Node Displacement Spectrum, Case 2, Formulation II

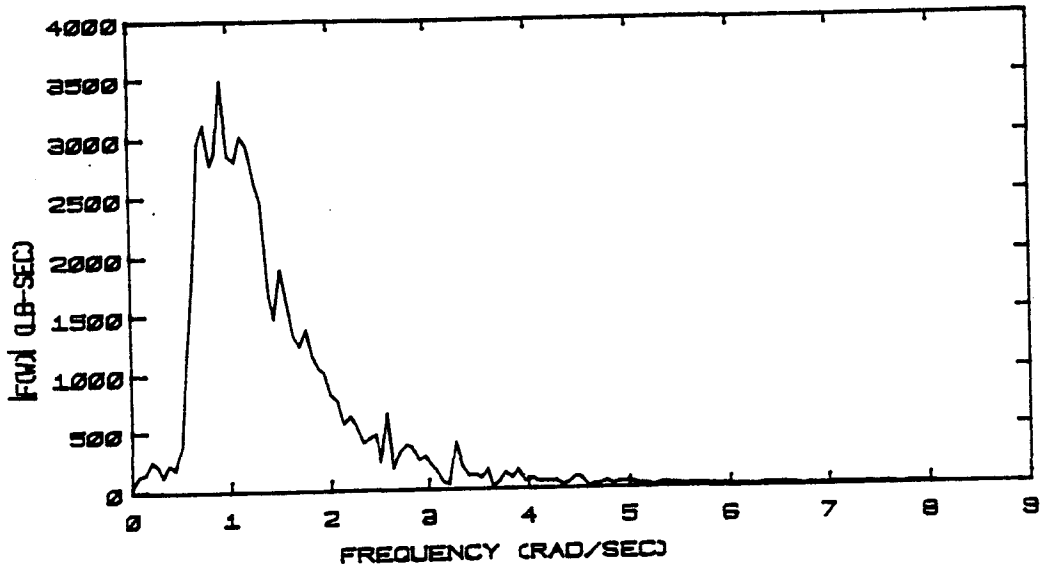

Fig. 5.20 Starting Force Spectrum, Case 3

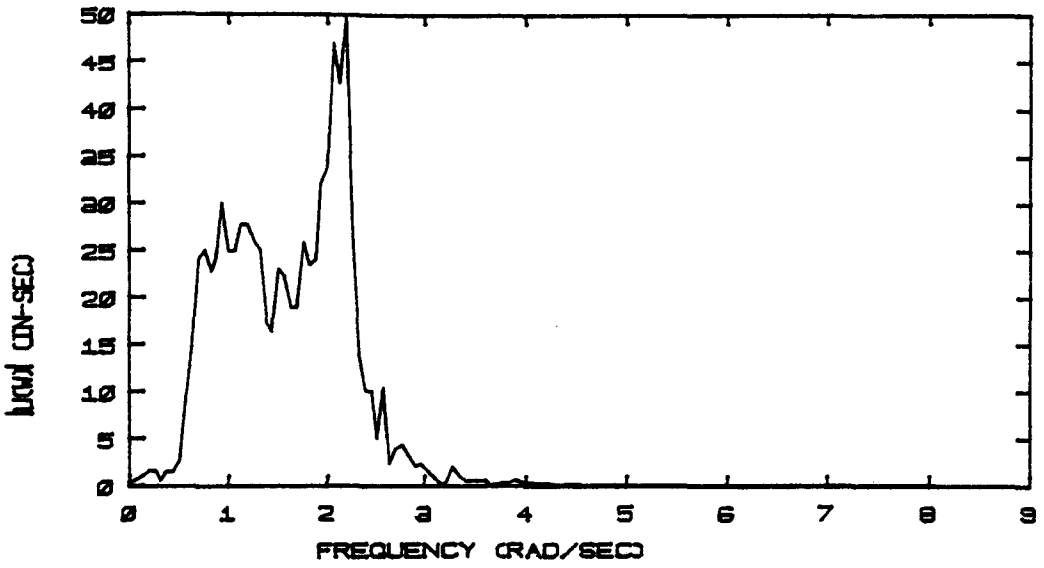

Fig. 5.21 Top Node Displacement Spectrum, Case 3, Formulation I

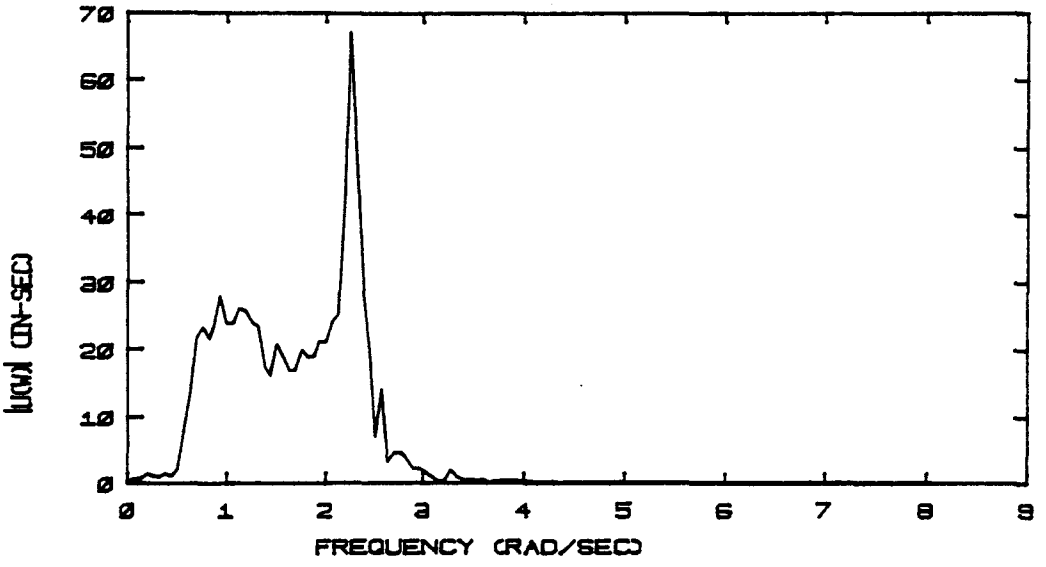

Fig. 5.22 Top Node Displacement Spectrum, Case 3, Formulation II

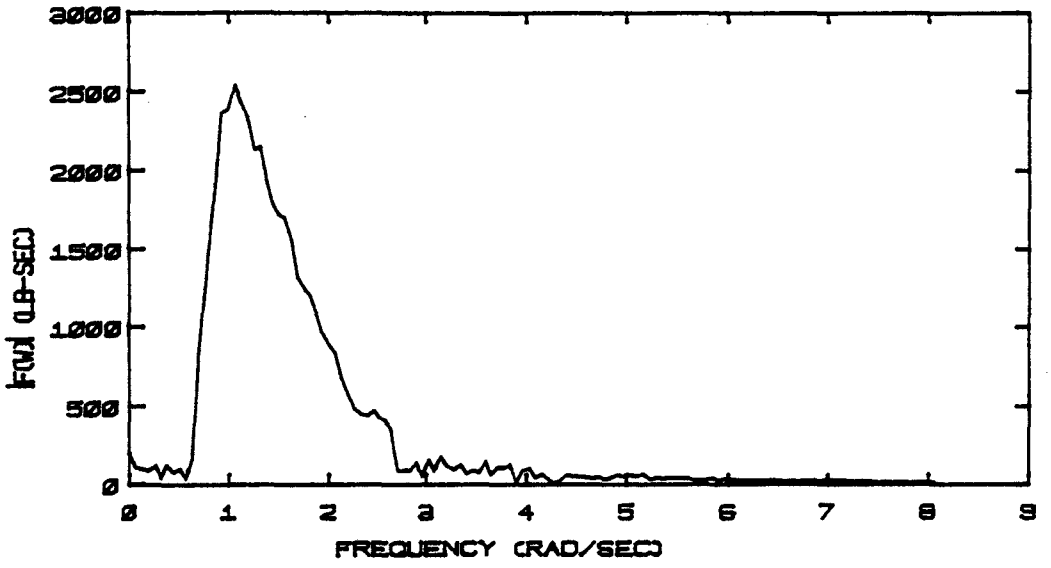

Fig. 5.23 Starting Force Spectrum, Case 4

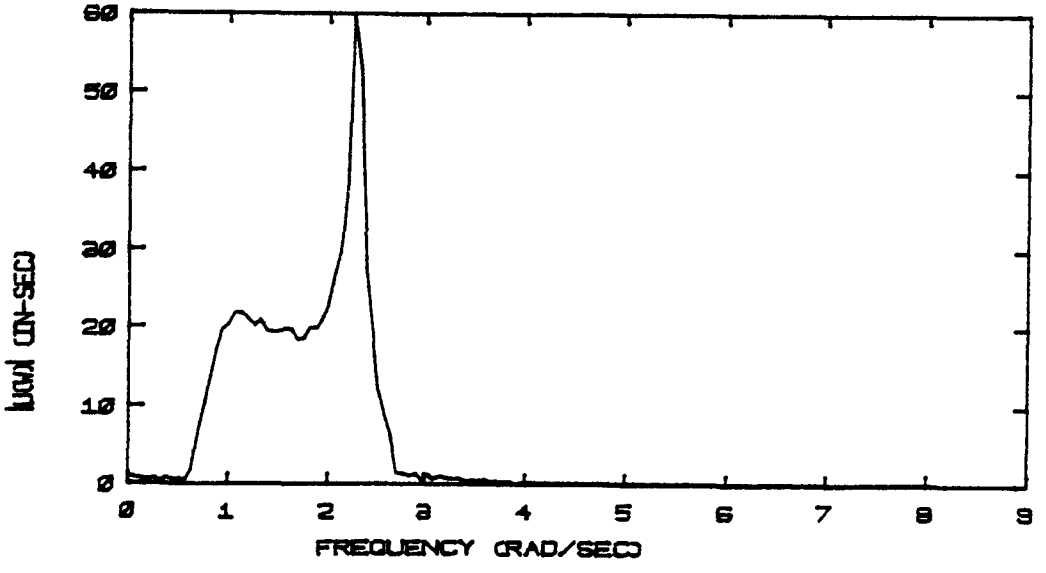

Fig. 5.24 Top Node Displacement Spectrum, Case 4, Formulation I

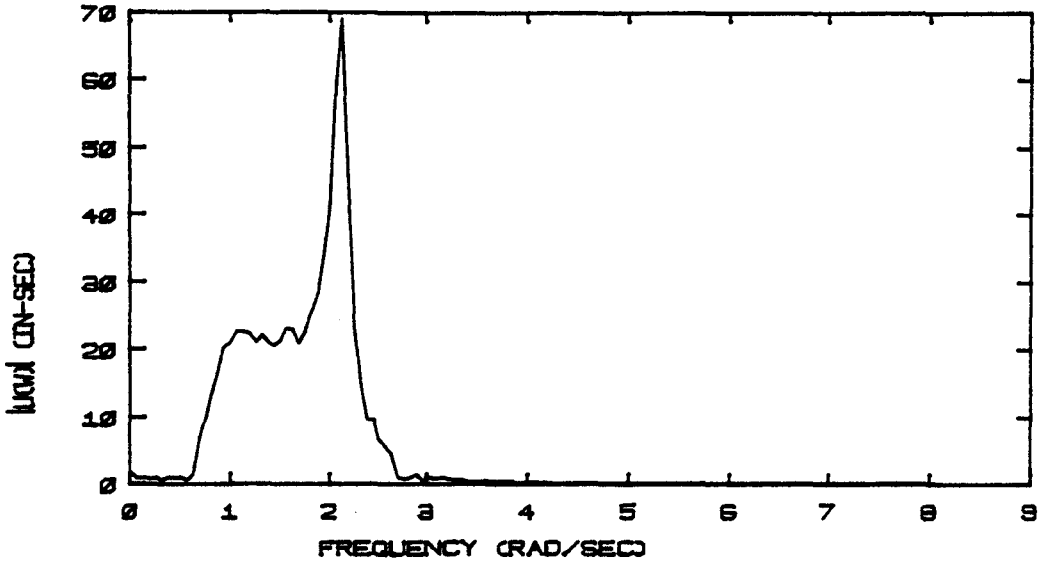

Fig. 5.25 Top Node Displacement Spectrum, Case 4, Formulation II

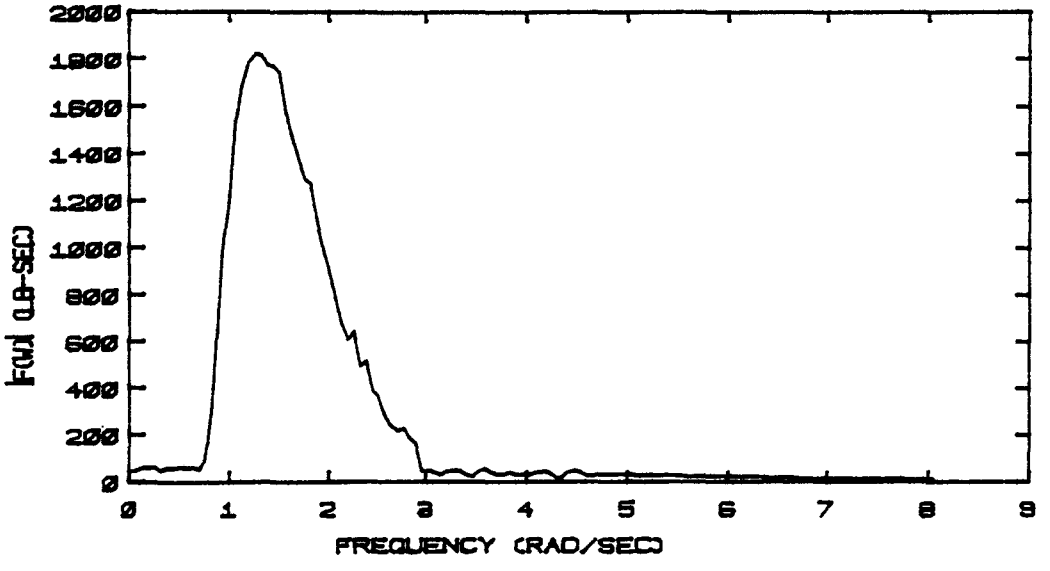

Fig. 5.26 Starting Force Spectrum, Case 5

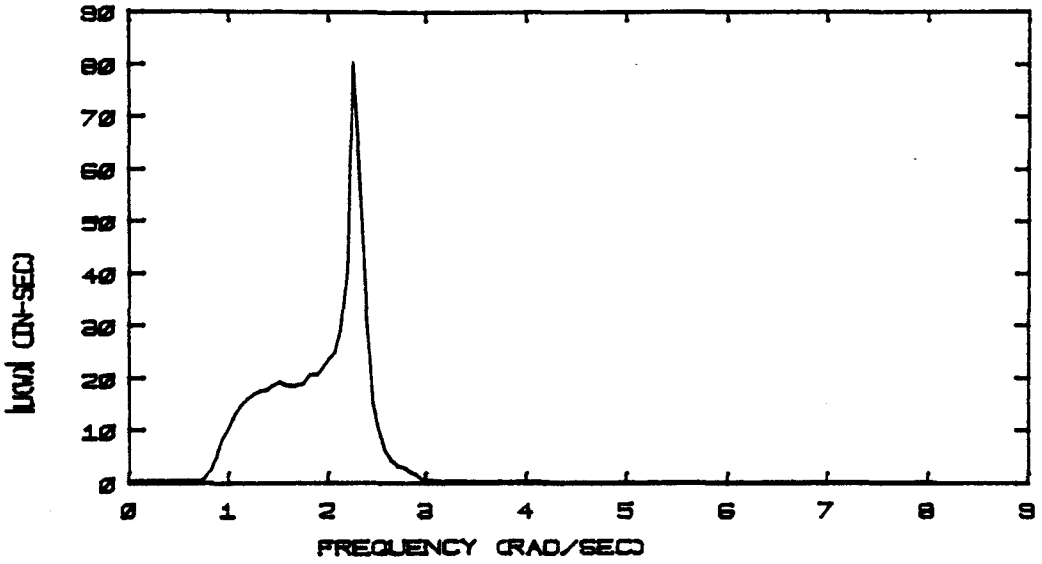

Fig. 5.27 Top Node Displacement Spectrum, Case 5, Formulation I

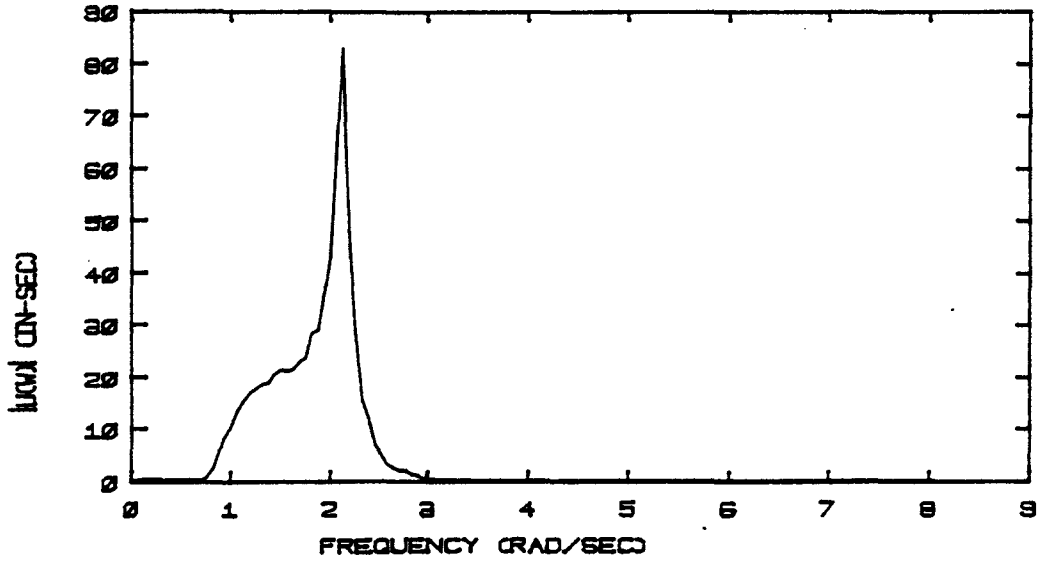

Fig. 5.28 Top Node Displacement Spectrum, Case 5, Formulation II

There is negligible hydrodynamic drag damping, and one cannot distinguish between the responses predicted by the two formulations.

CHAPTER 6

CONCLUSIONS

A computational model has been developed in this study to analyze the effect of structural motion on the hydrodynamic forcing for offshore steel structures. The main objective has been to investigate the sensitivity of the structural response to two different approaches for simulating fluid-structure interaction: the relative velocity and the independent flow fields formulations. The second approach, originally proposed for a steady current acting on an oscillating cylinder, has been extended to the case of an irregular wave acting on a flexible structure. A hydrodynamic forcing model which includes the nonlinearities present in the force formulations and partially accounts for the variability of the hydrodynamic coefficients with the flow parameters, has been coupled with the dynamic response model of a simplified offshore jacket consisting of a single vertical cylinder. The dimensions are selected such that the period is typical of a deep water platform and the diameter representative of a local member . A frequency domain deterministic iterative method which combines some features of time domain analysis has been developed and applied to solve the equations of motion. This method operates on a periodic pseudo-random load, deterministically generated through the specification of a set of random phase angles for the wave components, with the Discrete Fourier Transform. The equations

are solved in frequency domain, and the response is then transformed back into the time domain for evaluation of the response dependent force terms. This procedure does not require that the response have specific statistical properties, such as Gaussian, and therefore is a more fundamental approach than the the power series method proposed by Borgman [28].

Based on the limited number of sea state cases studied, it appears that the independent flow fields formulation generates less hydrodynamic damping than predicted by the relative velocity model. This difference increases with the severity of the sea state. For the "more" probable low sea state condition, the results for the amplitudes of vibration and r.m.s response are in close agreement since the drag force and therefore the hydrodynamic drag damping is negligible. As the sea state increases, the relative velocity is more appropiate for the submerged elements located in the upper zone of the strucuture where higher values of reduced velocity and Keulegan-Carpenter number are expected. In this case, the independent flow fields model will over-estimate the structural response if it is applied to the entire structure. The use of a relative velocity model is likely to under-estimate hydrodynamic damping in low to moderate sea states. Fatigue damage for a typical deep water platform is a maximum in this region [38] and hence experimental verification of the applicability of either formulation for random wave loading is of crucial importance.

Observations related to the performance of the numerical

procedure, drawn from the experience gained with its use in this study, are summarized below:

- Parallel application of time and frequency domain solution procedures is an effective method for treating the structural motion effects in the full nonlinear form of the hydrodynamic forcing expression. The suitability of the method is due to the efficiency of the Fast Fourier Transform (FFT) algorithm utilized to compute the Discrete Fourier Transform (DFT).

- Convergence is satisfactory. It improves with the use of appropiate counteracting damping components in the equations. Also, experience with other cases not presented here indicates that the convergence rate increases as the structure becomes stiffer.

- The force and therefore the response spectrum is reasonably insensitive to different specifications of random phase angles for generating the wave components. The force spectral moment statistics showed a slight improvement when the number of loading cases was increased from 10 to 20 (Sect. 5.1).

- Comparison of the computational cost of time domain schemes versus this "mixed" method indicates that the frequency domain method becomes less atractive as the number of degrees of freedom increases. The linear dynamic stiffness matrix has to be decomposed N/2 times, where N is

the number of time points. A time domain method requires only a single decomposition of the effective stiffness matrix and generates the solution through a sequence of back-substitutions of the effective load vector [25]. However, a nonlinear iterative time domain integration would not be feasible for the case of variable hydrodynamic coefficients. Also, an inherent problem of time domain methods is the presence of transients, they are difficult to isolate for the case of a random load and their effect may extend over a significant portion of the response records. A less significant disadvantage of the frequency domain method is its uneven convergence to the response time history. This is partly due to phase differences between consecutive response signals and the effect on the magnitude of the frequency domain response is much less. An r.m.s difference is a more appropiate convergence measure in this case.

It should be noted that the results are based on approximate models and therefore have to be interpreted carefully. The primary sources of uncertainty are:

- Both formulations neglect vortex shedding. Vortex shedding induced loads are known to be significant for the flow conditions associated with the sea state cases studied (see Sect. 2.5)

- The hydrodynamic coefficients have been evaluated through

weighted average measures of the random flow and fitted to Sarpkaya's data [15]. In some cases, extrapolation to an uncertain region ($6<K\text{-}C<25$, see Sect. 2.5) was necessary.

- A deterministic relation between the significant wave height and the zero average crossing period is used for the comparison studies. This is based on a least square fit to Wiegel's data [37] in a region of high scatter.

- A simple response model was employed. Experience indicates that this uncertainty is not as significant as the other three.

REFERENCES

Abreviations:

OTC Proceedings, Offshore Technology Conference, Houston, TX, 1969-1979.

BOSS Proceedings, International Conference on Behavior of Offshore Structures : Trondheim, Norway, 1976; London, U.K., 1979.

ASCE Proceedings, American Society of Civil Engineers.

[1] Moe, G. and Verley, R.L.P.: "An Investigation into the Hydrodynamic Damping of Cylinders Oscillated in Steady Currents of Various Velocities", Report of the River and Harbour Laboratory, Norwegian Institute of Technology, June 1978.

[2] Taylor, R.E.: "Structural Dynamics of Fixed and Floating Platforms in Waves", The Dynamics of Marine Vehicles and Structures in Waves, London 1974.

[3] Hobgen, N., Miller, B.L., Searle, J.W. and Ward, G.: "Estimation of Fluid Loading on Offshore Structures", Proc. Instn. Civ. Engrs., Part 2, 1977, 63, Sept., pp 515-562.

[4] Morison, J.R., O'Brien, M.P.,Johnson, J.W. and Schaaf, S.A.: "The Force Exerted by Surface Waves on Piles", Trans. Am. Inst. Min. Metall. Engrs., Petroleum Branch. Vol. 189, pp. 149-154, 1950.

[5] Garison, C.J. and Rao, V.S.: "Interaction of Wave with Submerged Objects", Journal of Waterways, Harbors and Coastal Eng., ASCE 97, No. WW2, pp. 259-277, 1971.

[6] Connor, J.J. and Shyam Sunder, S.: Wave Theories, Wave Statistics and Hydrodynamic Loads , Chapter for the Monograph on Introduction to Offshore Structures, Edited by D.V. Reddy and M. Arockiasamy (In Press).

[7] Det Norske Veritas (DNV): "Rules for the Design, Construction and Inspection of Offshore Structures", 1977, Oslo, Norway.

[8] Ottsen Hansen, N-E.: "Hydrodynamic Forces on Composite Risers and Individual Cylinders", OTC 1979, Paper No. 3541.

[9] Blevins, R.D.: Flow Induced Vibration. Van Nostrand Reinhold Company, New York, 1977.

[10] Borgman, L.E.: "Computation of the Ocean-Wave Forces on Inclined Cylinders", Transactions, American Geophysical Union, Vol. 39, No. 5, October 1958, pp. 885-888.

[11] Angelides, D.C.: "Stochastic Response of Fixed Offshore Structures in Random Sea", Research Report R78-37, Dept. of Civil Engineering, Massachusetts Institute of Technology, Cambridge, MA, Oct. 1978.

[12] Malhotra, A.K. and Penzien, J.: "Stochastic Analysis of Offshore Tower Structures", Report No. EERC 69-6, College of Engineering, University of California, Berkley, May 1969.

[13] Bernitsas,M.M.: "Contributions Towards the Solution of the Marine Riser Design Problem", Ph.D. Thesis, Dept. of Ocean Engineering, Massachusetts Institute of Technology, Cambridge, MA, Sept. 1979.

[14] Sarpkaya, T.: "Vortex Shedding and Resistance in Harmonic Flow About Smooth and Rough Cylinders", BOSS'76.

[15] Sarpkaya, T., Collins, N.J. and Evans, S.R.: "Wave Forces on Rough-Walled Cylinders at High Reynolds Numbers", OTC 1977, Paper No. 2901.

[16] Keulegan, G.H and Carpenter, L.H.: "Forces on Cylinders and Plates in an Oscillating Fluid", Journal of Research of the National Boreau of Standards, Vol. 60, No. 5, May 1958, pp. 423-440.

[17] Batchelor, G.K.: An introduction to Fluid Dynamics , Cambridge University Press, 1970.

[18] Pedley, T.J.: "Two-dimensional Boundary Layers in a Free Stream which Oscillates Without Reversing", Journal of Fluid Mechanics, 55, 2, pp. 359-383, 1973.

[19] Bardgett, J.J. and Irick, J.K.: "Construction of the Hondo Platform in 850 ft. of Water in the Santa Barbara Channel", OTC 1977, Paper No. 2059.

[20] "Recap of the 945 ft. Hondo Platform Installation", Ocean Industry, June 1977.

[21] Sterling, G.H.: "Design of the Cognac Platform for 1025 feet of Water Depth, Gulf of Mexico", OTC 1979, Paper No. 3494.

[22] Shyam Sunder, S. and Connor J.J.: "Sensitivity Analyses for Steel Jacket Offshore Platforms", Offshore Structures, Proceedings of the International Symposium on Offshore Structures held at COPPE, Federal University of Rio de Janeiro, Brazil, October 1979, Pentech Press Limited, 1980.

[23] Vandiver, J.K.: "Detection of Structural Failure on Fixed Platforms by Measurement of Dynamic Response", OTC 1975, Paper No. 2267.

[24] Shinozuka, M., Yun, C. and Vaicatis, R.: "Dynamic Analyisis of Fixed Offshore Structures Subjected to Wind Generated Waves", Journal of Struct. Mech., 5(2), pp. 135-146, 1977.

[25] Bathe, J.K. and Wilson, E.L.: Numerical Methods in Finite Element Analysis, Prentice-Hall, Englewood Cliffs, N.J., 1976.

[26] Sexton, R.M. and Agbezuge, L.K.: "Random Wave and Vessel Motion Effects on Drilling Riser Dynamics", OTC 1976, Paper No. 2650.

[27] Foster, E.T.: "Model for Nonlinear Dynamics of Offshore Towers", Journal the Engineering Mechanics Division, ASCE, Vol.96, No. EM1, Feb. 1970..

[28] Borgman, L.E.: "Ocean Wave Simulation for Engineering Design", Journal of Waterways and Harbour Divison, ASCE, Vol. 95, No. WW4, Nov.1969.

[29] Gudmestad, O.T. and Connor, J.J.: "Linearization Methods for Nonlinear Drag Force Loading Terms", Research Report R80- , Dept. of Civil Engineering, Massachusetts Institute of Technology, Cambridge, MA, Feb. 1980.

[30] Dunwoody, A.b.: "The Role of Separated Flow in the Prediction of the Dynamic Response of Offshore Structures to Random Waves", Ph.D. Thesis, Dept. of Ocean Engineering, Massachusetts Institute of Technology, Cambridge, MA, May 1980.

[31] Iyengar, R.N. and Dash, P.K.: "Study of the Random Vibration of Nonlinear Systems by the Gaussian Closure Technique", Journal of Applied Mechanics, Vol. 45, No. 2, pp. 393-399, June 1978.

[32] Smith, E.: "On Nonlinear Random Vibrations", Ph.D. Thesis, Division of Structural Mechanics, The Norwegian Institute of Technology, Trondheim, 1978.

[33] Fish, P.R. and Rainey, R.C.T.: "The Importance of Structural Motion in the Calculation of Wave Loads on an Offshore Structure", BOSS'79.

[34] Miller, B.L.: "Wave Slaming Loads on Horizontal Circular Elements of Offshore Structures", Journal of the Royal Institute of Naval Architects, May 1978.

[35] Kaplan, P. and Silbert, M.N.: "Impact Forces on Platform Horizontal Members in the Splash Zone", OTC 1976, Paper No. 2498.

[36] Oppenheim, A.V. and Schafer, R.W.: Digital Signal Processing, Prentice-Hall Inc., N.J., 1975.

[37] Shyam Sunder, S.: "Stochastic Modelling of Ocean Storms", S.M. Thesis/Research Report R79-7. Dept of Civil Engineering, Massachusetts Institute of Technology, Cambridge, MA, Feb. 1979.

[38] Kawamoto, J., Shyam Sunder, S. and Connor, J.J.: "An Assessment of Uncertainties in Fatigue Analysis of Steel Jacket Offshore Platforms". Journal of Applied Ocean Research, May 1980.

[39] Kawamoto, J., Shyam Sunder, S. and Laya, E.: "User Manual for POSEIDON-II, A program for Evaluating the Short Term and Long Term Frequency Domain Response of Offshore Steel Jacket Platforms", Research Report R80- , Dept. of Civil Engineering, Massachusetts Institute of Technology, Cambridge, MA, June 1980.

[40] Wade, B.G. and Dwyer, M.: "On the application of Morison's Equation to Fixed Offshore Platforms",OTC 1976, Paper No. 2723.

[41] Mercier, J.A.: "Large Amplitude of Oscillation of a cylinder in a Lowspeed Stream", Ph.D. Thesis, Stevens Institute of Technology, Dept. of Mechanical Engineering, 1973

[42] Mercier, J.A.:"The Forces on Circular Cylinders Due to Combined Action of Waves and and Currents", West Gulf Section, Soc. of Naval Arch. and Marine Engrs., Feb. 1976.

[43] See References [40], [41] and [42].

APPENDIX A

A COMPARISON OF FORCE FOURIER SPECTRA CORRESPONDING TO FIRST AND THIRD ORDER EXPANSIONS FOR THE DRAG FORCE

As discussed in Sect. 4.1, first and third order expansions are used in other solution methods to approximate the drag force term. We consider here a rigid cylinder, of length $\Delta\ell$, and investigate the effect of the different assumptions for the drag force. For convenience, we list the force expressions below:

Linear

$$f(t) \simeq \frac{1}{2}\rho D C_{DV} \frac{8}{\pi} \sigma_v v \, \Delta\ell + \frac{1}{4}\rho\pi D^2 C_{MV} \dot{v} \, \Delta\ell \qquad \text{(A-1)}$$

Cubic

$$f(t) \simeq \frac{1}{2}\rho D C_{DV} \frac{2}{\pi} \left[\sigma_v v + \frac{v^3}{3\sigma_v} \right] \Delta\ell + \frac{1}{4}\rho\pi D^2 C_{MV} \dot{v} \, \Delta\ell \qquad \text{(A-2)}$$

Full nonlinear

$$f(t) = \frac{1}{2}\rho D C_{DV} v|v| \, \Delta\ell + \frac{1}{4} \, D^2 C_{MV} \dot{v} \, \Delta\ell \qquad \text{(A-3)}$$

Data related to the member geometry, wave loading and spectral discretization is listed in table A-1.

Fourier transforms for the hydrodynamic force corresponding to different choices for the phase angles are "averaged" and the resulting smoothed transforms are plotted in Figs. A.1,2,3. The nonlinearity

TABLE A-1

CASE EXAMPLE FOR COMPARISON STUDIES

SEA STATE PARAMETERS			
Significant Wave Heigth	(H_S)	12	feet
Av. Zero Crossing Period	(T_Z)	6.91	sec
Lower Cut-off Frequency	(ω_1)	0.376991	rad/sec
Higher Cut-off Frequency	(ω_M)	2.513279	rad/sec
Frequency Increment	($\Delta\omega$)	0.062832	rad/sec
Still Water Depth	(d)	58.3	feet
CYLINDER PARAMETERS			
Length	($\Delta\ell$)	23.3	feet
Diameter	(D)	15	in
Relative Roughness	($\frac{k}{D}$)	0.01	
Depth to Center of Gravity	(y)	11.65	feet

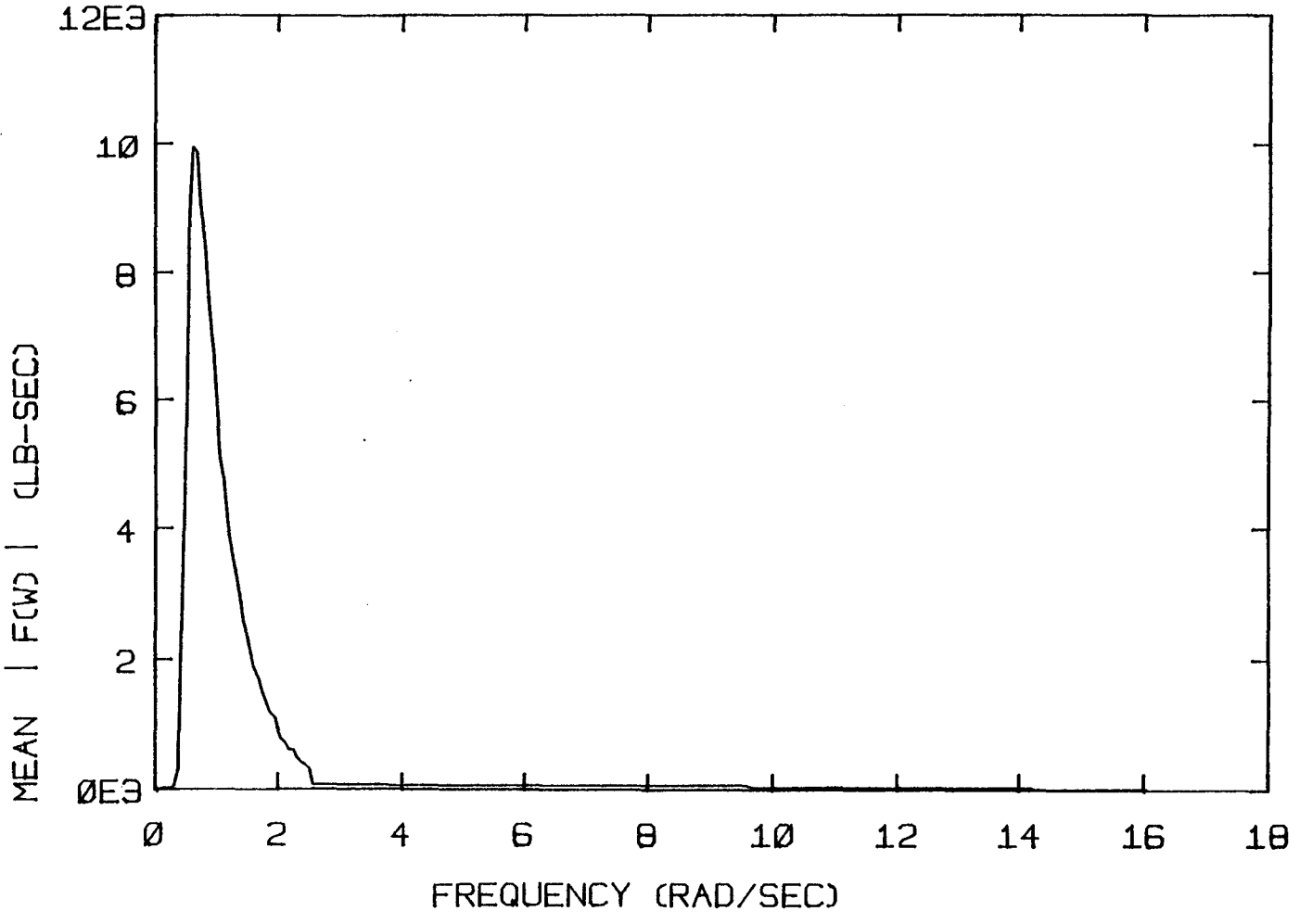

Fig. A.1 Mean Force Spectrum, Linear Expansion

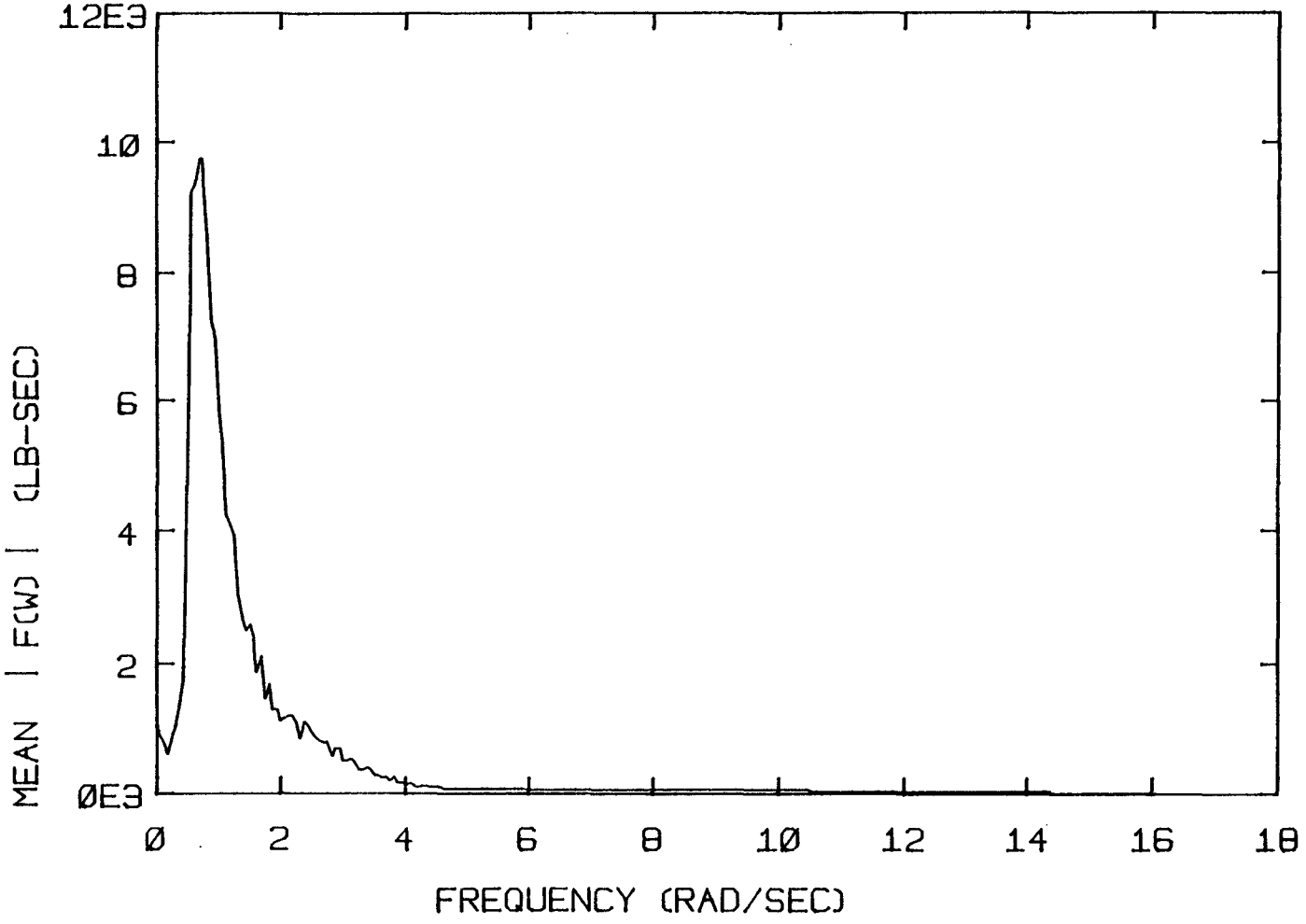

Fig. A.2 Mean Force Spectrum, Cubic Expansion

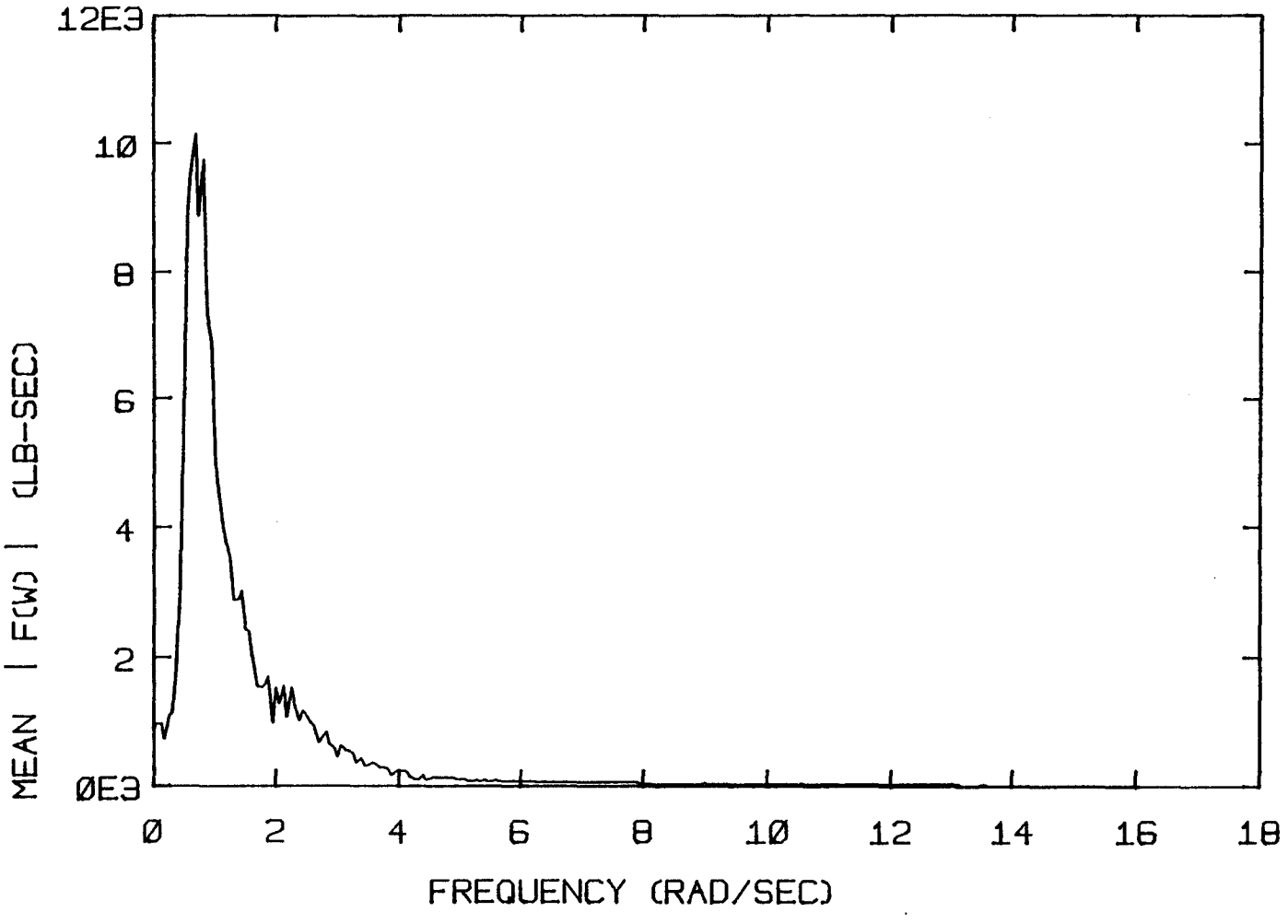

Fig. A.3 Mean Force Spectrum, Nonlinear Form

increases the contribution at both the low and high ends, and generates contributions in regions where the wave spectral density is negligible. Linearization eliminates this behavior, while the full nonlinear form produces the maximum contribution in the low frequency zone. The increased energy at the high frequency end may be a potential problem for structures having periods in the neighborhood of 5 seconds. Compliant towers are designed to have periods greater than the dominant wave periods, and according to the linear formulation there is negligible wave energy. However, a full nonlinear treatment indicates that this assumption is unconservative.